Investigation of Alternative Defrost Strategies

By

Nathan Hoffenbecker

A thesis submitted in partial fulfillment

Of the requirements for the degree of

Master of Science

(Mechanical Engineering)

At the

Solar Energy Laboratory

Industrial Refrigeration Consortium

University of Wisconsin – Madison

2004

Approved By:

Date: April 16, 2004

Abstract

We take for granted the abundance and variety of food that is available to us all year round. Grocery stores around the U.S and the world sell a wide variety of fruits and vegetables throughout the year no matter when the harvesting season took place; this in large part due to cold storage warehouses. Cold storage warehouses place otherwise perishable food items into freezers and coolers where they can be stored for months, or even years, until they are ready for sale.

Many food items placed in storage require the temperature to be held at low temperatures. Though the low temperatures are needed to maintain the quality of stored products, it has an adverse effect on the refrigeration system. By operating warehouses at temperatures below the freezing point, water (in the form of frost) will accumulate on the air-cooling evaporators used to cool the space. As frost builds up on an evaporator, the resistance to heat transfer between air and the refrigerant increases, airflow through the evaporator decreases, and the overall efficiency of the evaporator decreases.

The goal of this research project is to develop a better understanding of the factors that influence defrost performance as well as the parasitic impacts on system energy consumption by generating a transient computer model of the processes involved in a hot gas defrost cycle on an evaporator coil of known geometry. This study focuses on utilizing different refrigerant temperatures for melting frost accumulated on the evaporator's coils.

To evaluate an evaporator undergoing a defrost process; models of a dry coil as well as a frosted coil were developed using EES (Engineering Equation Solver). The models approximated the coil by representing it as a tube with a radial fin. The models themselves are made up of multiple nodes which are defined by energy boundaries. The nodes in the models are transient and are temperature driven. Freezer conditions as well as frost properties are also implemented in the programs to simulate different environments. The frosted fin model was used to record the time to melt a given mass of frost as well as find the distribution of energy associated with defrosting. The dry fin model was created to record the excess amount of energy that goes into a defrost process that lasts longer than the time required to melt the accumulated frost.

The last part of the study focuses on the estimating costs associated with the parasitic loads created by initiating a defrost cycle. Since the energy that is lost from convection, evaporation, and stored energy in the metal coils of the evaporator has to be reclaimed, the compressors in the refrigeration system are analyzed to estimate the energy costs associated with operating a compressor to circulate the refrigerant in order to capture the energy from the surroundings. The compressor cost evaluation is based on a single stage and a two stage system using different operating head pressures to simulate the effects of defrosting throughout a typical year.

Acknowledgements

My first and foremost thanks go to my advisors Prof. Sanford. A. Klein and Prof. Douglas T. Reindl whose knowledge and support was unsurpassed throughout my endeavor. Their constant encouragement and enthusiasm in this project, as well as their guidance, made this research possible.

I would like to thank Douglas Matousek and Kevin Broedlow at Atlas Cold Storage in Jefferson, WI. Their unconditional cooperation involving this project, as well as extending their friendship, made working with them a great learning experience.

I would also like to give thanks to all of my peers and professors in the Solar Energy Laboratory for their comments, suggestions, and knowledge. The environment in which they provided made my stay very enjoyable and memorable.

My thanks and love also goes out to my parents whose contributions and sacrifices made it possible for me to pursue greater things and never be content.

Last, but not least, I give thanks to my friends, especially Kristi, for their support and friendship which made living in Madison an enjoyable and unforgettable experience.

This project was supported by a grant from the Energy Center of Wisconsin.

Table of Contents

List of Figures

List of Tables

Nomenclature

Variables

A	area	[m]
A_p	profile area	[m^2]
C	specific heat	[kJ/kg-K]
D_{12}	binary diffusion coefficient	[m^2/s]
$\dot{E}$	energy transfer	[kJ]
g	gravitational constant	[m/s^2]
$\bar{g}_m$	mass transfer coefficient	[kg/m^2-s]
Gr	Grashof number	*N/A*
h	enthalpy	[kJ/kg]
h_C	convection	[W/m^2-K]
h_{ig}	enthalpy of fusion	[kJ/kg]
J	mass flux	[kg/m^2-s]
k	thermal conductivity	[W/m-K]
L	length	[m]
L_c	corrected fin length	[m]
Le	Lewis number	*N/A*
Nu	Nusselt number	*N/A*
m	mass	[kg]
m_{AIR}	mass fraction of dry air	*N/A*
m_{H_2O}	mass fraction of water	*N/A*
P,p	pressure	[kPa]
Pr	Prandtl number	*N/A*
q	heat transfer	[kJ]
$\dot{q}$	heat transfer rate	[kW]
r	radius	[m]
R	gas constant	[kJ/kmol-K]

Ra	Rayleigh number	*N/A*
RH	relative humidity	*N/A*
Sc	Schmidt number	*N/A*
Sh	Sherwood number	*N/A*
t	thickness	[m]
$time_{final}$	defrost completion time	[s]
T	temperature	[K, C, F]
u	specific internal energy	[kJ/kg]
v	specific volume	[m^3/kg]
V	volume	[m^3]
x	axial direction	*N/A*

Greek Symbols

Δ	change in	*N/A*
v	kinematic viscosity	[m^2/s]
θ	temperature difference	*N/A*
ρ	density	[kg/m^3]

Subscripts

b	base
cond	conduction
conv	convection
evap	evaporation
e	ambient
F	fin
∞	ambient
i	axial nodal direction
in	inside

ii	total number of nodes in the axial direction
jj	total number of nodes in the radial direction
n	neighboring node
out	outside
s	surface boundary
sat	saturated

Superscripts

.	rate
-	local (average)

Chapter 1 Refrigeration Background

1.1 Overview of Industrial Refrigeration

Industrial refrigeration, like all other refrigeration applications has a simple objective: remove heat from a source and discard it elsewhere. Operating on a larger scale, industrial refrigeration systems still utilize the same main components found in all vapor compression cycles: a compressor, condenser, an expansion device, and an evaporator.

A vapor compression refrigeration cycle, working under normal conditions, operates in the following manner: refrigerant is raised from low pressure, low temperature to a state of high temperature and pressure as it passes through the compressor. The refrigerant then enters a condenser where heat from the refrigerant is removed; thereby, liquefying in the process. The liquid refrigerant, still at a high pressure and temperature is then throttled through an expansion device where a portion flashes to a vapor as it cools from the saturated condensing temperature to the saturated evaporator temperature before entering the evaporator. In the evaporator the refrigerant, now at low pressure and temperature, passes through a heat exchanger (evaporator) and captures heat from the surroundings. As the refrigerant is heated, it boils from a liquid to a vapor and returns back to the compressor in a vapor state. Below, Figure 1-1 shows a vapor compression refrigeration cycle.

Figure 1-1: A schematic of a vapor compression refrigeration cycle

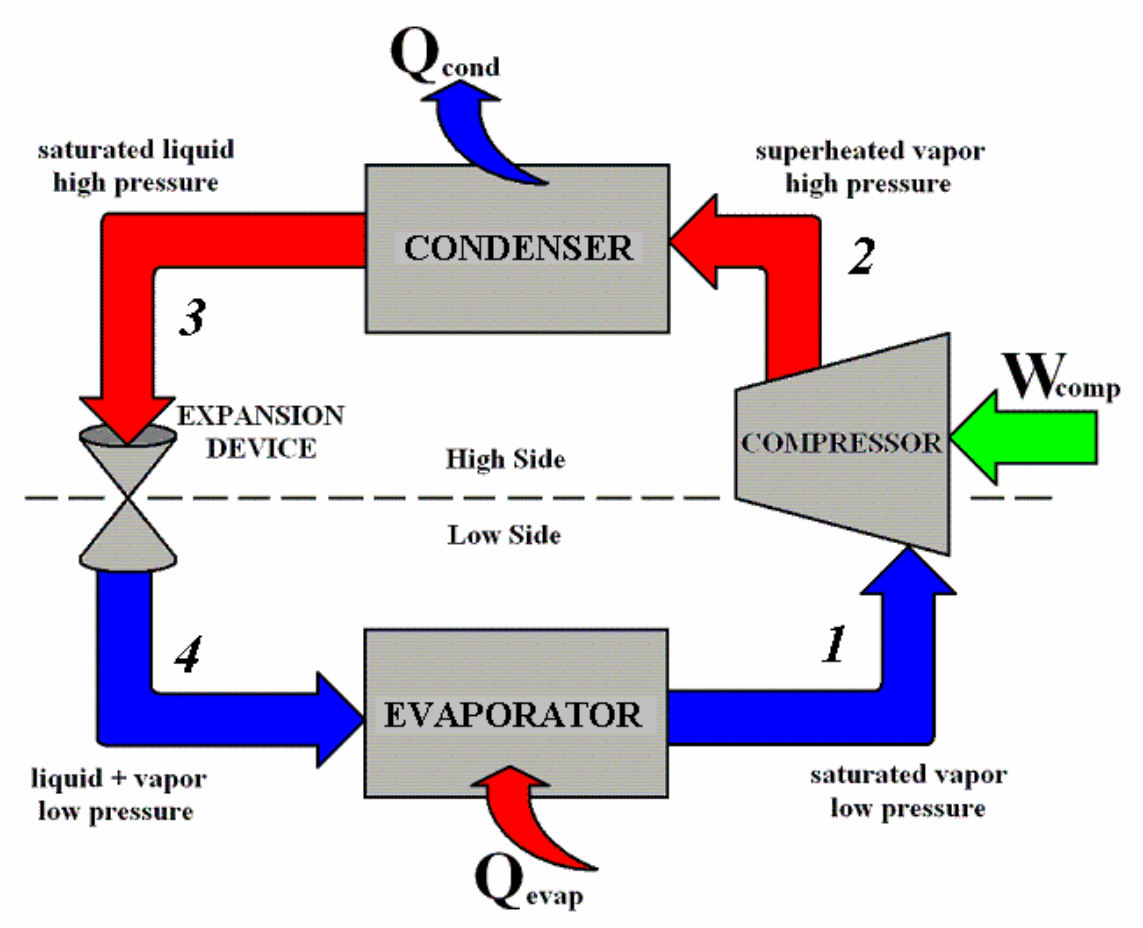

1.2 Property Diagrams

Referring to the above diagram, the properties of the refrigerant can be mapped as it goes through a typical vapor compression cycle. The plots shown below are for an ideal vapor compression cycle where losses and sources of inefficiency are not taken into account. The states of the refrigerant are tracked in the figures below.

Figure 1-2: T – s diagram of vapor compression cycle

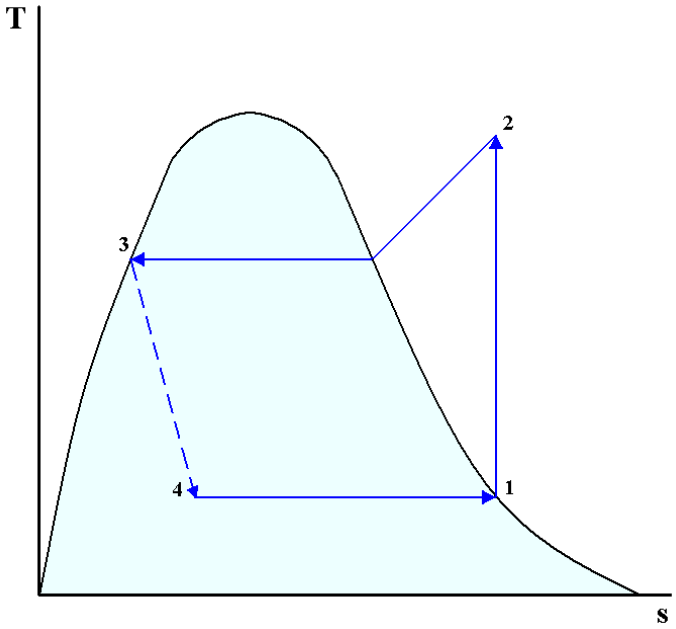

Following both the T-s and P-*h* plots, as the refrigerant goes through the compressor (1-2) the pressure and temperature of the refrigerant is elevated and the state of the refrigerant goes from saturated vapor to superheated vapor. There is no entropy generated in an ideal compression process. As the refrigerant continues through the condenser (2-3), the temperature decreases while the pressure remains constant. The refrigerant exits the condenser as a saturated liquid. The refrigerant then passes through the expansion valve (3-4) dropping both the pressure and temperature of the refrigerant. The expansion causes a portion of the refrigerant to 'flash' from a liquid to a vapor which means that the saturated liquid upstream of the expansion device will exit as a mixture of saturated liquid and vapor at low temperature and pressure. The refrigerant traveling through the evaporator (4-1) will absorb heat from the surroundings causing the liquid portion of the refrigerant to boil off, expanding the refrigerant as it feeds back to the compressor in a saturated vapor form.

Figure 1-3: P-h diagram of vapor compression cycle

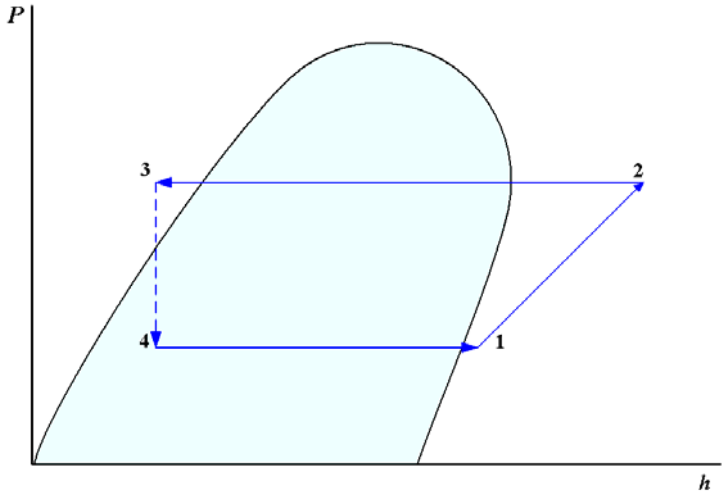

1.3 Use of Air as a Heat Transfer Medium

In refrigerated spaces, air is the principle medium used to accomplish useful cooling. The storage of product in spaces maintained at temperatures less than 0 ˚C (32 ˚F) results in a space that will be relatively dry. Moisture in low temperature spaces arises from multiple sources. First, products being moved into the refrigerated space where the product is at a higher temperature and humidity can give off moisture. Occupants add moisture to the space. Finally, moisture infiltrates the space from the outdoor environment as well as by virtue of adjacent spaces operating at a higher temperature and humidity level. As a result, the air used to cool the space must be capable of removing not only the sensible heat (for temperature control) but also the latent heat (for moisture control). This process is accomplished by cooling supply air to a lower temperature and humidity.

As the air is drawn past the evaporator coils, the heat is removed by cold refrigerant circulating through the circuits of the evaporator. As the air temperature decreases, moisture will be removed if the coil temperature is below the entering air dew point temperature. In situations where the surfaces of the evaporator operate below the freezing point of water, the

moisture extracted from the air will be deposited on the evaporator surface in the form of frost. The air exiting the evaporator is now at a lower temperature and moisture content and, as a working fluid, will be able to absorb sensible and latent heat once again.

1.4 Defrost Background

A consequence of cooling and dehumidifying low temperature air is a deposition of moisture (in the form of frost) on the evaporator coil tubes and fins (if equipped). Any given evaporator has a limit to the amount of frost that can accumulate on the coil surface before it begins to experience operational problems. When too much frost accumulates, the coil's heat transfer performance is decreased because the frost itself behaves like an insulator. The frost also hinders the amount of air that can be drawn through the evaporator by decreasing the free area available for air to flow between adjacent frosted fins. To compensate for these effects, the evaporator must halt its cooling duty, and go into a "defrost mode."

Defrosting is a process intended to remove accumulated frost from the evaporator coils so it may, again, provide cooling in an effective and efficient manner. There are many ways to remove frost from evaporator coils; the various processes are explained in the following section.

1.4.1 Methods of Defrost

To rid of accumulated frost from evaporator coils, it is necessary to raise the temperature of the evaporator coil surfaces above the freezing point of water. An alternative strategy is to avoid accumulation of frost in the first place using a desiccant solution. Using a solution that has a lower freezing point than water and freezer operating conditions, moisture from the air in the freezer is captured by the solution that drips over the fins. However, energy penalties are associated with using brine solutions as well. The concentration of the brine becomes reduced over the hours of evaporator operation. The captured moisture from the air into the brine solution must be boiled off to maintain the low freezing temperature. This can be considered a "defrost process" itself.

There are various ways of removing frost collected on evaporator coils. It can be dealt with by using electrical resistance heating, spraying warm water, or using hot gaseous refrigerant. Using electrical resistance heating for defrost is plainly mounting a resistive heater in contact with the evaporator coil assembly. Though the first cost of this method is inexpensive, the cost of electricity makes this strategy quite expensive to operate. Using water to defrost requires water to be sprayed on the surface of the evaporator coils. The warm water mixes with the accumulated frost and over time clears the finned surface of the evaporator. Stoecker (1998) recommends water around 18 ˚C (65 ˚F) and a flow rate of 2 to 3 kg/s per m^2 (0.4096 to 0.6144 ft/s per ft^2) of face area. Using hot gaseous refrigerant is the most practiced method in industrial refrigeration and is detailed in the section following.

1.4.2 Hot Gas Defrost (principles and sequences of operation)

Hot gas defrosting is popular because everything that is needed for the defrosting process is used in the cooling process as well, ignoring minor piping strategies to utilize it. The hot gas defrosting method uses hot refrigerant vapor that is discharged from the compressor. Instead of the entire hot refrigerant going into the condenser, a portion of it is piped to the evaporator during defrost. The evaporator must be out of the cooling mode when this takes place in order to accommodate the hot refrigerant. Two figures of an evaporator, one while operating in the cooling mode, the other while it is operating in the hot gas defrost mode are presented below. The evaporator represented in the figures is a direct expansion evaporator, though other evaporator types such as flooded evaporators generally use the same concept.

Figure 1-4: An evaporator in normal cooling mode, Reindl (2004)

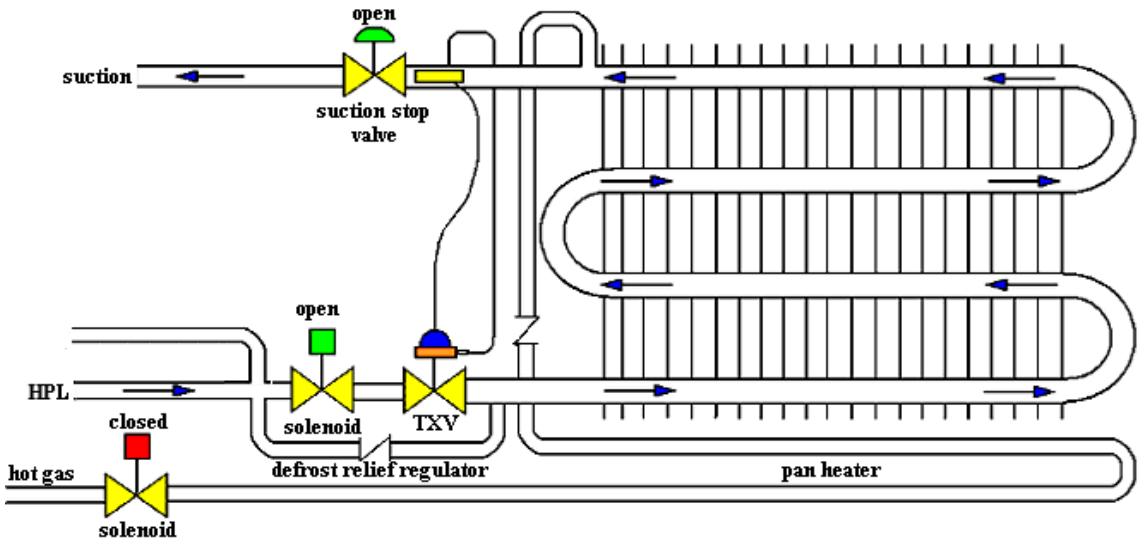

In Figure 1-4, the evaporator is in cooling mode. The refrigerant first passes through a liquid feed solenoid (a valve that operates either fully open or fully closed) followed by a refrigerant flow control device - a thermostatic expansion valve. The thermostatic expansion valve modulates the flow of refrigerant into the coil where a portion of the high-pressure liquid is flashed to resulting in a mixture of saturated liquid and vapor at a low temperature and pressure that is delivered to the coil. When the refrigerant absorbs heat from the coils it boils off and continues up the coil circuitry flowing out the coil through the suction stop valve where it is delivered back to the compressor.

The figure below (Figure 1-5) is the same evaporator undergoing hot gas defrosting. The solenoid valve is closed and the cold refrigerant is halted. After a time delay that allows the remaining refrigerant in the coil to boil off, the hot gas solenoid valve is opened. Hot gas first flows to the drain pan allowing hot refrigerant to warm the pan. Condensed liquid and hot gas leaves the drain pan and rises vertically through the pan check valve and enters the top of the coil. The hot gaseous refrigerant flows through the coil giving up heat as it condenses. When the pressure in the coil reaches the setting of the defrost relief regulator, it opens wide allowing the refrigerant to escape to the defrost return.

Figure 1-5: An evaporator in a hot gas defrost process, Reindl (2004)

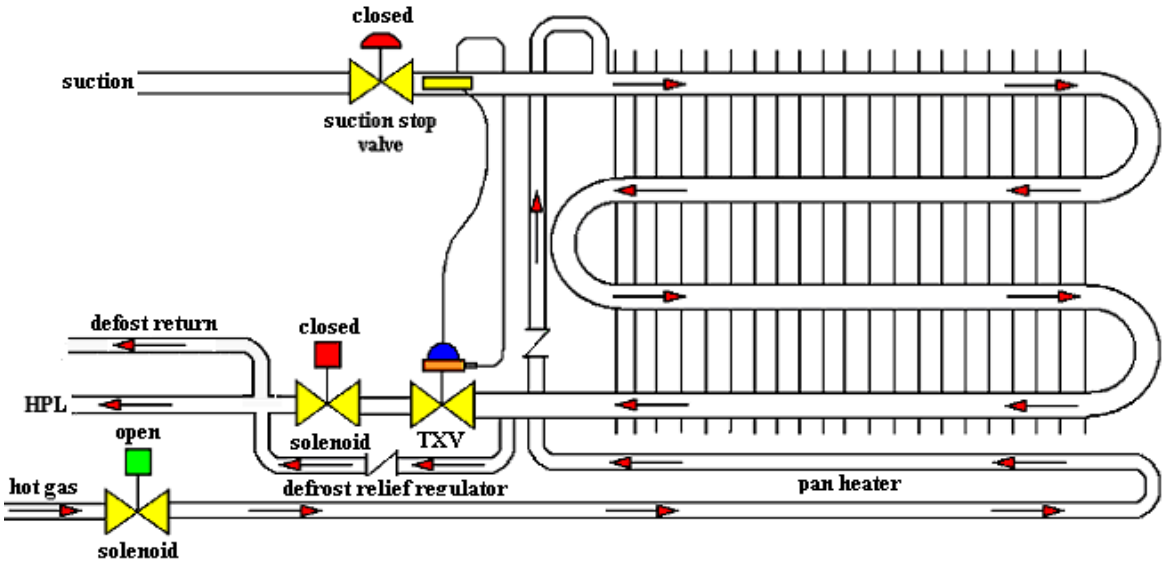

1.4.3 System Effects during Defrost (space parasitic loads, Compressor Behavior, Head Pressure, etc.)

Because the most prevalent method of defrosting is using hot gaseous refrigerant, the implications presented here are for hot gas defrosting, though other defrost strategies may share some areas of concern. When an evaporator is defrosting, it can affect the overall refrigeration system as a whole. The evaporators that are sharing a cooling load with the evaporator that is in defrost must pick up the extra cooling load not being met by the evaporator in defrost. A defrosting evaporator also generates sensible and latent heat loads in the space while it is in defrost.

The areas of concern presented next are also tabulated in Reindl, et al. (2004). In some cases, compressors are operated at higher condensing pressures than necessary throughout the year to accommodate moving hot gaseous refrigerant to evaporators when they go into defrost. Even when the head pressure could be lowered, and in most cases should be lowered, most facilities maintain high head pressures to make sure there is an adequate supply of hot gas for defrosting evaporators.

Plants generally use a time-initiated and time-terminated defrost sequence. Based loosely on the freezer conditions (observations by the systems operators), an evaporator

scheduled to operate for a given number of hours, either in real time or accumulated liquid feed solenoid open time, between defrost cycles. When the operating time criteria are met, the system will initiate an evaporator defrost sequence, whether the evaporator coil has a significant or little amount of frost accumulated. The defrost cycle, on a timer as well, runs too long and thereby introduces excessive parasitic loads to the freezer.

For systems that do not incorporate defrost drainers such as float valves (Figure 1-6), excessive hot gas supply dwell periods can falsely load compressors as a result of hot gas bypassing the evaporator and returning to suction late in a defrost sequence. This 'hot gas bypass' is common in facilities that use long hot gas supply periods for defrost. Defrost drainers are one alternative that allows the evaporator to maintain high pressures while in defrost, but allow only the refrigerant condensate to leave.

Figure 1-6: Defrost drainer, Hansen Technologies Corporation (1998)

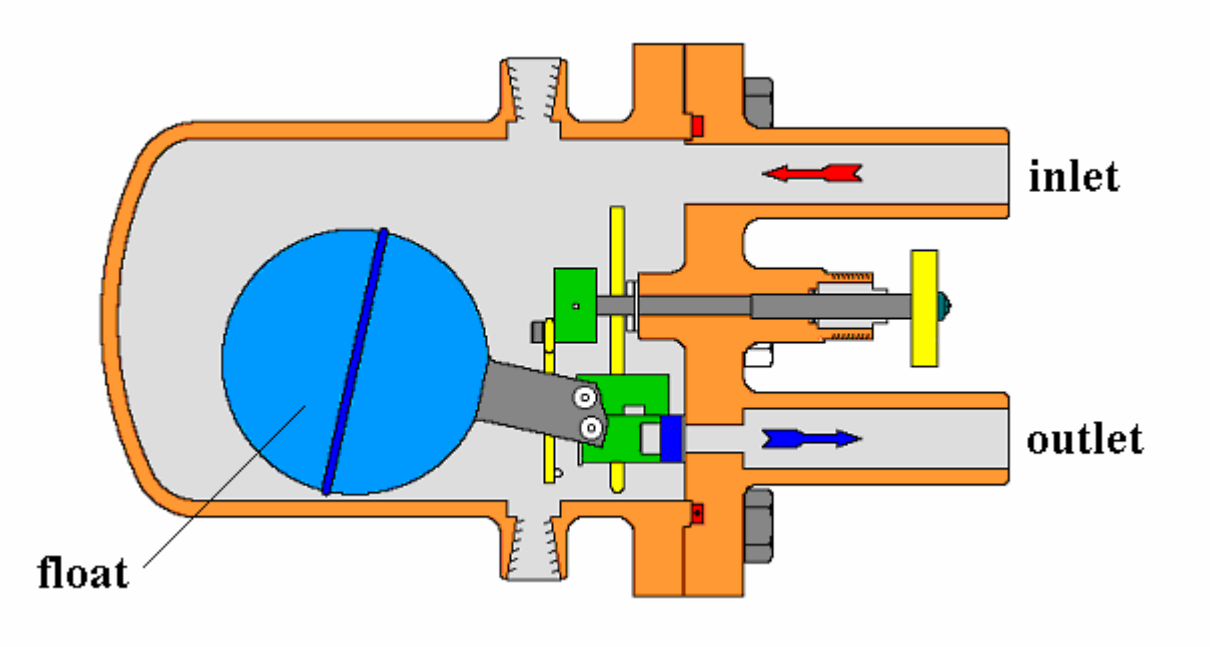

1.4.4 Energy Impacts of Defrost

There are many energy implications to a refrigeration system's performance when an evaporator initiates defrost. As stated above, the compressor head pressure is maintained at a high level to accommodate moving the hot gaseous refrigerant. Maintaining higher head pressures than necessary results in increased compressor energy usage. False loads are

applied to the compressor due to hot refrigerant bypassing the evaporator and returning to the compressor as hot vapor. The sensible and latent heat that escapes into the freezer during defrost is of concern because all of the energy has to be reclaimed from the freezer. Excessively supplying coils with hot gas for longer periods than necessary during a defrost sequence adds unnecessary parasitic loads in the freezer. The huge amount of energy that goes into heating the evaporator fin and tube mass as well as the casing and drain pan also need to be reclaimed following the defrost cycle. Cole (1989) stated that the most of the energy required to defrost an evaporator goes back into the system, above 80% of the supplied energy, resulting in e defrost efficiency of less than 20%.

1.5 Detailed Evaporator Layout/Description

Air cooling evaporators are all comprised of the following basic components:

- tubes that carry the refrigerant
- fins that are attached to the tubes to improve heat transfer
- fans to pull surrounding air past the tube and fin structure,
- a housing to hold all of the components together, and
- a drain pan used to carry water away after a defrost

The figure below shows the major components in an air-cooling evaporator. Further details of evaporator construction are given in the sections following.

Figure 1-7: An industrial evaporator detailing the major components, Evapco (2001)

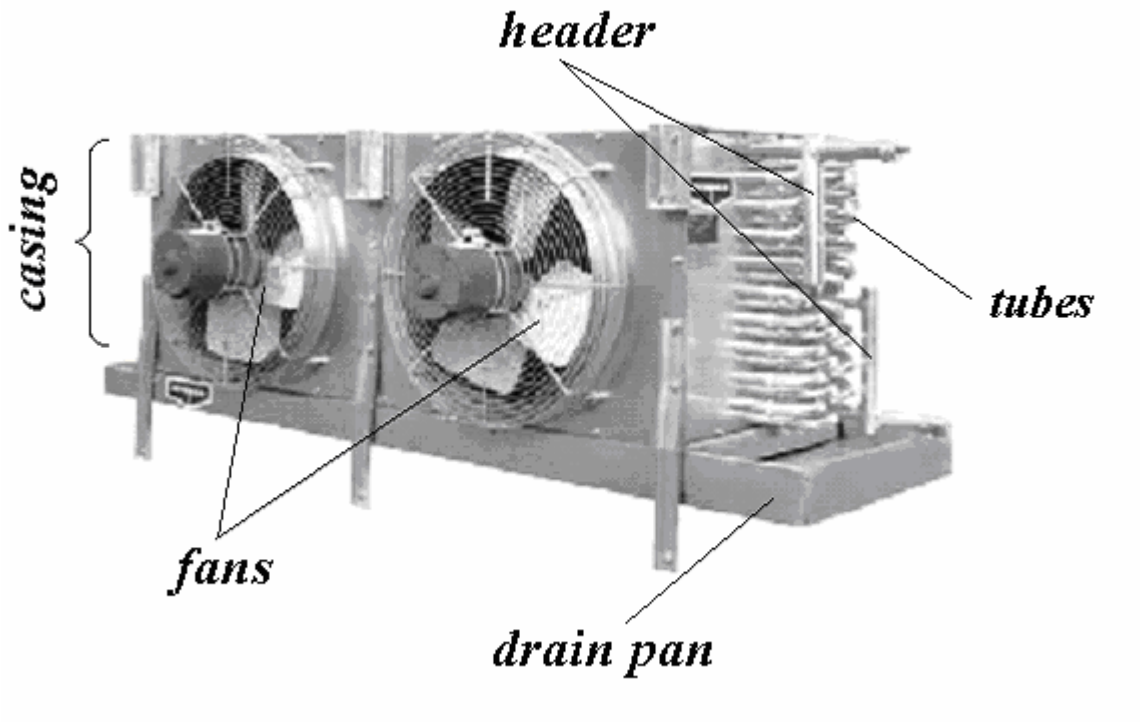

1.5.1 Tube/Fin Assembly

Air cooling evaporators are comprised of a series of tubes with fins attached to their exterior surfaces. Each tube in an evaporator comprises a single circuit. A circuit consists of a single tube that runs horizontally down the length of the evaporator and back several times from the face of the evaporator to the exit. Depending on the evaporator, a circuit can consist of a tube running the length of the evaporator and back several times – referred to as the number of passes. Each evaporator is made up of several circuits, and each circuit is attached to a header. A header is a larger pipe that connects to all of the circuits and supplies the circuits with the refrigerant. The fins are large sheets of very thin metal that increase the heat transfer area of the tubes. The fins also allow contact with multiple tubes as seen in Figure 1-8.

Figure 1-8: A section of a tube and fin assembly, Evapco (2001)

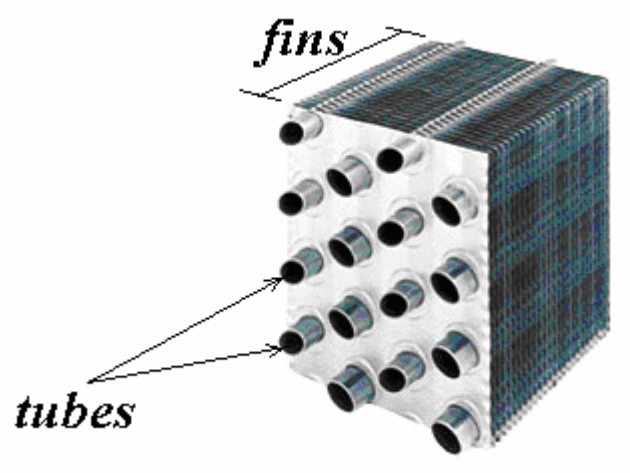

1.5.2 Other Evaporator Components

Figure 1-7 shows an entire evaporator including the casing, fans, and drain pan. The casing holds all of the tubing circuitry as well as the fins that the tubes pass through. The casing also provides a mounting surface, since most evaporators are ceiling hung. Below the casing is the drain pan. The drain pan collects, and when connected to a pipe, removes water from the freezer space when the evaporator defrosts. Mounted on the evaporator's casing are fans that draw air through the evaporator. The fans optimize the heat transfer from the refrigerant to the air in the space. The sizes of the fans are dependent on the size of the evaporator used as well as the required airflow rate.

1.5.3 Materials of Construction

Materials used for evaporators vary between the types of refrigerant used. Most evaporators however use aluminum for their fin construction. Though it has a higher specific heat than steel, the density of aluminum is much less than steel. Therefore less energy is required to raise the aluminum's temperature, relative to steel. This is important when considering that a defrost sequence requires all of the fins be heated above the freezing point of water to remove the frost from its surface. The tubes in the evaporator are generally made of steel, but aluminum or stainless steel can be used as well. The tubes are very thin,

generally around the order of 0.060 inches (1.524 mm). The casing and drain pan are also made from aluminum with steel brackets to mount the unit.

1.6 Research Objectives

At a high level, the objective of this research project is to identify methods to improve the efficiency of industrial refrigeration systems that utilize air-cooled evaporators operating at temperatures below freezing. The primary focus of the research is aimed at achieving energy efficiency improvements by developing strategies for reducing the parasitic impacts of evaporator defrosting with hot gas defrosting systems.

As the hot gas circulates inside the evaporator, the outside surface warms and the accumulated frost melts. There are many parameters that potentially can be varied in this process such as:

- time between defrost cycles (related to mass of frost accumulated on the coil)
- the refrigerant pressure and temperature used for defrost
- hot gas defrost time period
- piping and valve arrangements for hot gas supply and defrost (condensate) return

In addition to the above parameters, the materials of coil construction (i.e. aluminum, stainless, steel coil materials) may also influence the ease of defrost.

A goal of this research project is to develop a better understanding of the factors that influence defrost performance as well as the parasitic impacts on system energy consumption by generating a transient computer model of the processes involved in a hot gas defrost cycle on an evaporator coil of known geometry. The model provides a tool to optimize both the temperature and time of the process to decrease the sensible and latent gains to the space as a consequence of evaporator defrosting. There is particular interest in estimating the impact of the parameters listed above on hot gas defrosting latent loads to spaces. The latent parasitic load due to hot gas defrosting represents the amount of moisture that is re-evaporated to the space during the defrost cycle. Minimizing the parasitic space sensible and latent gains will directly improve the energy efficiency of the overall refrigeration cycle serving controlled

environment spaces. The study will compare the simulated results of the program to available experimental results in order to both validate the model and evaluate the energy savings potential of optimizing the defrost process.

1.6.1 Energy Distribution during Defrost Cycle

The energy that is given up from the hot gaseous refrigerant goes into melting the frost accumulated on the coil surface. It also raises the temperature of the evaporator coil, convects energy out to the freezer, and releases energy associated with evaporation of water into the freezer. These types of dispersed energies are well known, but the extent to which they impact refrigeration system efficiency is not well known. The optimum parameters for hot gas defrost are also unknown.

The main purpose of the model is to evaluate the *total* amount of energy that re-enters a refrigerated space with a given defrost cycle. By understanding the amount of energy that is related to each mode, proper adjustments can be made to minimize them. Although the energy that re-enters a refrigerated space during and after a defrost cycle is a major factor that establishes the defrost efficiency, the time it takes to defrost is just as important when deciding the best defrost strategy. If a certain defrost strategy allows more energy out to the freezer during defrost than another, but also takes much less time than the latter, it may be fitting to choose the former strategy because the evaporator returns to the cooling mode sooner.

1.6.2 Temperature of Refrigerant vs. Time to Defrost

A hot gas defrost uses a portion of the system's hot gaseous refrigerant from the compressor outlet that would otherwise feed into the condenser. Depending on the system's head pressure and the defrost relief regulator valve set point, the saturation temperature of refrigerant in the evaporator during defrost can range from 50˚F to 100˚F. At higher refrigerant temperatures, the frost accumulated on the evaporator coils melts at a faster rate, decreasing the amount of time it takes to complete the defrost cycle. Though the time it takes the hot gas defrost cycle to terminate is reduced, the rate of energy that escapes into the refrigerated space may be greater. After the defrost process is completed, the evaporator

coils are at an elevated temperature and have to be cooled back to the normal cooling mode operating temperature; thereby, increasing the load on the refrigeration equipment.

1.6.3 Minimize Loads of Freezer during Defrost

Every air-cooling evaporator that is used in refrigeration systems that operates below 32˚F [0˚C] needs to be defrosted periodically, and with every defrost come efficiency penalties. When an evaporator goes into defrost mode it no longer provides cooling to the surrounding space. In order to maintain a cold environment, the other evaporators in the freezer must pick up the excess load. When hot gas begins to flow through the coils of the defrosting evaporator, the fins and tubes are heated. With the melting of frost on the coil surface, there is also heat transfer into the freezer space by convection. As the frost melts, some water evaporates increasing the moisture content of the air in the freezer. If the defrost process is controlled by a timer and allowed to continue after the frost is gone, the fins and tubes of the evaporator will continue to convect heat to the surroundings, increasing the sensible load on the refrigeration equipment. Finally, as the defrost terminates, the cool refrigerant in the evaporator will then have to remove the heat stored in the coils it acquired from the hot refrigerant.

All of the points stated above, not to mention the added head pressure of the refrigeration system, add great loads to the system. It is because of these excess loads that finding an optimum defrost strategy to minimize the losses, and cost, is invaluable.

1.7 References

Reindl, Douglas T., Jekel, Todd B., Elleson, James S. *Industrial Refrigeration Energy Efficiency Guidebook*. Industrial Refrigeration Consortium. 2004.

Cole, R.A. *Refrigeration Loads in a Freezer Due to Hot Gas Defrost and Their Associated Costs*. ASHRAE Trans. 1989, vol. 95, part 2, 1149-1154.

Evapco Inc. *NT Series Industrial Evaporators (Product Brochure)*. http://www.evapco.com/indexb.html 2001.

Hansen Technologies Corporation. *Specifications, Applications, Service Instructions & Parts*. http://www.hantech.com/Literature/PDF/d409.pdf. 1998

Chapter 2 Dry Fin Model

The purpose of creating a model of a dry fin is to introduce the main concepts that will be used later in a more complex model. While most of the concepts for both models (the dry fin model explained in this section and the frosted fin model detailed in chapter 3) are the same, validation of the dry fin model with known sources can be obtained and applied to the more in-depth frosted fin model.

2.1 Geometry

Air-cooling evaporators used in industrial refrigeration systems are comprised of a series of multi-row tubes with hundreds of fins pressed over the tubes to provide an extended heat transfer surface. Figure 2-1 is a drawing of a typical air-cooling evaporator that has multiple fins and tubes. If a single fin is examined, it can be noted that the symmetry of the fin surrounding each tube resembles a hexagon. The multiple hexagonal areas can then be used to approximate a single fin of an evaporator. For further approximation, each hexagonal area can be approximated as a disc, or more appropriately, an annular fin as shown in Figure 2-3. Like the hexagonal area around each evaporator tube, the annular fin area profile can also be used to approximate a single evaporator fin.

Figure 2-1: A general sketch of evaporator fins with tubes passing through

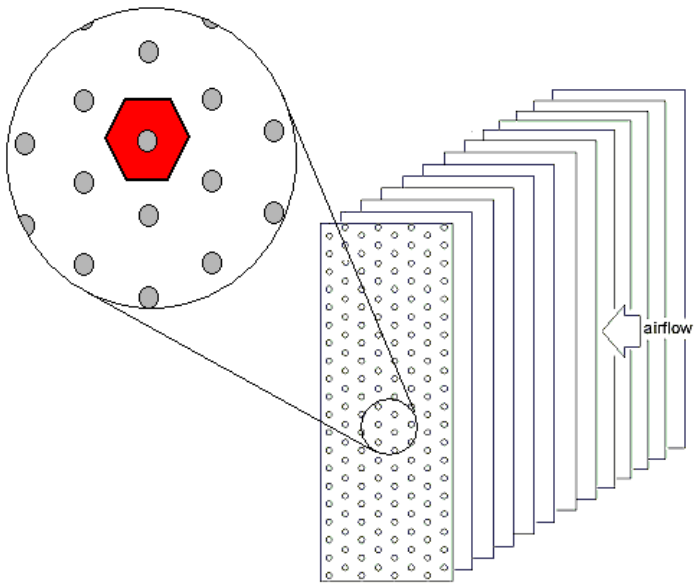

Figure 2-2 shows multiple annular fins approximating a single evaporator fin. Since all of the annular fins are alike, a single annular fin can be modeled and scaled-up to model the temperature distribution for a complete evaporator tube/fin assembly.

Figure 2-2: An estimate of the area distribution around each tube on a single fin

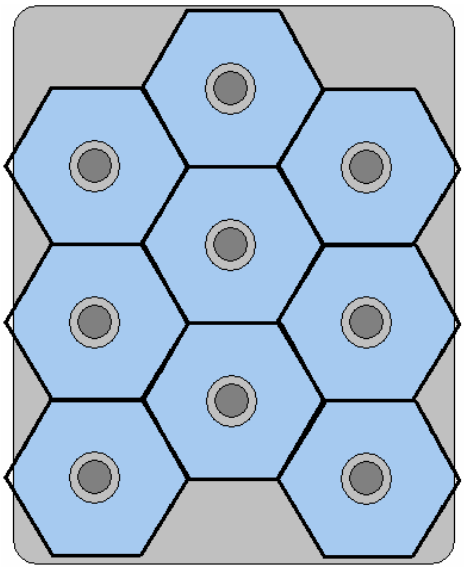

Figure 2-3: A further estimate of the area distribution using annular fins

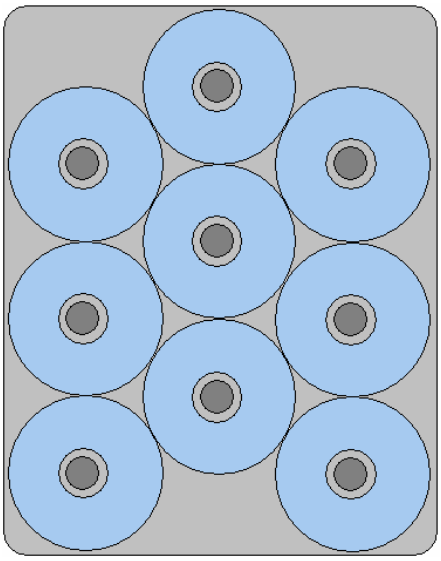

Applying symmetry, a typical tube in the evaporator with its fin attached forms the basis for establishing a model of the defrost process. Figure 2-4 shows an isolated portion of the evaporator coil after applying symmetry and the approximation of a circular fin from the hexagon.

Figure 2-4: Dry fin model representation

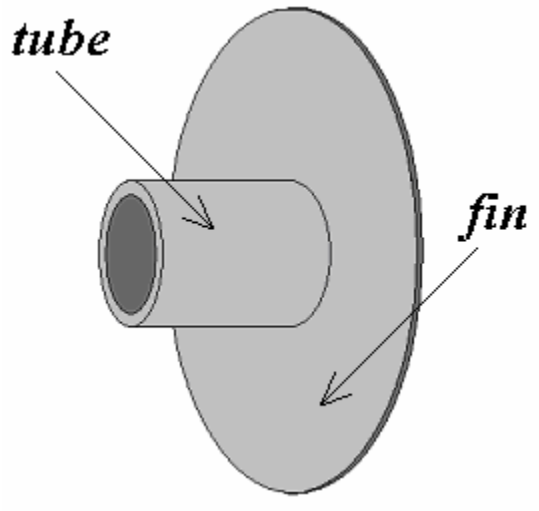

2.2 Analytical Solution

Heat transfer for extended surfaces is well known and their equations are common. For an annular fin the general forms of the fin equations found in Incropera and DeWitt (2002) are shown in equations 2-1 and 2-2 for steady state conditions.

Eq. 2-1

$$\frac{d^2T}{dr^2}+\frac{1}{r}\frac{dT}{dr}-\frac{2h}{kt}\left(T-T_\infty\right)=0$$

Eq. 2-2

$$\frac{d^2\theta}{dr^2}+\frac{1}{r}\frac{d\theta}{dr}-m^2\theta=0 \quad ; \quad m=\frac{2h}{kt} \quad \& \quad \theta=T-T_\infty$$

2.2.1 Temperature Distribution

Equation 2-2 is a modified Bessel equation of zero order. The general solution is of the form:

Eq. 2-3

$$\theta(r)=C_1I_0(mr)+C_2K_0(mr)$$

Assuming the annular fin has an adiabatic tip, $d\theta/dr\big|_{r_2} = 0$ (symmetry condition), and the temperature at the base of the fin is known, $\theta(r_1) = \theta_b$, C_1 and C_2 can be solved for, resulting in an equation for the temperature distribution given by Incropera and DeWitt (2002).

Eq. 2-4

$$\frac{\theta}{\theta_b} = \frac{I_0(mr)K_1(mr_2) + K_0(mr)I_1(mr_2)}{I_0(mr_1)K_1(mr_2) + K_0(mr_1)I_1(mr_2)}$$

The steady state temperature distribution for a fin of inside radius 1.27 [cm] (0.5 inches), outside radius of 3.81 [cm] (1.5 inches), a thickness of 0.0254 [cm] (0.01 inches), a convective coefficient of 6.7 [W/m^2-K], a thermal conductivity of 240 [W/m-K], and a base temperature of 310.93 ˚K (100 [˚F]) is shown in the figure below.

Figure 2-5: Temperature distribution of annular fin

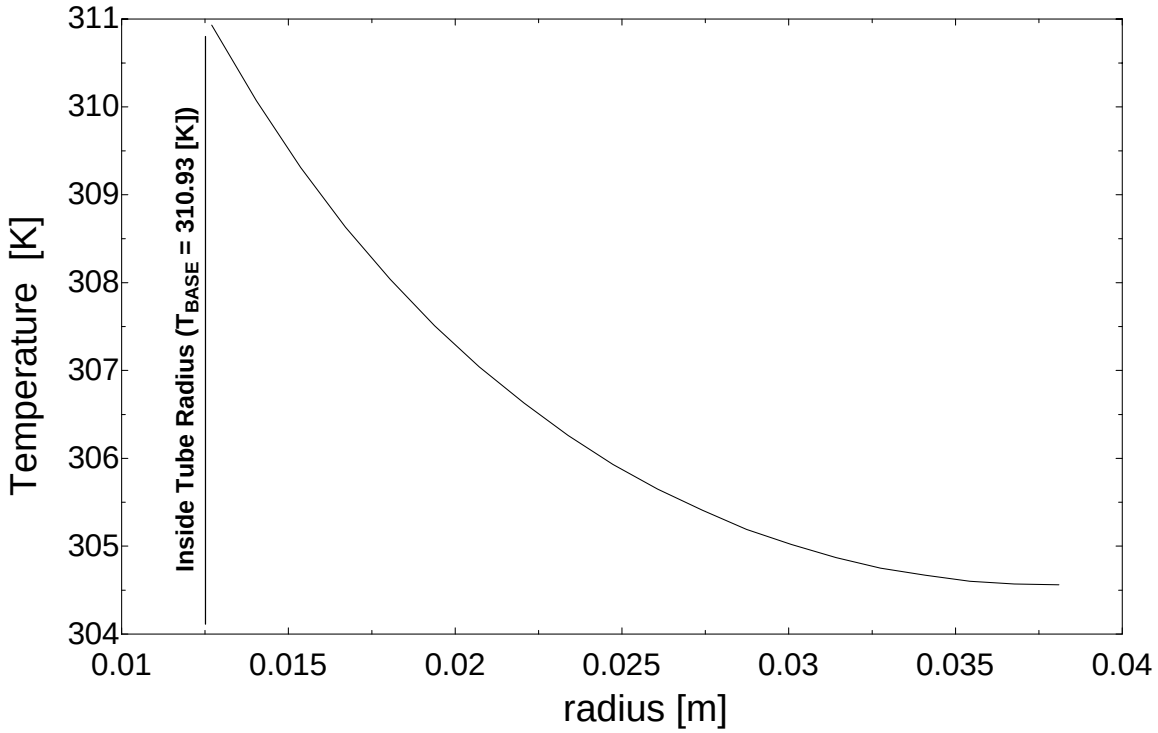

2.2.2 Fin Efficiency

Like the temperature distribution function, the steady state fin efficiency is also a Bessel function of the first order. The relationship between the zero and first order Bessel functions are tabulated in Incropera and DeWitt (2002). The conduction heat transfer rate is given by:

Eq. 2-5

$$q_f = -kA_{C,b}\frac{dT}{dr} = -k(2\pi r_1 t)\frac{d\theta}{dr}$$

Inserting the derivative of the temperature distribution in equation 2-4 results in the heat flux from the fin as given in equation 2-6.

Eq. 2-6

$$q_f = 2\pi k r_1 t \theta_b m \frac{K_1(mr_1)I_1(mr_2) - I_1(mr_1)K_1(mr_2)}{K_0(mr_1)I_1(mr_2) - I_0(mr_1)K_1(mr_2)}$$

The relationship between heat transfer rate and fin efficiency (Incropera and DeWitt), the equation for the fin efficiency for a fin of non-uniform cross sectional area is provided in equation 2-7.

Eq. 2-7

$$\eta_f = \frac{2r_1}{m\left(r_2^2 - r_1^2\right)}\frac{K_1(mr_1)I_1(mr_2) - I_1(mr_1)K_1(mr_2)}{K_0(mr_1)I_1(mr_2) - I_0(mr_1)K_1(mr_2)}$$

The figure below (Figure 2-6) is the fin efficiency for different sized fins expressed as ratios of the outside and inside radii.

Figure 2-6: Efficiency of annular fins of rectangular profile

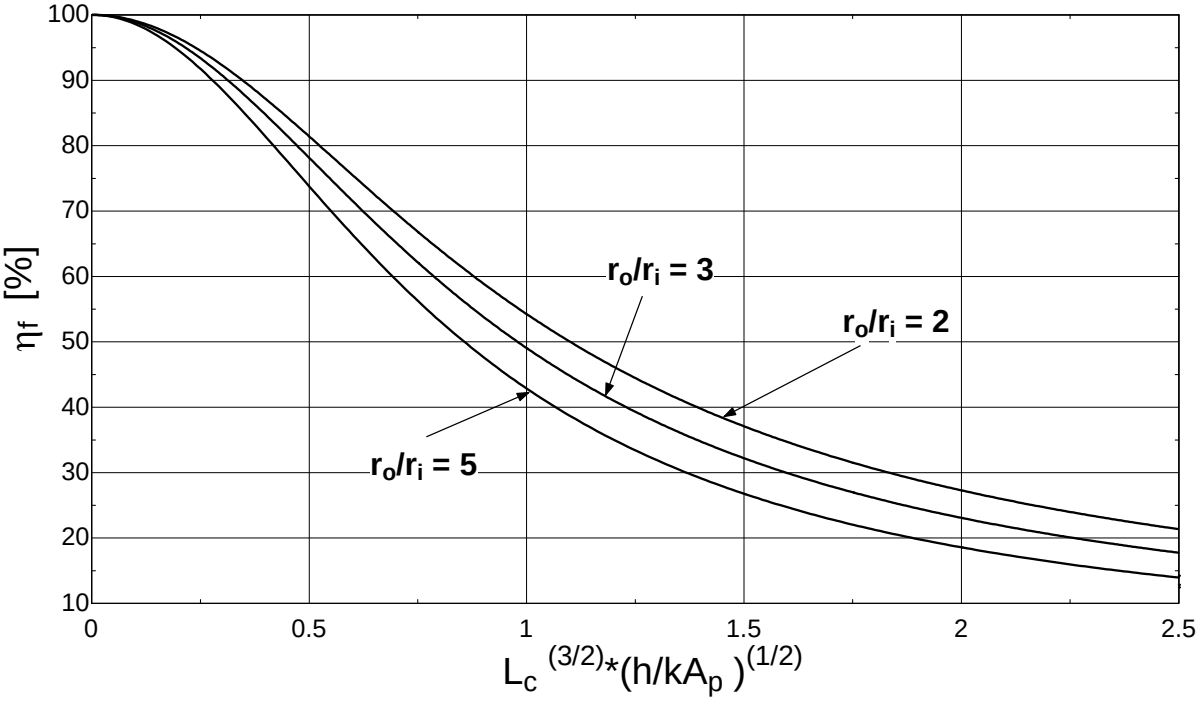

2.3 Finite Difference Solution

A finite difference model of an annular fin is an initial step toward the development of a more complicated model that includes frost. The existence of frost on the fin presents a more complex finite difference model that does not have a readily available analytical solution, as discussed in chapter 3. An advantage of developing a numerical model of the fin itself is that the analytical solution can be used to verify both the numerical model formulation and solutions strategy. As a first step, a verification of the simple case of an annular fin's finite difference solution is provided.

2.3.1 Model Formulation

The finite difference approach is a numerical method that approximates the analytical method. In order to get a model expressed in terms of finite differences, the general form of the fin equation must be modified. A start for this is given by the figure below where a control volume with radial coordinates is shown.

Figure 2-7: Control volume involving radial coordinates

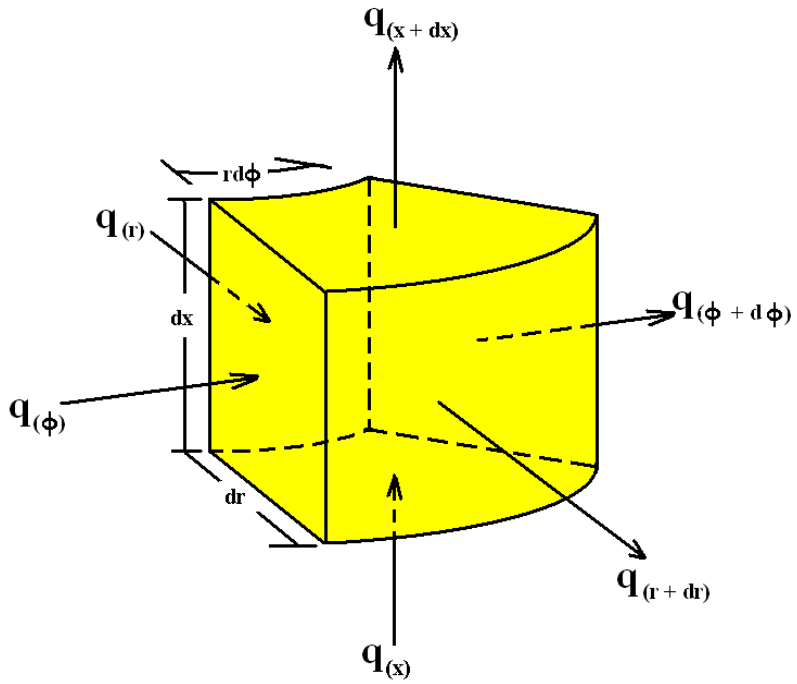

Figure 2-7 shows heat flux components in the axial, radial, and circumferential directions. In the annular fin, the heat flux is assumed to be uniform in the circumferential direction, reducing the problem from three to two dimensions. An energy balance for a general control volume is found in equation 2-8:

Eq. 2-8

$$\dot{E}_{in} + \dot{E}_{g} - \dot{E}_{out} = \dot{E}_{st}$$

Relating this energy balance for a control volume of an annular fin with no circumferential heat flux (Figure 2-8) the energy balance breaks into the equations below.

Figure 2-8: A single node of an annular fin

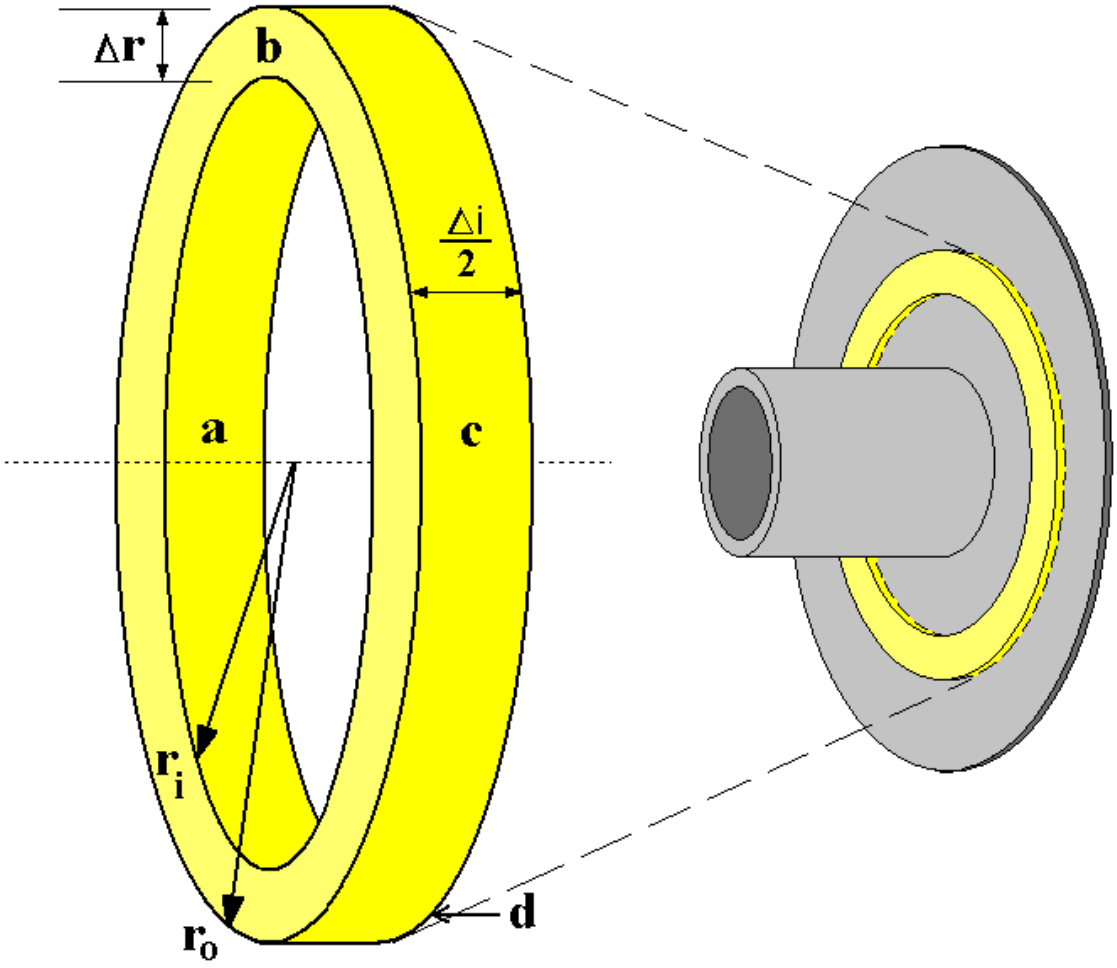

From Figure 2-7 and applying it to Figure 2-8, there are four possible different sides (*a-d*) of the node where energy transfers occur. Taking the geometry of the fin into consideration the right side (*d*) of the node is adiabatic due to symmetry. The top and bottom of the node (*a* and *c*) experience heat transfer by conduction. Finally, the left side of the node (*b*) undergoes a convective interaction with the space surrounding it. From Figure 2-7 to Figure 2-8, some differences are present. The height of the node in the axial direction of Figure 2-7 is labeled as *dx*. This corresponds to the dimension $\Delta i/2$ in Figure 2-8 to agree with the variable names used in the annular fin model. All of the terms in the finite difference equations are written to represent energy into the node, so there is no rate of

energy out ($\dot{E}_{out}$). Assuming there is no energy generated within the node, the term ($\dot{E}_g$) also drops out. The energy stored in a node is expressed as equation 2-9.

Eq. 2-9

$$\dot{E}_{st} = \frac{dU}{dt} = \frac{d(mu)}{dt} = m\frac{du}{dt} = \rho VC\frac{dT}{dt} = mC\frac{dT}{dt} = \dot{q}_{st}$$

Equation 2-8 then becomes $\dot{E}_{in} = \rho VC\frac{dT}{dt}$; where $\dot{E}_{in}$ is the energy into the node by conduction or convection. $\dot{q}_{st}$ is substituted for $\dot{E}_{st}$ when discussing energy transfer by mode of heat. To complete the transformation, the general energy balance takes form of a nodal equation where each side of the node is expressed separately. The energy balance is then equation 2-10.

Eq. 2-10

$$\dot{q}_a + \dot{q}_b + \dot{q}_c + \dot{q}_d = \dot{q}_{st}$$

When energy is of the conduction form in the radial direction, the energy is expressed as equation 2-11, and when it is convective in the radial direction it is shown in the form of equation 2-12.

Eq. 2-11

$$\dot{q}_{cond} = kA\frac{dT}{dr} = \underbrace{k(2\pi\, dx)\frac{(T_{j-1} - T_i)}{\ln[(r_i + \Delta r)/r_i]}}_{boundary\ \ a} \ \ or \ \ \underbrace{k(2\pi\, dx)\frac{(T_{j+1} - T_i)}{\ln[r_i/(r_i - \Delta r)]}}_{boundary\ \ c}$$

Eq. 2-12

$$\dot{q}_{conv} = hAdT = \underbrace{h \cdot 2\pi\, rdx(T_{i-1} - T_i)}_{boundary\ \ b}$$

Finally, equation 2-10 can be expressed as the equation below which is the finite difference formulation.

Eq. 2-13

$$\underbrace{\rho VC\frac{dT}{dt}}_{\dot{E}_{st}} = \underbrace{k(2\pi\,dx)\frac{(T_{j-1}-T_i)}{\ln[(r_i+\Delta r)/r_i]}}_{boundary\ \ a} + \underbrace{h\pi(r_{out}^2-r_{in}^2)(T_{i-1}-T_i)}_{boundary\ \ b} + \underbrace{k(2\pi\,dx)\frac{(T_{j+1}-T_i)}{\ln[r_i/(r_i-\Delta r)]}}_{boundary\ \ c}$$

2.3.2 Boundary Conditions

The boundary conditions for the dry fin are important in generating the appropriate nodal equations to represent the annular fin. Only half of the fin is used due to symmetry therefore, one side of the fin will be adiabatic and experience no heat flux on that surface. Each node in the fin will then be adiabatic on side'*d*'. The fin also is adiabatic on the outermost surface because of its direct contact with a neighboring annular fin (symmetry boundary condition). This means that the furthest node in the radial direction will be adiabatic on its '*c*' face. The energy into the fin comes from the outer radius of the tube. Assuming a very thin tube wall, the temperature of the condensing refrigerant that heats the tube is determined to be the same temperature at the base of the fin. Therefore the node with the smallest radius will have a temperature input of known value (T_b) and a lumped convective coefficient (h_{BASE}). The nodes that are between the inner and outer most nodes will have a conductive heat transfer boundary at faces '*a*' and '*c*'. The annular fin experiences convection off of its face, so every node will then have a convective boundary at boundary '*b*'. By breaking up these boundary conditions, three types of nodes express the entire annular fin. The types of nodes are expressed as nodes '*J*', '*K*', and '*L*'. '*J*' is the outermost node, '*K*' is representative of the nodes in the middle of the fin. Node type '*L*' is the node in which energy is put into the fin. The equations below are shown in their entirety.

Eq. 2-14: Node type 'J'

$$\rho\pi\left(r_{jj,out}^2 - r_{jj,in}^2\right)\frac{\Delta i}{2}\cdot C_F\left(\frac{dT}{dt}\right)_{jj} = k_F\,\frac{2\pi\cdot(\Delta i/2)\left(T_{jj-1}-T_{jj}\right)}{\ln\left[r_{jj}\Big/\left(r_{jj}-\Delta r\right)\right]} + h_C\cdot\pi\left(r_{jj,out}^2 - r_{jj,in}^2\right)\left(T_\infty - T_{jj}\right)$$

Eq. 2-15 Node type 'K' for j = 2, jj-1

$$\rho\pi\left(r_{j,out}^2 - r_{j,in}^2\right)\frac{\Delta i}{2}\cdot C_F\left(\frac{dT}{dt}\right)_{j} = k_F\,\frac{2\pi\cdot(\Delta i/2)\left(T_{j-1}-T_{j}\right)}{\ln\left[r_{j}\Big/\left(r_{j}-\Delta r\right)\right]} + h_C\cdot\pi\left(r_{j,out}^2 - r_{j,in}^2\right)\left(T_\infty - T_{j}\right) + k_F\,\frac{2\pi\cdot(\Delta i/2)\left(T_{j+1}-T_{j}\right)}{\ln\left[\left(r_{j}+\Delta r\right)\Big/r_{j}\right]}$$

Eq. 2-16: Node type 'L'

$$\rho\pi\left(r_{1,out}^2 - r_{1,in}^2\right)\frac{\Delta i}{2}\cdot C_F\left(\frac{dT}{dt}\right)_{1} = h_{BASE}\cdot 2\pi\, r_{1,in}\,\frac{\Delta i}{2}\left(T_{BASE}-T_1\right) + h_C\cdot\pi\left(r_{1,out}^2 - r_{1,in}^2\right)\left(T_\infty - T_1\right) + k_F\,\frac{2\pi\cdot(\Delta i/2)\left(T_2-T_1\right)}{\ln\left[\left(r_1+\Delta r\right)\Big/r_1\right]}$$

The subscript *jj* is the number of nodes that is expressing the annular fin. For example, if *jj* = 10 then type '*J*' node would be node 10, type '*K*' node would be nodes 2 through 9, and type '*L*' node would be 1. Changing the number of nodes only changes how many nodes are represented by type '*K*', since type '*J*' and '*L*' are set at the outer and innermost positions of the annular fin.

2.4 Comparison of the Analytical and Finite Difference Approaches

To further extend the model of the annular fin and introduce more complex boundary conditions, it is essential to first compare the finite difference approach of the simpler dry

annular fin to the analytical solution. Though the analytical solutions are steady state and the finite difference model is transient, comparisons of the two methods were taken when the finite difference model reached steady state.

Figure 2-9: Temperature distribution comparing the analytical solution and finite difference approach

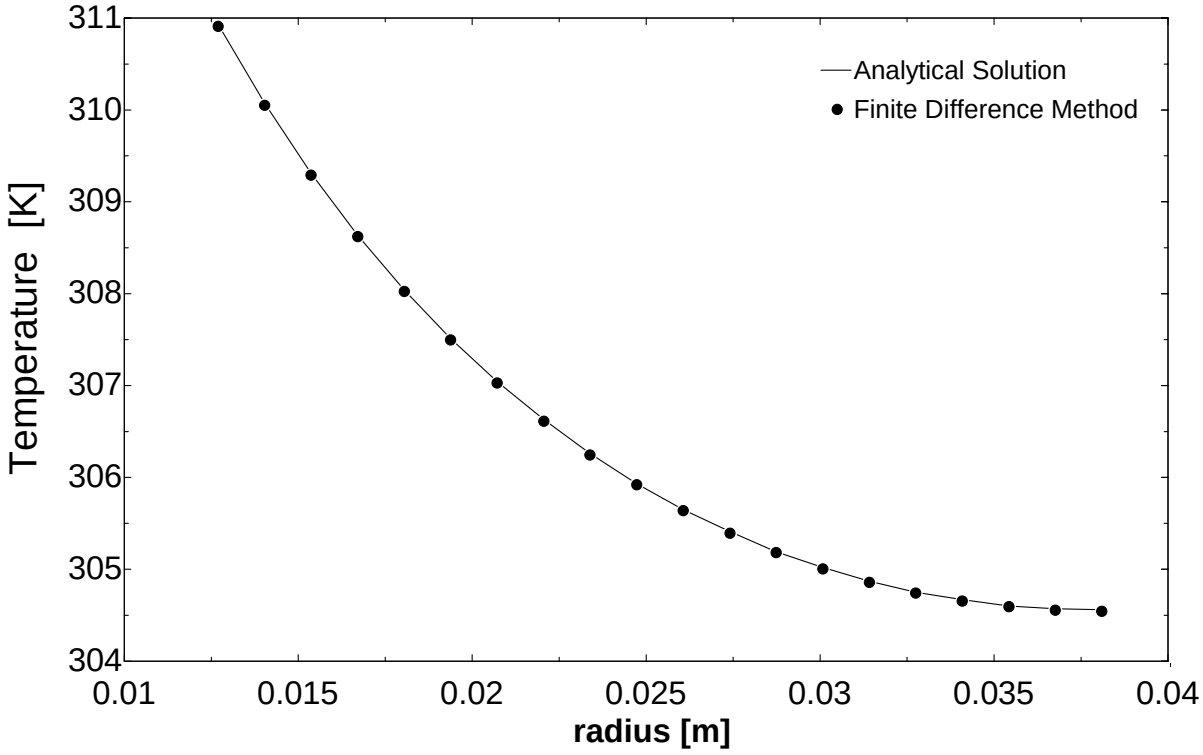

Above in Figure 2-9 is the analytical solution of the temperature distribution with the finite difference method. The conditions are the same as they were in Figure 2-5. Below is a plot of the number of nodes used in the finite difference formulation.

Figure 2-10: Temperature distribution of analytical solution compared to various finite difference mesh sizes

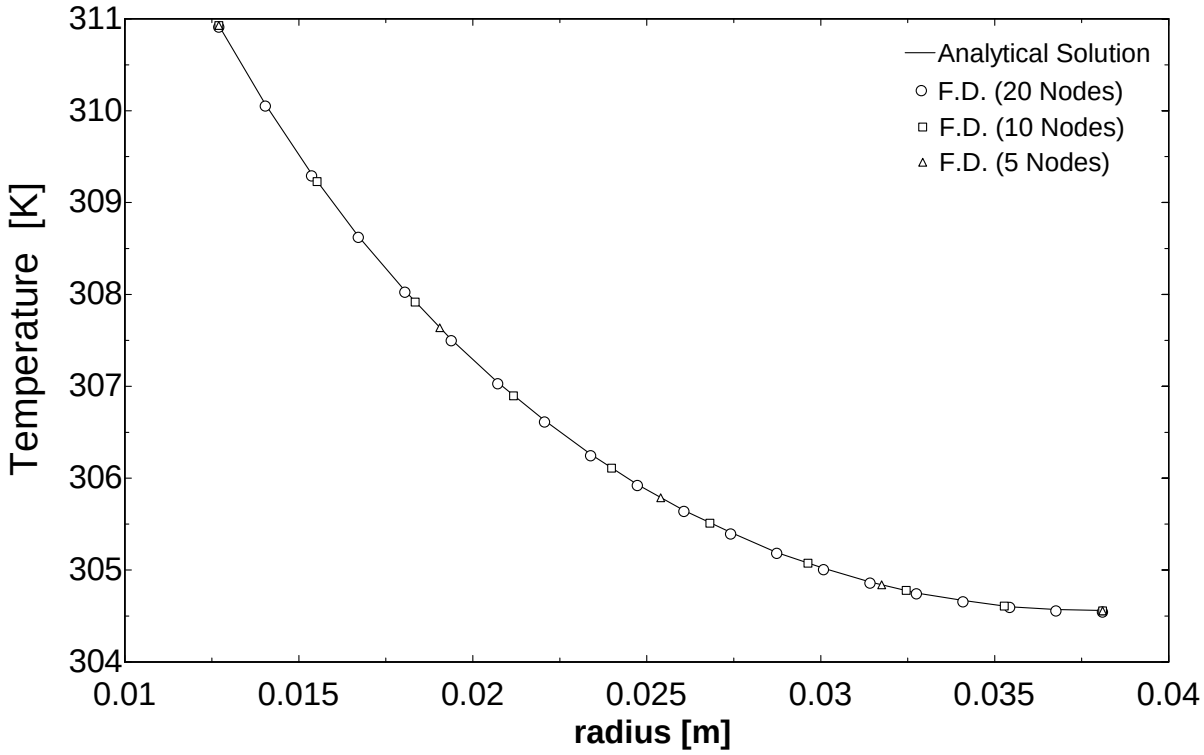

As for the fin efficiency, several simulations of the dry fin were taken at different ratios of radii. Since the fin efficiency is dependent on the geometry, the efficiency for each run was the same as it was for the analytical solution. The number of nodes used in the simulations does not make a difference because the inner and outer radii are set in the model. In the figure below, several runs were taken at different radii ratios as well as for different length radii.

Figure 2-11

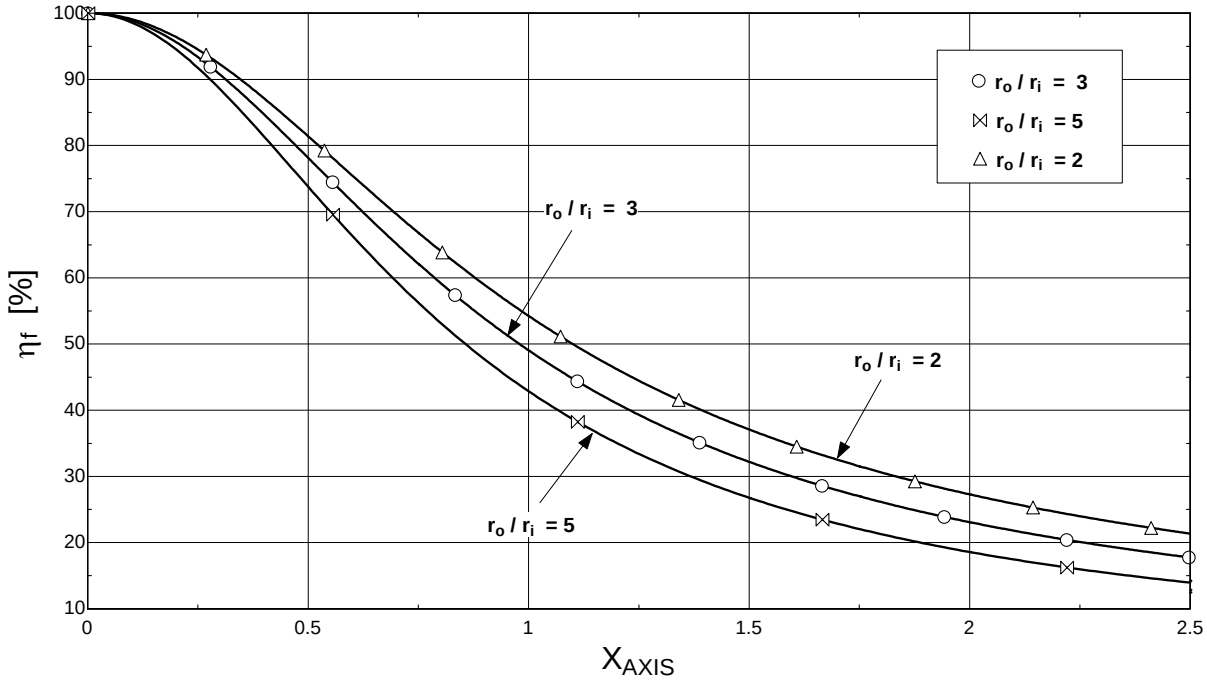

Comparison of the analytical solution to the finite difference approach gives confidence that the finite difference approach taken is a good representation of the analytical solution. This model is expanded in Chapter 3 to include the contribution of ice on the fin.

2.5 References

Incropera, F. P., and D. P. DeWitt. *Introduction to Heat Transfer 4th Ed*. John Wiley & Sons, 2002.

Chapter 3 Frosted Fin Model

The goal of this chapter is to establish a methodology that allows the prediction of the defrost process for an air-cooling evaporator. The methodology uses symmetry to reduce an entire evaporator to a typical evaporator fin with frost on the external finned surface. The model must have the capability of simulating the processes involved during the defrost sequence of an evaporator using hot gas. The energy for defrosting originates from warm refrigerant vapor condensing inside the evaporator tubes. The heat given up by the condensing vapor refrigerant warms the base of the fin attached to the tubes and maintains, essentially, a constant temperature boundary condition at the fin base assuming that the process occurs at constant pressure.

3.1 Layout of Model

The geometry of a typical air-cooling evaporator is presented and simplifying assumptions are used to reduce the entire evaporator down to a single finned surface. Boundary conditions are presented and qualitative expectations of the defrost process discussed.

3.1.1 Geometry

The model should accommodate varying amounts of initial thickness of frost on the fin ranging from allowable operational blockage of frost on the fin to no frost accumulation on the fin. The dry fin model is discussed in chapter 2. The model must also be able to accommodate the different geometries of commercial evaporators.

Figure 3-1: The geometry of a single tube/fin assembly used for model representation

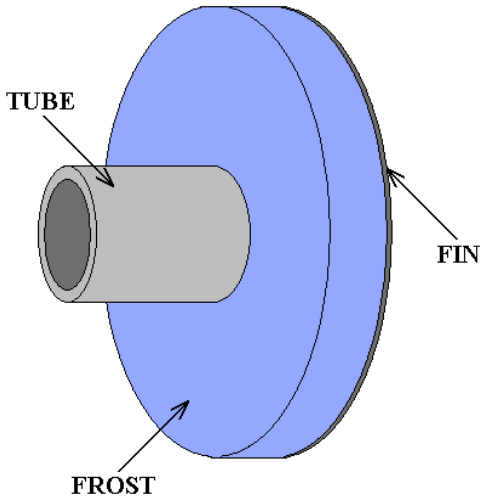

3.1.2 Boundary Conditions

The boundary conditions used in the model need to both reflect the simplifying geometric assumptions (i.e. symmetry) and attempt to replicate conditions that real evaporators experience. The centerline of the annular fin is adiabatic by symmetry considerations, as it was in the dry fin model.

With the added layer of frost on the surface of the annular fin, boundary conditions in the existing model are not the same as the dry fin model, though some conditions do remain unchanged. The energy imparted into the frosted fin model does not change because the fin itself does not change. The energy continues from the base of the fin from the refrigerant. Tube wall thermal resistance is assumed to be negligible. The changes in the boundary conditions occur between the fin and frost, and also between the frost and surrounding space. Instead of the fin convecting energy out to the surroundings, it conducts energy to the frost attached to its surface. The surface of the frost will convect energy to the space as well as release energy due to evaporation as it warms. The frost not only convects from the axial surface, but also from its inside radial surface. The convection from the inside radial surface must be considered because the frost that is bonded to the tube melts very quickly due to the high refrigerant temperature, causing a gap between the frost and tube. Like the dry fin in

the previous chapter, the outermost radius is adiabatic because of the symmetrical conditions. It also applies to the frost at the outside radius for the same purposes.

3.1.3 Frost Melting Assumptions

Just before initiating the hot gas defrost process, the frost adhered to the finned surface is entirely in a solid state. As hot gas is supplied to the coil, the fin base temperature rises causing the frost near the base of the finned surface to warm and melt. The frost at the top of the fin will remain in place until sufficient energy moves up the fin to melt it. The frost that melts will naturally drain by gravity causing a discontinuity in the computational domain. That is: the nodes that reach a liquid state will then be removed and will no longer aid in the energy transport from the base of the fin to the nodes that have not reached the melting point and the finite difference method will be invalid.

To account for this, the model developed assumes that all frost melted remains in-place in a liquid phase within the computational domain until the farthest frost point is melted after which all liquid is assumed to drain from the computational domain. The model assumes that the density of the frost does not change when the frost turns into water although the densities differ by 11%; however, the thermal conductivities change to account for the phase change. The thermal conductivity of the frost changes to the thermal conductivity of air once the node is melted because the melted frost will normally drain, leaving an air gap in the computational domain. Additional discussion and justification of this assumption is provided in section 3.3 below.

As previously stated, the densities of the nodes do not change during the phase change. Though this would not be true because of the water draining, it is reasonable to do so. Given the computational domain in Figure 3-4, the frost that melts first will be the frost closest to the fin. When these nodes are water, they stay in the domain rather than drain. If the nodes disappeared, the remaining nodes surrounding the melted nodes would experience convection on their energy boundaries. That convection that the nodes would experience, given the low conductivity of air, would be approximate to the water nodes conducting energy to the remaining nodes. Therefore the change in thermal conductivity from frost to air while density remains constant is a plausible estimate.

3.2 Two Dimensional Heat Transfer

Looking back at Chapter 2, the finite difference formulation was based on the energy balance equation. Solving for the fin in the previous chapter, this chapter will focus on acquiring the energy balances for the frost nodes. Equation 3-1 is the energy rate balance equation.

Eq. 3-1

$$\dot{q}_{in} + \dot{q}_{g} - \dot{q}_{out} = \dot{q}_{st}$$

The energy earlier expressed by (E) is replaced by (q) because the energy transfer is in the form of heat. Looking at Figure 2-7 and Figure 2-8 there is again energy that enters and leaves in both the radial and axial directions. Using the strategy of writing finite difference equations, all energy is directed into the node. There is also no internal energy generated by the node. The energy into the node can be broken up to energy that crosses each energy boundary surface, thus the energy equation looks like equation 2-10.

The mode of thermal energy exchange into or out of a control volume can be by conduction, convection, and evaporation. Energy transfer by conduction and convection are displayed in equations 2-11 and 2-12 and are further discussed in the sections following. Energy transfer from evaporation is described by the equation below.

Eq. 3-2

$$\dot{q}_{evap} = \bar{g}_m A\left(m_{H_2O,s} - m_{H_2O,e}\right)\cdot h_{ig} = \underbrace{\bar{g}_m \pi\left(r_{out}^2 - r_{in}^2\right)\left(m_{H_2O,s} - m_{H_2O,e}\right)\cdot h_{ig}}_{boundary\ \ b}$$

The stored energy in the fin is expressed as the change in temperature of the control volume. However, when a control volume for the frost experiences a phase change, like from ice to water, the stored energy within the control volume (or the rate of stored energy) cannot be calculated by using temperature. The temperature of the mass does not change through the phase transition, although its specific internal energy does. In this case, the

energy stored in the control volume can be expressed in terms of enthalpy, pressure and specific volume using the relationship in equation 3-3.

Eq. 3-3

$$u = h - pv \quad \rightarrow \quad \frac{du}{dt} = \frac{dh}{dt} - \left(p\frac{dv}{dt} + v\frac{dp}{dt} \right)$$

If the phase change is melting ice in ambient conditions, pressure does not change with time. The density of water is approximately 11% higher than that of ice, so an assumption is made that the specific volume (the inverse of density) of the control volume does not change. Both terms involving the pressure and specific volume then drop out of the equation resulting in equation 3-4.

Eq. 3-4

$$\frac{du}{dt} = \frac{dh}{dt}$$

Looking back to equation 2-9 and the relationship in equation 3-4, another way to express energy stored is found.

Eq. 3-5

$$\dot{q}_{st} = m\frac{du}{dt} = m\frac{dh}{dt}$$

3.3 Transient Conduction

Conduction plays a role in the energy balances for each node in the fin. It also plays a role in the frost that is attached to the fin. This section describes the transient nature of the thermal conductivity of the frost which is driven by temperature change.

Initially, the frost attached to the fin is solid. An equation that relates the thermal conductivity of the frost with respect to the density is found in Tao et al. (1993) shown

below, followed by a plot for the range of frost densities used in the model. The operating conditions used in correlating the frost densities to the thermal conductivities ranged from temperatures between -25˚C to -5˚C, relative humidity between 0.3 and 0.9, and a Reynolds number in the range of 2840 and 5680.

Eq. 3-6

$$k = 0.02422 \; + \; 7.214\times10^{-4}\cdot\rho_f \; + \; 1.01797\times10^{-6}\cdot\rho_f^2$$

Figure 3-2: Frost density vs. conductivity using equation 3.6 from Tao et. al. (1993)

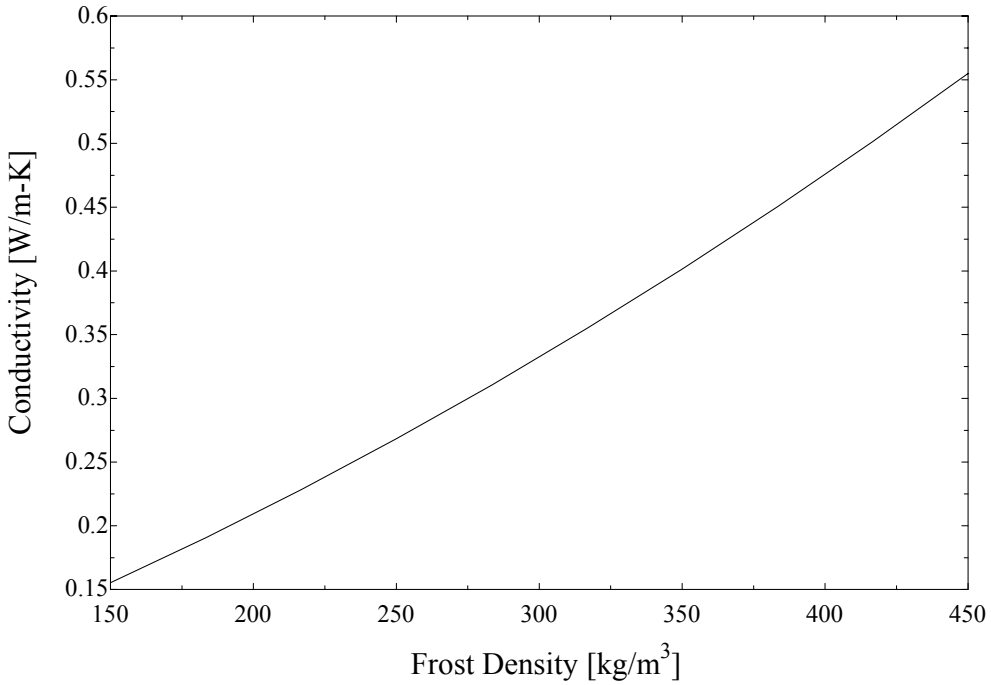

After the node melts, the model switches the thermal conductivity of the node to the thermal conductivity of air using the temperature of the node. The thermal conductivity of air is determined by the function used in EES (Engineering Equation Solver). Thermal conductivity changes to that of air is because the melted frost would likely drain leaving an air pocket between the frost and the fin. Since the frost nodes that have been melted stay in place during the simulation to avoid energy imbalances, the switch from frost to air thermal

conductivity help by having the melted nodes conduct as air nodes for the rest of the simulated run.

The justification for keeping the density of the node constant and changing the thermal conductivity is as follows: When the frost in a node melts, the water will drain, resulting in the infiltration of air into the vacant space created by the drained water. In a realistic situation, the temperature of that nodal space will stay relatively constant because it has a nearly infinite heat sink from the huge amount of air in the freezer space continuously removing the air in the nodal space by new air. This effect is captured by not changing the density of the node to air, to retain a larger effective nodal mass. Having a larger mass for the node makes it possible for the sum of its superficially large amount of mass times the specific heat of the air to result in a relatively constant temperature, which would be expected due to the continuous infiltration of new freezer air.

Since the model is transient, nodes in different areas are at different temperatures, so the thermal conductivities must be averaged between the two neighboring conducting nodes in order to satisfy the energy balance.

3.4 Natural Convective Heat and Mass Transfer

3.4.1 Nusselt Correlation for Natural Convection

When defrosting, the fans are turned off while the hot refrigerant circulates through the tubes in the evaporator. This situation causes the air in the surrounding freezer space to be stagnant while defrost is in progress. To model this phenomenon, it was important to find an appropriate natural convection correlation with respect to the geometry of the evaporator as well as the temperature of frost on the fins in the evaporator. A correlation for Nusselt number was found in Jaluria (1980). The correlation was taken for a flat vertical plate undergoing natural convection. The correlation is as follows:

Eq. 3-7: Nusselt correlation for vertical plate with natural convection

$$\overline{Nu}_L = 0.13(Ra)^{1/3} \qquad for \qquad 10^9 < Ra < 10^{13}$$

The Rayleigh number appearing in equation 3-7 is the product of the Grashof and Prandtl numbers, as defined in equations 3-8 and 3-9.

Eq. 3-8

$$Gr_L = \frac{\left(\Delta\rho / \rho_M\right) \cdot g \cdot L_{EVAP}^3}{\nu^2}$$

Eq. 3-9

$$\Pr = \frac{\nu}{\alpha}$$

In the above equations, the $\Delta\rho$ and ρ_M are the difference in densities and average densities of moist air in the freezer surroundings and at the face of the convecting nodes. g is the gravitational constant and the length of the fin is cubed (L_{FIN}^3). The variable 'ν' is the dynamic viscosity of the air. The alpha (α) in the Prandtl number equation is the thermal diffusivity of the freezer air. The evaporator fin length is set at 5 feet, since the behavior of the natural convection is estimated for an entire evaporator fin to obtain an accurate Rayleigh number.

The densities of the air in the freezer space and at the convecting node surfaces are determined using the mass fractions of water in the air at each position, ρ_e, and ρ_s, respectively. The mass fractions are determined by solving for the density of dry air and the density of water vapor in the air. The equations of state are used to calculate the densities of the air and water in the air *in the surrounding freezer* by the equations below. The density of humid air in the freezer (ρ_e) is the sum of the densities of water in the air ($\rho_{H_2O,e}$) and the dry air ($\rho_{AIR,e}$) in the freezer. The density of the water vapor in the air ($\rho_{H_2O,e}$) is solved by using the saturated pressure at the freezer temperature times its relative humidity. The pressure used for calculating the density of the dry air ($\rho_{AIR,e}$) is the atmospheric pressure minus the pressure used for the water vapor equation of state.

Eq. 3-10

$$\rho_e = \rho_{H_2O,e} + \rho_{AIR,e}$$

Eq. 3-11

$$\rho_{H_2O,e} = \frac{P_{H_2O,e} \cdot MW_{H_2O}}{R \cdot T_\infty} \quad , \quad P_{H_2O,e} = RH \cdot P_{SAT,\infty}$$

Eq. 3-12

$$\rho_{AIR,e} = \frac{P_{AIR,e} \cdot MW_{AIR}}{R \cdot T_\infty} \quad ; \quad P_{AIR,e} = P_{ATM} - P_{H_2O,e}$$

The densities for the dry air ($\rho_{H_2O,s}$) and the water vapor ($\rho_{AIR,s}$) at the faces of the *convecting nodes* are found in the same manner. The pressure used for solving the density of the water vapor at the node face is the saturation pressure at the nodes temperature. The pressure for the dry air at the node face is then the atmospheric pressure minus the saturated pressure. The total density is then the sum of the two densities found ($\rho_s = \rho_{H_2O,s} + \rho_{AIR,s}$).

The kinematic viscosity in the Prandtl and Rayleigh equation is solved for by using the viscosity (μ) divided by the average density of air (ρ_M). The thermal diffusivity is calculated by using the thermal conductivity of the air (k_{AIR}) divided by the product of the average density and specific heat of the air (C_{AIR}). The properties of the air are calculated using the average temperature of the freezer air and the temperature at the node surface.

The above equations are all used to solve for the Nusselt number. In turn, the Nusselt number determines the convective heat transfer coefficient with the following equation:

Eq. 3-13

$$\bar{h}_C = \frac{k_{AIR}}{L_{FIN}} \cdot \overline{Nu}_L$$

The heat transfer coefficient is continuously changing during a simulation because of the changing temperature differences between the node surface and the surrounding freezer space.

3.4.2 Evaporation due to Vapor Pressure's

Mass transfer of water into air (evaporation) is due to the difference in vapor pressures at each location as described by Mills (1995). The driving force for water evaporating into air is the difference in partial pressures of water vapor at the surface of the frost and at a location in the freezer far from the evaporator. Although there is a driving force, at low temperatures it is relatively small. The mass fractions of water in the air at the respective locations are ratios of the densities of the water vapor in the air at each location divided by the total density of the humid air in each location. The densities are found by using partial pressures related to the saturated pressure at each location. The equations below aid in the explanation.

Eq. 3-14

$$\Delta m = m_{H_2O,e} - m_{H_2O,s}$$

The driving force for mass transfer is the same as it is for the convective heat transfer, but explained in more detail with mass fractions. The difference in mass fractions of water in the air at the surface of the liquid and in the surrounding air drives the water to leave the surface and escape into the surrounding air. The mass fractions are simply the ratios of the water vapor density in the air divided by the total density of air.

Eq. 3-15(a) & (b)

$$m_{H_2O,e} = \frac{\rho_{1H_2O,e}}{\rho_e} \qquad\qquad m_{H_2O,s} = \frac{\rho_{H_2O,s}}{\rho_s}$$

The densities are determined by summing the densities of the dry air and the water vapor in the air. The ideal gas equation of state is used to find the respective densities.

Eq. 3-16

$$\rho_e = \rho_{H_2O,e} + \rho_{AIR,e} \quad ; \quad \rho_{H_2O,e} = \frac{P_{H_2O,e} \cdot MW_{H_2O}}{R \cdot T_\infty} \quad , \quad \rho_{AIR,e} = \frac{P_{AIR,e} \cdot MW_{AIR}}{R \cdot T_\infty}$$

The pressure used in the equations of state for the water vapor in the surrounding air is the saturated vapor pressure of the air times the relative humidity of the air. The pressure used in the dry air calculation is the atmospheric pressure minus the pressure used for the water vapor calculation. The equations of state use the temperature of the air in the surrounding space.

Eq. 3-17

$$P_{H_2O,e} = RH \cdot P_{SAT,\infty} \quad , \quad P_{AIR,e} = P_{ATM} - P_{H_2O,e}$$

The equations of state for the water vapor and dry air at the liquid interface use the saturated pressure of air and atmospheric pressure less the saturated, respectively. The temperature in the equations of state is the temperature of the liquid at the surface.

Eq. 3-18

$$\rho_s = \rho_{H_2O,s} + \rho_{AIR,s} \quad ; \quad \rho_{H_2O,s} = \frac{P_{H_2O,s} \cdot MW_{H_2O}}{R \cdot T_S} \quad , \quad \rho_{AIR,s} = \frac{P_{AIR,s} \cdot MW_{AIR}}{R \cdot T_S}$$

Eq. 3-19

$$P_{H_2O,s} = P_{SAT,S} \quad , \quad P_{AIR,s} = P_{ATM} - P_{H_2O,s}$$

3.4.3 Sherwood Correlation

The process of convective mass transfer is analogous to convective heat transfer. The difference between the correlations of mass and heat transfer is to replace the Prandtl number by the Schmidt number (*Sc*). This replacement is then expressed as the Sherwood number instead of the Nusselt number. The equation below is the mass transfer correlation for a vertical plate under natural convection, turbulent in nature. The following correlation can be found in Jaluria (1980).

Eq. 3-20: Sherwood correlation for vertical plate undergoing natural convection

$$\overline{Sh}_L = 0.13(GrSc)^{1/3} \qquad for \quad 10^9 < GrSc < 10^{13}$$

The Schmidt number (Sc) is expressed much like the Prandtl number. The difference between the Prandtl number and the Schmidt number is the thermal diffusivity is replaced by the mass diffusivity, or D_{12}.

Eq. 3-21

$$Sc = \frac{\nu}{D_{12}}$$

3.4.4 Lewis Number

The Lewis number is a dimensionless group that correlates mass transfer to heat transfer. It is the ratio of the Schmidt number over the Prandtl number.

Eq. 3-22

$$Le = \frac{Sc}{\mathrm{Pr}}$$

As stated in A.F. Mills (1995), The Lewis number for water vapor-air mixtures is somewhat greater than unity (Le taken to be Pr/Sc). The Lewis number for air – water vapor systems can therefore be approximated ≈ 0.95, using the inverse relation from equation 3-22.

3.4.5 Binary Diffusion Coefficient

The binary diffusion coefficient (D_{12}), or mass diffusivity is analogous to thermal diffusivity. The Schmidt number uses the mass diffusivity while the Prandtl number uses the thermal diffusivity coefficient. They are tied together using the Lewis number. Fick's First Law of Diffusion uses the mass diffusivity and the mass fraction of the species to find the diffusive mass flux, given in equation 3-23.

Eq. 3-23

$$J_1 = -\rho D_{12} \frac{dm_1}{dz}$$

The diffusive mass flux (J_1) is dependent on the local mixture solution density (ρ) and the change in mass fractions of species '1' with respect to position. Fick's First Law is to mass transfer as Fourier's Law is to heat transfer.

3.4.6 Mass Transfer Coefficient

The mass transfer coefficient can be found from the Sherwood correlation just as the heat transfer coefficient can be found by the Nusselt correlation. When the Prandtl number is solved, and using the assumed Lewis number, the Schmidt number is also found. The binary mass diffusion coefficient (D_{12}) is obtained from the Schmidt number.

Eq. 3-24

$$\overline{g}_m = \frac{\rho_M \cdot D_{12}}{L_{FIN}} \cdot \overline{Sh}_L = \frac{\rho_M \cdot \nu}{Sc \cdot L_{FIN}} \cdot \overline{Sh}_L$$

Like the heat transfer coefficient, the mass transfer coefficient is relies on the temperature-dependent properties. Since the temperatures in the simulation change throughout a run, the properties change, hence the mass transfer coefficient changes. The changing mass transfer coefficient makes the conditions in the model more like the conditions an actual evaporator would experience.

3.5 Finite Difference Approach

The frosted fin model builds on the dry annular fin model. New concepts are introduced to the model that includes a two dimensional nodal system and mass transfer by evaporation. However like the first model, the frosted fin model still incorporates convection and conduction that is temperature dependant, as explained in the previous section.

3.5.1 Finite Difference Formulation

The governing differential equations are discretized using a finite difference approach. In all, the finite difference model consists of 12 different types of nodal energy balances (A-L) as indicated in Figure 3-4. Each type of nodal balance represents a general node that has, potentially, different boundary conditions. The three types of fin nodes were explained in Chapter 2; however, the boundary conditions on the side exposed to frost are different.

Given the figure below (Figure 3-3) four nodes from the frosted fin model are shown up close. The nodes are labeled '*D*', '*E*', '*F*', and '*K*', this will become clearer later on. The node on the left side is a frost node that convects to the freezer on its left side, conduction occurs between itself and the frost node to the right of it, and there is conduction from the inside and outside radii from the neighboring nodes above and below it (not shown). The second node to the right is a frost node with conduction from all four of its energy boundaries. The third node is a frost node that has energy conducted from three of its energy boundaries and conduction from a fin node on its right boundary. The last node is a fin node type '*K*' that was discussed earlier in Chapter 2; only the left boundary is now conducting with the frost node instead of convecting to the surroundings.

The energy balances for the nodes in Figure 3-3 are worked out below, starting with node type '*D*' and working through to type '*K*'. All equations follow from the simple energy balance shown previously in equation 2-10.

Eq. 3-25: Node type 'D'

$$\underbrace{\rho V\left(\frac{dh}{dt}\right)_{1,j}}_{\dot{E}_{st}} = \underbrace{\left(\frac{k_{1,j-1}+k_{1,j}}{2}\right)\cdot 2\pi\frac{\Delta x}{2}\cdot\frac{\left(T_{1,j-1}-T_{1,j}\right)}{\ln\left[\left(r_i+\Delta r\right)/r_i\right]}}_{boundary\ \ a}$$

$$+\ \underbrace{h_C\pi\left(r_{j,out}^2-r_{j,in}^2\right)\left(T_\infty-T_{1,j}\right)+\overline{g}_{m,D}\cdot\pi\left(r_{j,out}^2-r_{j,in}^2\right)\cdot\left(m_{H_2O,s}-m_{H_2O,e}\right)\cdot h_{ig}}_{boundary\ \ b}$$

$$+\ \underbrace{\left(\frac{k_{1,j+1}+k_{1,j}}{2}\right)\cdot 2\pi\frac{\Delta x}{2}\cdot\frac{\left(T_{1,j+1}-T_{1,j}\right)}{\ln\left[\left(r_i+\Delta r\right)/r_i\right]}}_{boundary\ \ c} + \underbrace{\left(\frac{k_{2,j}+k_{1,j}}{2}\right)\frac{\pi\left(r_{j,out}^2-r_{j,in}^2\right)\left(T_{2,j}-T_{1,j}\right)}{\Delta x}}_{boundary\ \ d}$$

Eq. 3-26: Node type 'E'

$$\underbrace{\rho V\left(\frac{dh}{dt}\right)_{i,j}}_{\dot{E}_{st}} = \underbrace{\left(\frac{k_{i,j-1}+k_{i,j}}{2}\right)\cdot 2\pi\frac{\Delta x}{2}\cdot\frac{\left(T_{i,j-1}-T_{i,j}\right)}{\ln\left[\left(r_i+\Delta r\right)/r_i\right]}}_{boundary\ \ a} + \underbrace{\left(\frac{k_{i-1,j}+k_{i,j}}{2}\right)\frac{\pi\left(r_{j,out}^2-r_{j,in}^2\right)\left(T_{i-1,j}-T_{i,j}\right)}{\Delta x}}_{boundary\ \ b}$$

$$+\ \underbrace{\left(\frac{k_{i,j+1}+k_{i,j}}{2}\right)\cdot 2\pi\frac{\Delta x}{2}\cdot\frac{\left(T_{i,j+1}-T_{i,j}\right)}{\ln\left[\left(r_i+\Delta r\right)/r_i\right]}}_{boundary\ \ c} + \underbrace{\left(\frac{k_{i+1,j}+k_{i,j}}{2}\right)\frac{\pi\left(r_{j,out}^2-r_{j,in}^2\right)\left(T_{i+1,j}-T_{i,j}\right)}{\Delta x}}_{boundary\ \ d}$$

Eq. 3-27: Node type 'F'

$$\underbrace{\rho V\left(\frac{dh}{dt}\right)_{ii-1,j}}_{\dot{E}_{st}} = \underbrace{\left(\frac{k_{ii-1,j-1}+k_{ii-1,j}}{2}\right)\cdot 2\pi\frac{\Delta x}{2}\cdot\frac{\left(T_{ii-1,j-1}-T_{ii-1,j}\right)}{\ln\left[\left(r_i+\Delta r\right)/r_i\right]}}_{boundary\ \ a}$$
$$+\underbrace{\left(\frac{k_{ii-2,j}+k_{ii-1,j}}{2}\right)\frac{\pi\left(r_{j,out}^2-r_{j,in}^2\right)\left(T_{ii-2,j}-T_{ii-1,j}\right)}{\Delta x}}_{boundary\ \ b}$$
$$+\underbrace{\left(\frac{k_{ii-1,j+1}+k_{ii-1,j}}{2}\right)\cdot 2\pi\frac{\Delta x}{2}\cdot\frac{\left(T_{ii-1,j+1}-T_{ii-1,j}\right)}{\ln\left[\left(r_i+\Delta r\right)/r_i\right]}}_{boundary\ \ c}$$
$$+\underbrace{2k_{ii-1,j}\frac{\pi\left(r_{j,out}^2-r_{j,in}^2\right)\left(T_{ii,j}-T_{ii-1,j}\right)}{\Delta x}+2k_F\frac{\pi\left(r_{j,out}^2-r_{j,in}^2\right)\left(T_{ii,j}-T_{ii-1,j}\right)}{\Delta i}}_{boundary\ \ d}$$

Eq. 3-28: Node type 'K'

$$\underbrace{\rho VC\left(\frac{dT}{dt}\right)_{ii,j}}_{\dot{E}_{st}} = \underbrace{k_F\cdot 2\pi\frac{\Delta i}{2}\cdot\frac{\left(T_{ii,j-1}-T_{ii,j}\right)}{\ln\left[r_i/\left(r_i-\Delta r\right)\right]}}_{boundary\ \ a}$$
$$+\underbrace{2k_{ii-1,j}\frac{\pi\left(r_{j,out}^2-r_{j,in}^2\right)\left(T_{ii-1,j}-T_{ii,j}\right)}{\Delta x}+2k_F\frac{\pi\left(r_{j,out}^2-r_{j,in}^2\right)\left(T_{ii-1,j}-T_{ii-1,j}\right)}{\Delta i}}_{boundary\ \ b}$$
$$+\underbrace{k_F\cdot 2\pi\frac{\Delta i}{2}\cdot\frac{\left(T_{ii,j+1}-T_{ii,j}\right)}{\ln\left[\left(r_i+\Delta r\right)/r_i\right]}}_{boundary\ \ c}$$

As in the earlier case for the nomenclature '*jj*', the '*ii*' is the number of nodes that are selected for the '*x*' or axial direction. If '*ii*=10', then the '*E*' type node would represent the axial nodes 2 through 8. The types '*D*', '*F*', and '*K*' would remain the same and only depend on what '*jj*' was selected. Further examination of the mesh is explained in a following section.

Figure 3-3: Nodes taken from the frosted fin model

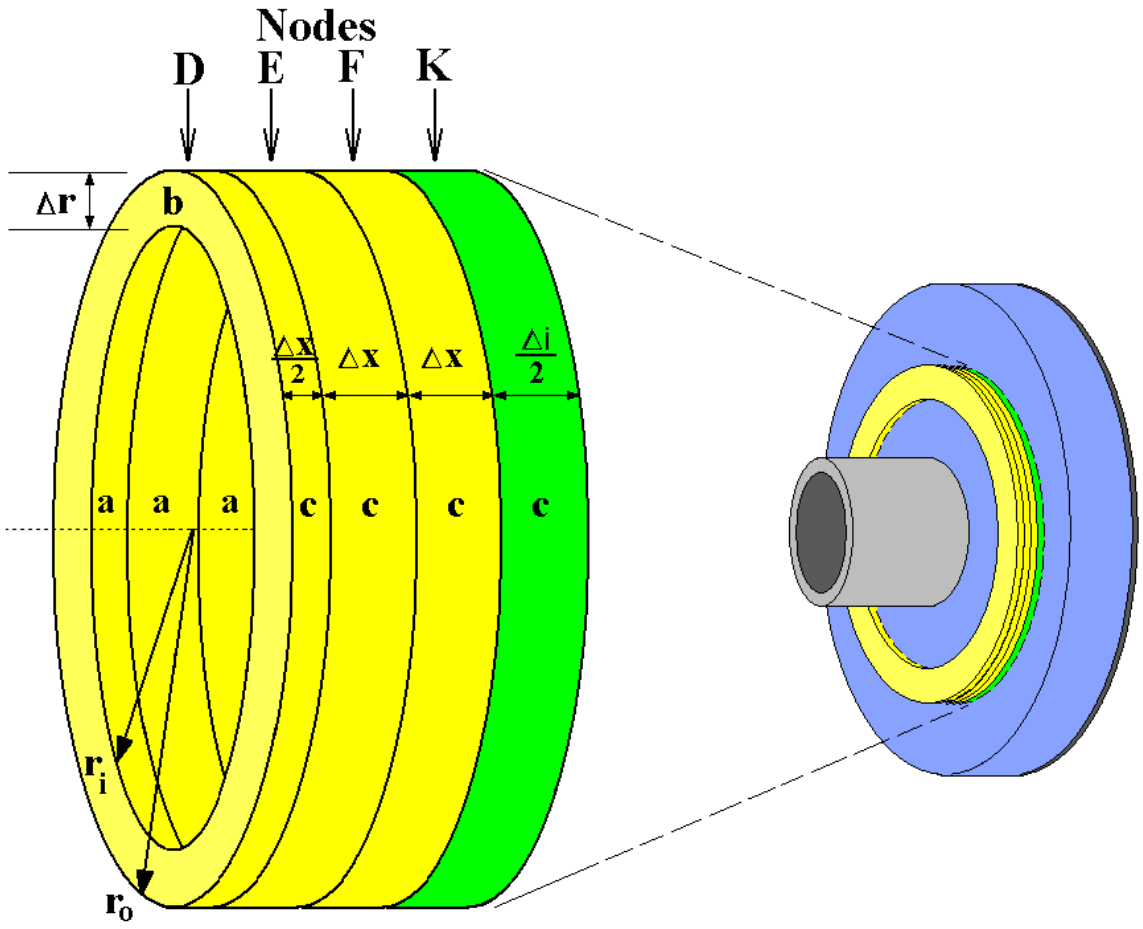

Figure 3-4 is a cross section of the frosted fin that shows the boundary conditions for each node. There are 12 different types of nodal energy balances, labeled A-L. The nodes are represented by the dots and the energy balances for each node are given by the dashed lines that bound the dots.

Figure 3-4: Computational domain for the defrost numerical model (not to scale).

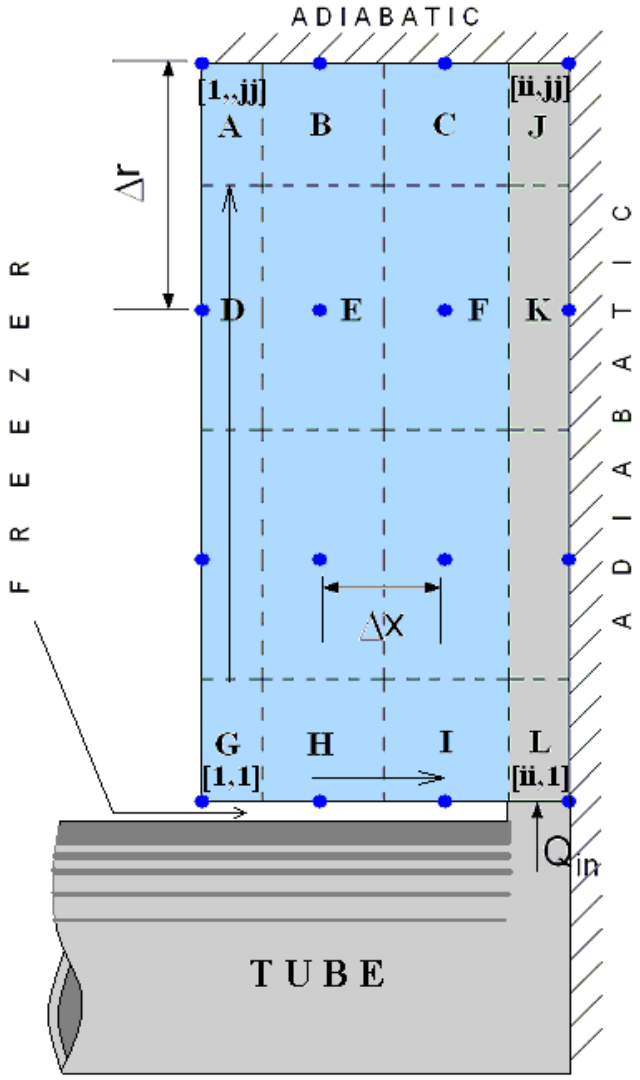

3.5.2 Mesh Size (mesh refinement)

The model allows both the fin spacing and the fin thickness to be specified. The number of nodes in the model can be varied both in the vertical and horizontal directions. The layout of the nodes in the model are [1, 1] at the bottom left corner of the model (node '*G*'). The nodes increase in magnitude in the vertical direction to [1, *jj*] at node '*A*'. The nodes

increase in the horizontal direction to [*ii*, 1] at node '*L*'. The upper right hand corner of the model (node '*J*') is the highest number node for the system. For example, if a 10 x 20 matrix is desired, the '*J*' type node would be [10, 20]. The spacing of the nodes in the model (Eq. 3-29 (a) and (b)) is determined by the number of nodes so the entire model can be set to a specific size without independent of the mesh size.

Eq. 3-29 (a) & (b)

$$\Delta x = \frac{Length}{ii - 3/2} \qquad (a)$$

$$\Delta r = \frac{r_{out} - r_{in}}{jj - 1} \qquad (b)$$

The total number of nodes in the vertical and horizontal direction is represented by '*jj*' and '*ii*' respectively. The spacing between the nodes in the horizontal direction of the ice is represented by Δx, and in the fin corresponds to Δi. The spacing between the nodes in the vertical direction for both the ice and fin are represented by Δr. *Length* is the pre-determined span of frost and fin set for the entire model.

3.6 Transient Behavior

The frosted fin model is a transient model that simulates a defrosting period for an evaporator. The transient program was written in the software package Engineering Equation Solver (EES, 2003). The EES software has multiple thermodynamic properties for an even greater multitude of materials and fluids. It also incorporates many mathematical functions. The frosted fin model takes advantage of these programming abilities by utilizing the property data as well as employ integration functions in order to solve for the transitory conditions.

3.6.1 Enthalpy of Frost vs. Time

The behavior of the model is transient in nature. Constant integration of variables over time steps makes it critical that the variables are changing throughout the process. The model integrates the energy balances of each node and resolves for a temperature at each time interval. For the frost nodes, the change in temperature with respect to time does not constantly change when it encounters a phase change. Therefore, the enthalpy is used instead of temperature. The enthalpy changes from -332.8 [kJ/kg] to 0 [kJ/kg] within the phase change from ice to water, whereas the temperature remains constant at 0 [˚C]. This makes it possible for the integration to continue and the model to reach a solution.

Figure 3-5: Temperature vs. Enthalpy diagram

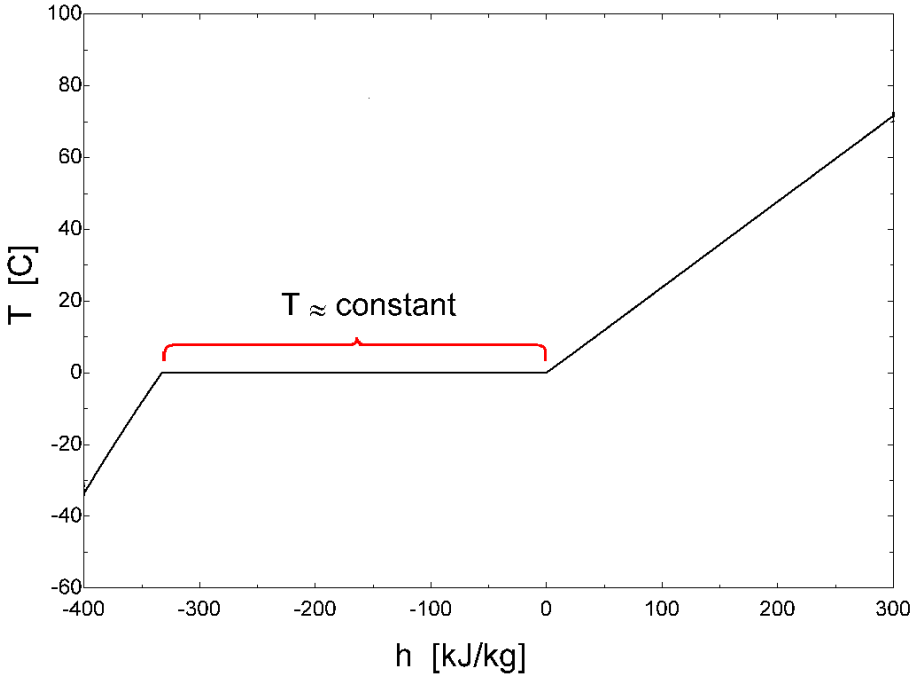

3.6.2 Temperature of Fin vs. Time

The fin reaches the a steady temperature distribution within a small time frame, so the change in temperature for each time step may be too great to iterate if the step size is too great. The energy in to defrost (Q_{in}) is dependant on the convective coefficient (h_{base}). With

the convective coefficient rising to minimize resistance, the time step for the model needs to decrease to ensure that the temperature change at the base of the fin is stable.

3.7 Variables in Model

The model is set up to mimic any type of air-cooled evaporator that may be encountered in the field. Evaporators are made of different materials and have different geometries. The spacing between the fins varies from one fin per inch to multiple fins per inch. Along with the fin spacing, the fin thickness changes with different types of evaporators. The tubes in evaporators are also spaced out differently, making the length of the annular fin protruding from the tube fluctuate. The diameters of the tubes are also a variable from evaporator to evaporator. The frost that is encountered on the evaporator fins is never the same. The amount of frost that accumulates on the fin change depending on the product that is in the freezer space. Temperatures of the freezer, the refrigerant, and the frost/fin structure are dependent on the environment as well. The model was written to be easily changed for every variable encountered.

3.7.1 Size of Model

The size of the model can be set up to represent a single fin-tube assembly. The profile of the annular fin extends from the outside tube diameter, at $r_{i,1}$, to half the distance to the surrounding tubes, $r_{o,jj}$. The temperature distribution for each fin-tube assembly will then be the same for each. If the inside radius is taken to be 0.5 inches, making the outside tube diameter 1 inch, and the outside radius of the annular fin is taken to be 1.5 inches, a tube spacing of 2 inches (O.D. to O.D.) will be set.

Eq. 3-30

$$\Delta r = \frac{r_{jj} - r_1}{jj - 1}$$

The mesh spacing is determined by the number of nodes chosen for the model. Each node has the height of Δr by the use of equation 3-30. The exception to this is the innermost

nodes (*G, H, I, L*) and the outermost nodes (*A, B, C, J*) which have a height of $\Delta r/2$. The equations below (Eq. 3-31, Eq. 3-32) are used to make the inside node start at the O.D. of the tube and the outside node end at the end of the annular fin profile.

Eq. 3-31

$$r_{out,jj} = r_{jj}$$
$$r_{in,jj} = r_{out,jj} - \frac{\Delta r}{2}$$

Eq. 3-32

$$r_{in,1} = r_1$$
$$r_{out,1} = r_1 + \frac{\Delta r}{2}$$

Equation 3-33 is the code written to make the inside nodes in the model have the same spacing throughout. As the number of nodes in the vertical direction change, specified by *jj*, the Δr changes as well. The changing Δr in return, varies the height of each node to account for this.

Eq. 3-33

$$\textit{Duplicate} \quad j = 2, jj-1$$
$$r_j = r_{j-1} + \Delta r$$
$$r_{out,j} = r_j + \frac{\Delta r}{2}$$
$$r_{in,j} = r_j - \frac{\Delta r}{2}$$
$$\textit{End}$$

3.7.2 Mesh Size (Number of Nodes)

The model is written in a way so that the number of nodes used can vary depending on the user's preferences. As the number of nodes increases (decreasing mesh), the accuracy also increases. The computational time is affected by the number of nodes used in the model.

Under the same transient conditions for a specified amount of time the energy supplied into the frosted fin model was recorded. A table is given below that shows the relative error as the number of nodes increases in both the axial and radial directions from the least number of nodes ($ii = 4, jj = 3$). As the number of nodes is increased radially, there is little change in the models accuracy. As the nodes in the axial direction are increased the relative error decreases more rapidly. The relative error is taken to be the difference in supplied energy (Q_{in}) between the mesh size analyzed and the finest mesh, and dividing it by the finest mesh's supplied energy and multiplying by a factor of 100.

The computational time increased as the mesh size became dense. The appropriate number of nodes chosen to both decrease the computational time and maintain accuracy was the ($ii = 10, jj = 10$) mesh size.

Table 3-1: Mesh size and relative error

Number of Nodes		Q_{in}	$T_{1,jj}$	Time	Rel. Error
ii (axial)	jj (radial)	[kJ]	[K]	[sec]	[%]
5	5	0.63941	273.150	78.1	12.53
5	10	0.63177	273.150	102.4	11.19
10	5	0.63074	273.150	268.4	6.01
10	10	0.59456	272.975	304.0	4.64

3.7.3 Size of Fin for Energy Distribution (Length, Thickness)

The fin used in the model is a single row of nodes. The fins used in evaporators are sufficiently thin and conduct energy very efficiently that more than one row is not needed. However, the thickness of the fin can be changed within the model without changing any of the other parameters. The thickness of the fin is represented by 'Δi' in the model. The reason for keeping the fin thickness variable (Δi) separate from the frost nodal spacing variable (Δx) is to ensure that when the number of nodes changes the thickness of the fin stays constant.

3.7.4 Initial Amount of Frost

The amount of frost used in the program is adjusted by using an estimate of fin spacing blockage. If frost covers the entire gap from fin to fin, it has 100% blockage. If there is no frost on the fin, it has 0% blockage.

Eq. 3-34

$$Length_{FROST} = Percent_{BLOCKAGE} \cdot Fin_{SPACE} - \frac{\Delta i}{2}$$

Eq. 3-35

$$Fin_{SPACE} = \frac{1}{Fins_{PER\_INCH}}$$

The length of the frost (Eq. 3-34) is dependent on the fin spacing. The fin spacing is just the length of the gap between the fins. If there were 3 fins per inch, the fin spacing would be 0.33 inches. If the percent blockage of frost is also set at 100%, the length of the frost would be 0.33 inches minus the fin thickness since the fin is also part of the 0.33 inch spacing.

3.7.5 Time of Simulation

The model simulates a defrost process and stops when all of the frost nodes have reached at least 0˚C [32˚F]. The time it takes for the model to do this depends on the temperature of the refrigerant, the temperature of the surrounding environment, and the initial conditions. The properties of the frost also affect the time for defrost to complete. Time increases as the density of the frost increases. The geometry of the tube and fin also affect the outcome. If the tube spacing is large, the frost nodes will be farther away from the tube; increasing simulation time. Every variable in the model affects the time it takes to defrost.

3.7.6 Temperatures of Freezer, Refrigerant

Freezer conditions are chosen depending upon the products that are stored within. That is why it is important to be able to change these conditions. The main variable in the model is the temperature of the refrigerant used to melt the frost on the fin. The refrigerant temperatures are usually varied from 10˚C to 37.78˚C (50 [˚F] to 100[˚F]). The model is used to aid in the understanding of what the energy distributions and parasitic loads on the freezer are, depending on the refrigerant temperatures.

3.7.7 Relative Humidity of Freezer Air

The conditions of the freezer also include the humidity in the space. The relative humidity set in the model is at 80%. This variable can be changed; however, there is little effect in doing so. Since the temperatures of the surrounding space is below the freezing point of water, the amount of water that the air can hold does not change much with different humidity ratios.

3.8 References

Jaluria, Yogesh. Natural Convection – (*HMT, the science and applications of heat and mass transfer*; vol. 5). Pergamon Press 1980.

Klein, S. A., and F. L. Alvarado (2003). Engineering Equation Solver. Middleton, WI, F-chart
software.

Mills, Anthony F. *Heat and Mass Transfer*. Richard D. Irwin Inc, 1995.

Tao, Y.-X., R.W. Besant, and K.S. Rezkallah. 1993a. A mathematical model for predicting the densification and growth of frost on a flat plate. *Int. L. Heat Mass Transfer*, vol. 36 (2):353-363.

Chapter 4 Validation of the Model's Results

4.1 Distribution of Energy in Model Simulation

The model tracks the distribution of energy while a defrost simulation is in progress. The energy flows quantified by the model include:

- Q_{in} - the total amount of energy supplied to the coil during a defrost cycle.
- $Q_{out/stored}$ - the amount of thermal energy that is stored in the tubes and fins plus the energy that is released during the defrost cycle. Should equal Q_{in}.
- Q_{evap} - the latent energy that transfers to the surroundings during a defrost cycle by re-evaporation of water from the coil surfaces.
- Q_{frost} – the amount of thermal energy stored within the frost nodes after a defrost cycle is complete.
- Q_{conv} - the sensible energy convected back to the space during a defrost cycle.
- Q_{fin} and Q_{tube} - the total thermal energy stored within the fin and tube after a defrost cycle is complete.
- Q_{excess} – the energy provided beyond that needed to heat given frost nodes past the melting point of water.
- Q_{melt} - is the amount of energy it takes for the mass of frost to reach 0 [˚C] and change phase from ice to water.

The results presented in this section are for a single air-cooling evaporator. The simulations conducted are based on an evaporator model studied in the field (Imeco Model FCLS). Details for this heat exchanger are given in the table below.

Table 4-1: Detailed table of Imeco industrial evaporator

Imeco evaporator specifications Model: FCLS 96103.4.3 Serial: 7191.1 RHI		
coil volume	21.4	ft^3
coil mass	9,479	lb_m
coil metal	galvanized steel	
fin metal	aluminum	
fin pitch	3	fins/inch
# of fins	800	n/a
# of rows	10	n/a
# tubes on face	18	n/a
tube wall thickness	0.060	in
tube outside diameter	1.05	in
total coil surface area	11,119	ft^2
# of fans	4	n/a
installed fan power (each)	3	hp
total air flow rate	72,416	ft^3/min
air face velocity	741	ft/min

4.1.1 Energy Supplied during a Defrost Cycle

The rate of energy supplied to the evaporator during a defrost cycle is quantified as $\dot{Q}_{in}$. As shown in equation 4-1 and explained in section 2.3.2, it is the convective heat transfer from the hot refrigerant to the base of the fin at node type '*L'*. It is lumped as a convective interaction because the tube wall is very thin and when h_{base} is high, the base of the fin (T_b) is essentially the temperature of the refrigerant. The rate at which the energy is supplied depends on the refrigerant temperature. Figure 4-1 is a plot of the rate of supplied energy into the frosted fin model for a frost density of 150 [kg/m^3] and a frost blockage of 20%.

Eq. 4-1

$$\dot{Q}_{in} = h_{base} \frac{\Delta i}{2} \cdot 2\pi \cdot r_{in,1} \left(T_{base} - T_{ii,1} \right)$$

Figure 4-1: Rate of supplied energy to the coil during defrost

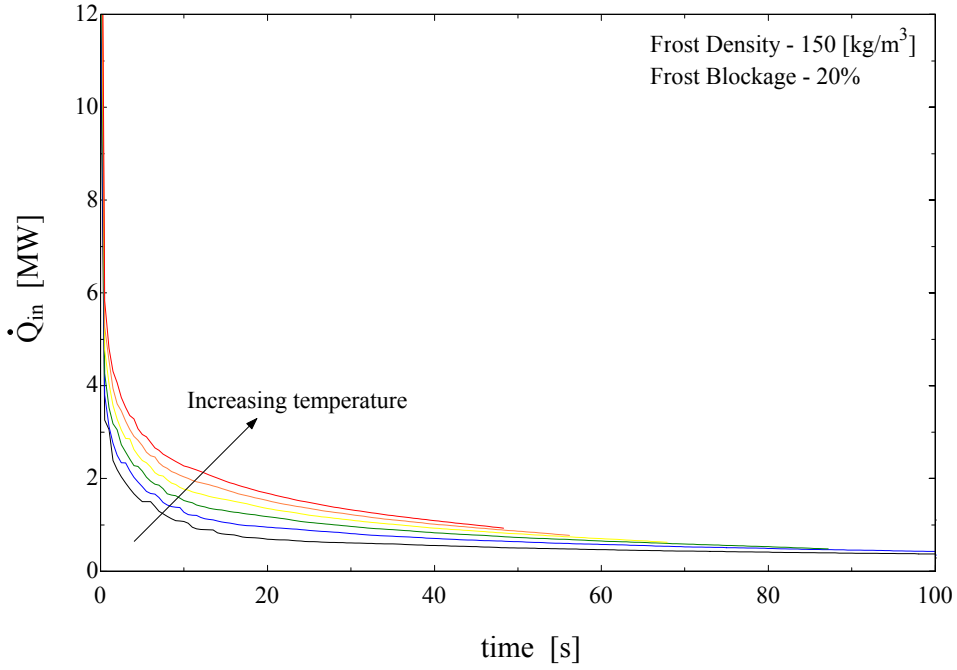

The total quantity of energy supplied during a defrost cycle is represented by Q_{in}, defined in equation 4-2. It is simply the integral of the energy supply rate for the entire defrosting period. This energy represents the total amount of energy supplied for defrost, including the losses from stored and released energy.

Eq. 4-2

$$Q_{in} = \int_{0}^{time\ final} \left[h_{base} \frac{\Delta i}{2} \cdot 2\pi \cdot r_{in,1} \left(T_{base} - T_{ii,1} \right) \right] \cdot dt$$

The total amount of supplied defrost energy is shown in Figure 4-2 along with the time required to fully melt accumulated frost for frost densities ranging between 150 - 450 [kg/m^3] and a constant frost blockage of 20%.

Figure 4-2: Total supplied energy and defrost time for a defrost cycle at 20% frost blockage and varied refrigerant temperatures

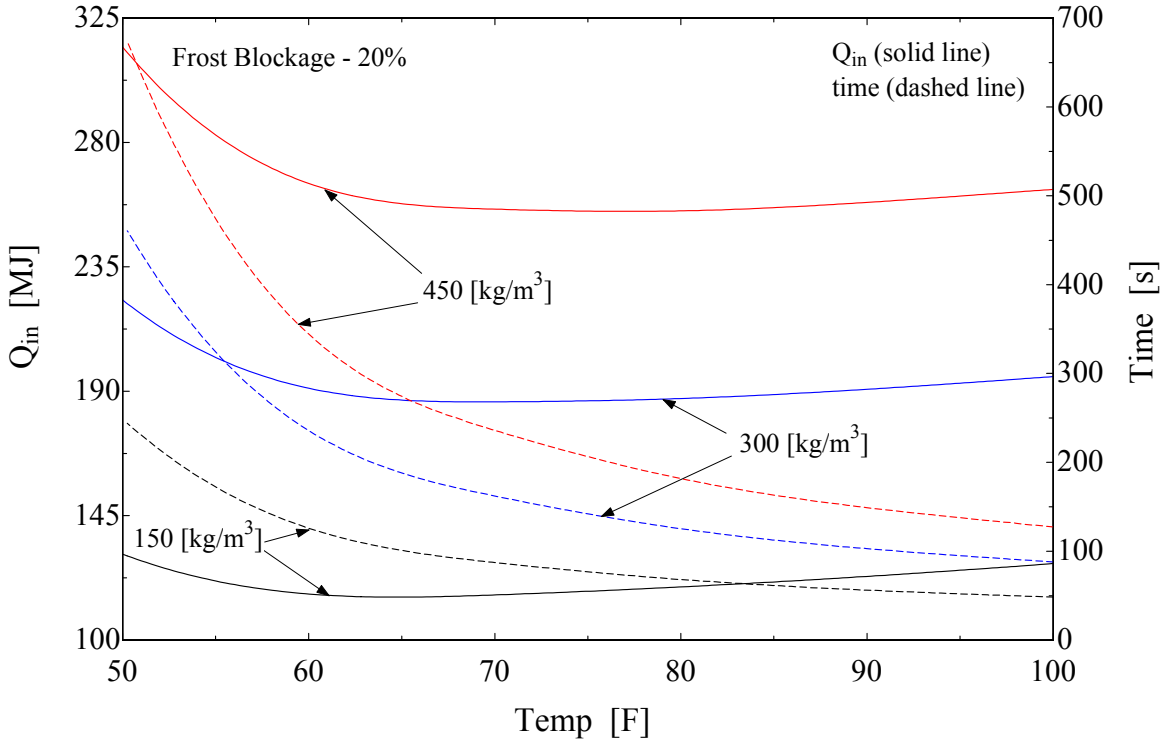

The energy supplied for a defrost is particularly useful for defrost cycles that operate for a predetermined time. Q_{in} is includes the excess energy, defined as the energy that convects to the freezer after all of the frost melts and before the cycle is terminated. The excess energy is determined with the dry fin model described in Chapter 2. This subject is discussed later in this Chapter.

4.1.2 Energy Transfer by Convection

The rate of energy that convects from the face of the frost nodes during a defrost cycle to the freezer is defined as $\dot{Q}_{conv}$. The total convection to the surroundings for each node is represented by Q_{conv}, the integral of $\dot{Q}_{conv}$. Equation 4-3 is the convected energy from a single face node (*A, D, G, H,* or *I*) in the frosted fin model. Q_{conv} is the sum of all the convecting nodes. Each node on the air interface experiences a changing heat transfer coefficient, h_C, as explained in section 3.4.

Eq. 4-3

$$Q_{conv,i} = \int_{0}^{time\ final} \left[\overline{h}_C \cdot \pi\left(r_{out}^2 - r_{in}^2\right)\left(T_\infty - T_i\right)\right]_i \cdot dt$$

The rate of convection for a frost density of 150 [kg/m^3] and a frost blockage of 20% is shown in the Figure 4-3 for different entering refrigerant temperatures.

Figure 4-3: Rate of convecting energy during a defrost cycle

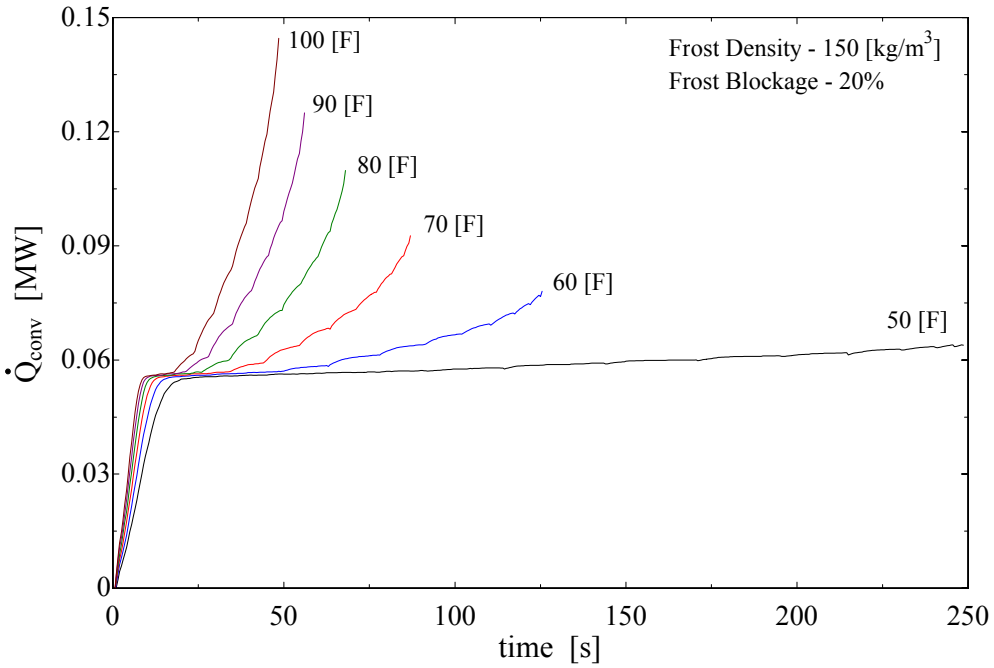

In addition to the convective losses, there is a sensible energy term representing the amount of energy required to raise the temperature of the melted frost above 0 ˚C. Since the melted nodes are assumed to be drained and the conductivity of the node transitions to that of air, the amount of energy that raises the melted frost nodes above 0 ˚C (32 ˚F) is considered to be a convective loss. The excess energy in the melted frost nodes is represented by the left hand side of the frost nodal equations (*A-I*), the difference being the change in enthalpy is the final enthalpy minus the enthalpy of water at temperature 0 ˚C (32 ˚F), which is 0 [kJ/kg]. All of frost nodes excess stored energy are then summed up and represented as Q_{excess}. Further explanation of Q_{excess} is in section 4.1.6. Figure 4-4 shows the total amount of

convected energy and sensible heat above 0˚C that is released for a frost density of 150 [kg/m^3] and varying frost blockages at the time the defrost is complete.

Figure 4-4: Total amount of convected energy released during defrost, including Q_{excess}

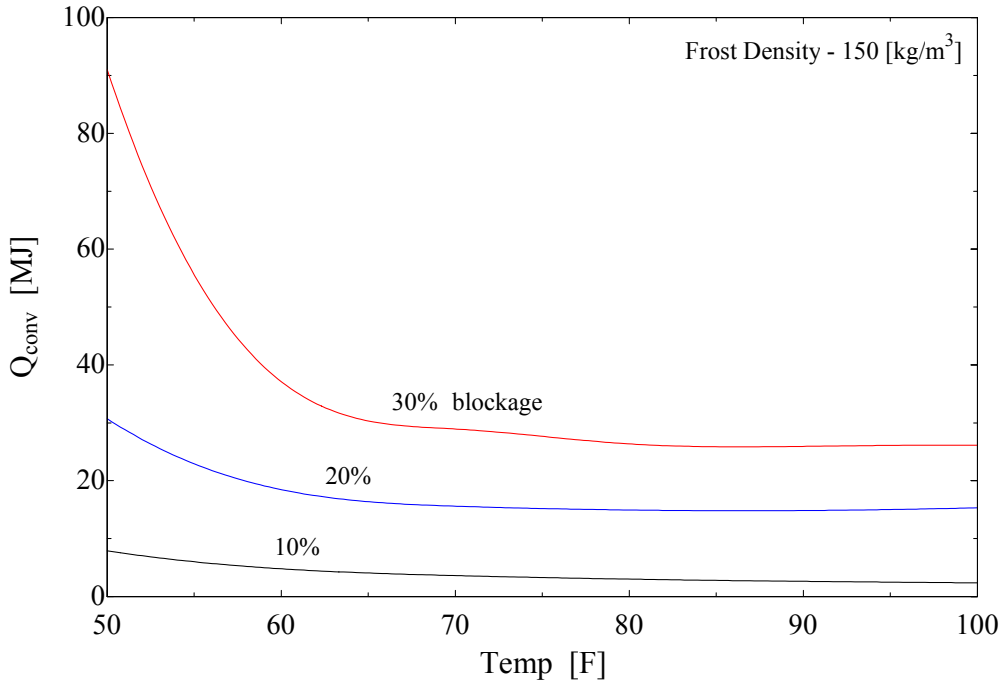

Convection remains relatively constant when different refrigerant temperatures are selected for coils having frost blockages of 10 and 20%. As the frost increases to 30% however, the convection increases noticeably with decreasing refrigerant temperatures. The rate of convection is smaller with the lower temperature refrigerants, but the extensive amount of time needed to melt the frost on the coils allows the total convective losses to overwhelm the defrost process.

4.1.3 Energy Transfer due to Evaporation

As sensible energy is transferred from the coil during a defrost cycle due to thermally driven convection, there are also latent energy losses due to the re-evaporation of water from the coil surface to the surroundings during a defrost cycle. The total latent energy loss for a defrost cycle is represented by Q_{evap}, the term for a single node is in equation 4-4.

Eq. 4-4

$$Q_{evap,i} = \int_{0}^{time\ final} \left[\overline{g}_m \cdot \pi \left(r_{out}^2 - r_{in}^2 \right) \left(m_{1s} - m_{1e} \right) \cdot h_{ig} \right]_i \cdot dt$$

The rate of latent heat associated with re-evaporated moisture during a hot gas defrost cycle for a frost density of 150 [kg/m^3] and a frost blockage of 20% is shown in the figure below for varying refrigerant temperatures.

Figure 4-5: Rate of latent energy lost during re-evaporation of moisture during a defrost cycle

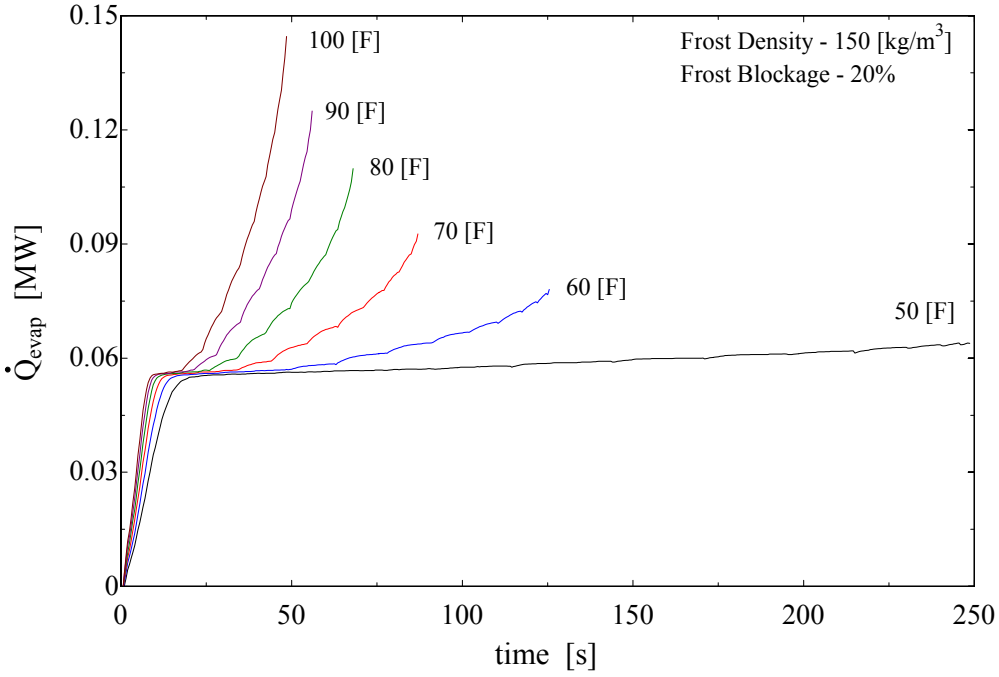

Figure 4-5 shows that as the refrigerant temperature is increased, the rate of evaporative losses also increases. However, the total energy lost due to the re-evaporation of water into the freezer is less, based on the total energy supplied, because of the short defrost times (shown by the discontinuation of the curves).

Although the rate of latent energy loss due to evaporation is greater using increased refrigerant temperatures, the integrated latent energy loss from evaporation is less due to the shorter defrosting times experienced at elevated temperatures. Figure 4-6 is the integrated latent energy loss energy for a frost density of 150 [kg/m^3] and varying frost blockages.

Figure 4-6: Integrated latent energy loss during a hot gas defrost cycle

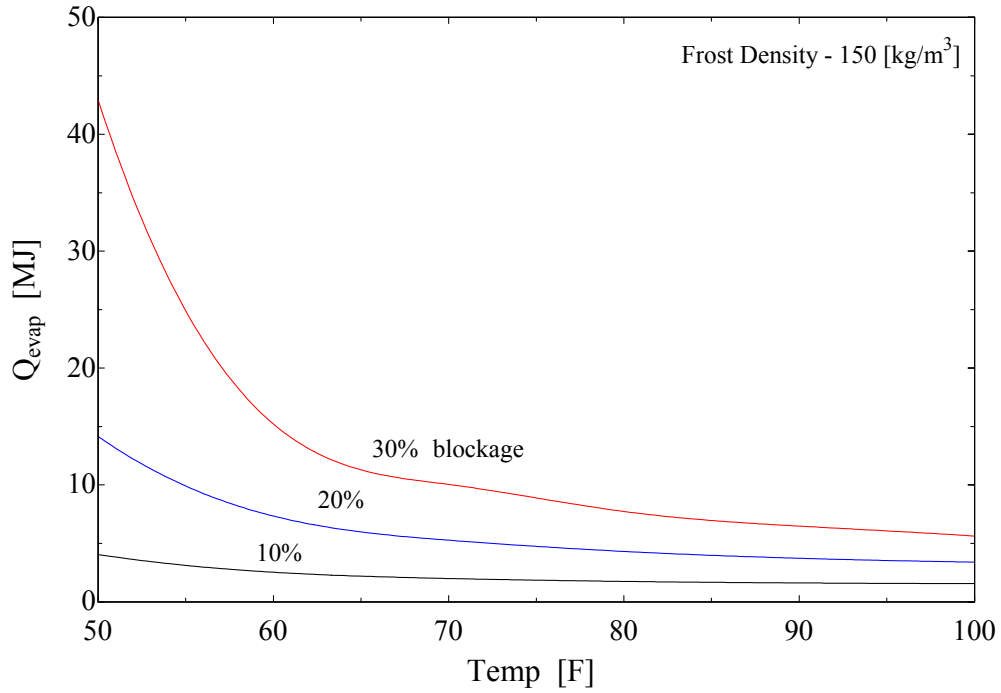

Figure 4-6 shows the increase in total evaporative losses with decreasing refrigerant temperatures. The losses are always greater with lower refrigerants but not significantly until frost blockages reach 20% and higher. The evaporative losses make up 2 to 18% of the total supplied energy depending on the refrigerant temperature and frost blockage. Evaporative losses exceed the total amount of energy stored in the fins and tubes of the evaporator when low refrigerant temperatures are in combination with increased frost blockages. Evaporative losses range from 0.25 to 0.5 to that of convective losses, depending on the refrigerant temperature.

4.1.4 Energy Stored in Tube

The energy stored in the tube after a defrost cycle is completed given in equation 4-5.

Eq. 4-5

$$Q_{tube} = m_{tube} C_{p,tube} \cdot \left(T_{base} - T_{initial}\right)$$

The wall of the tube is highly conductive and thin so that the assumption is made that the tube wall reaches the saturation temperature of the condensing gaseous refrigerant used for

defrosting. This effectively results in the transfer coefficient being near infinity. A value of 100,000 [W/m^2-K] is used in the model to obtain the desired base fin temperature. This assumption also affects the way Q_{in} is calculated, since the fin receives energy from the tube at the temperature of the refrigerant. Before the evaporator can help cool the freezer again it must first transfer the energy stored in the tube by removing the heat using cold refrigerant once the hot gas sequence is complete. Since the tube is not part of the mesh in the frosted fin model, equation 4-5 uses the difference in the final and initial temperatures to calculate the energy stored in the tube.

4.1.5 Energy Stored in Fin

Like the tube, energy stored in the finned surfaces after the defrost cycle is completed contributes to the parasitic defrost load. The energy stored in the fin after a defrost process terminates is represented by equation 4-6.

Eq. 4-6

$$Q_{fin,j} = \int_0^{time\,final} \left[\rho_F \frac{\Delta i}{2} \cdot \pi \left(r_{out,jj}^2 - r_{in,jj}^2 \right) \cdot C \frac{dT}{dt} \right]_j \cdot dt \qquad for\ \ j = 1, jj$$

The equation above for the stored energy in the fin is representative of the left hand sides of equations 2-14, 2-15, and 2-16 in the dry fin model. Figure 4-7 shows the total amount of energy that is stored in the fin after a defrost cycle is complete for a frost density of 150 [kg/m^3] and for frost blockages of 10, 20, and 30%. There is more energy stored in the fin as the amount of frost increases because the fin has more time to reach steady state temperature. The defrost times are shown with dotted lines in this figure.

Figure 4-7: Stored energy in total evaporator fin surface after the defrost cycle terminates

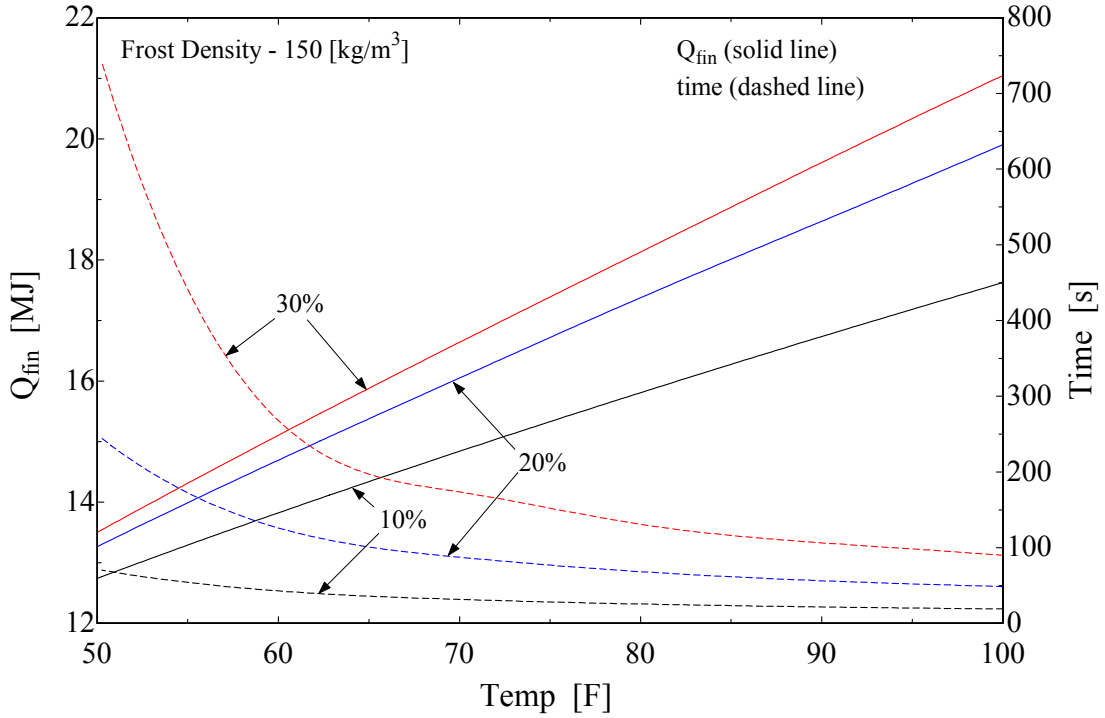

4.1.6 Energy Stored in Frost

The energy stored in the melted frost nodes (Q_{frost}) is unique in that it does not create another load on the freezer. Once the defrost has terminated, the portion of the frost that does not re-evaporate is melted and washed away in the drain pan. Even though the energy stored in the frost is greater when the refrigerant temperature is increased, only the excess energy added to raise the frost nodes temperature above 0 °C (32 °F) (Q_{excess}) affects the amount of energy that re-enters a freezer because the energy that goes into heating the water would otherwise be convected out to the freezer.

4.1.7 Energy Required to Melt Frost

The defrost efficiency is a ratio used to express the amount of energy that is needed to melt the frost compared to the total amount of energy that is provided during a defrost cycle. The total amount of energy supplied was already defined as Q_{in}. The amount of energy it takes for the frost to reach a water state at 0 [˚C] from its initial temperature is then expressed as Q_{melt}.

Eq. 4-7

$$Q_{melt} = Q_{frost} - Q_{excess}$$

where Q_{frost}, shown in equation 4-9, is the left hand side of the frost energy balance equations.

Eq. 4-8

$$Q_{frost} = \int_{0}^{time\ final} \left[\rho V \left(\frac{dh}{dt} \right)_{i,j} \right] \cdot dt \qquad for \quad i = 1, ii-1 \quad and \quad j = 1, jj$$

The energy it takes to melt the frost (Q_{melt}) can also be defined as the difference between the energy that is stored in the frost after a defrost cycle terminates and the energy that raises the frost's temperature and enthalpy above 0 [˚C] and 0 [kJ/kg] respectively; the definition of Q_{excess}.

The defrost efficiency is expressed in the equation below. It is the amount of energy that is required to melt the frost adhered to the fin with respect to the total energy supplied to the evaporator coil for a defrost cycle. The defrost efficiency defined is consistent with Cole (1989).

Eq. 4-9

$$\eta_{defrost} = \frac{Q_{melt}}{Q_{in}}$$

A plot of the defrost efficiency for a frost density of 150 [kg/m^3] and frost blockages ranging from 10% to 30% is shown in Figure 4-8. At lower refrigerant temperatures, the defrost efficiency is heavily dependent on the time it takes for the accumulated frost to melt. Referring to the refrigerant of 50°F, at 10% frost blockage the defrost efficiency is approximately 0.3 because with such little accumulated frost, most of the supplied energy goes into heating the evaporator coils. At 20% frost blockage the efficiency increases to 0.38 because the amount of energy needed to melt the frost is higher than the energy stored in the coils. Also, the frost melts in a timely manner making the convective and evaporative losses less of an issue. As frost blockage increases to 30% the efficiency for defrost decreases once

again to 0.32 because the long period of time to complete the defrost cycle allows for greater convective and evaporative losses. For every unit of energy that goes into melting the accumulated frost, 1.675 units are lost by convection and evaporation.

Figure 4-8: Defrost efficiency for varied refrigerant temperatures

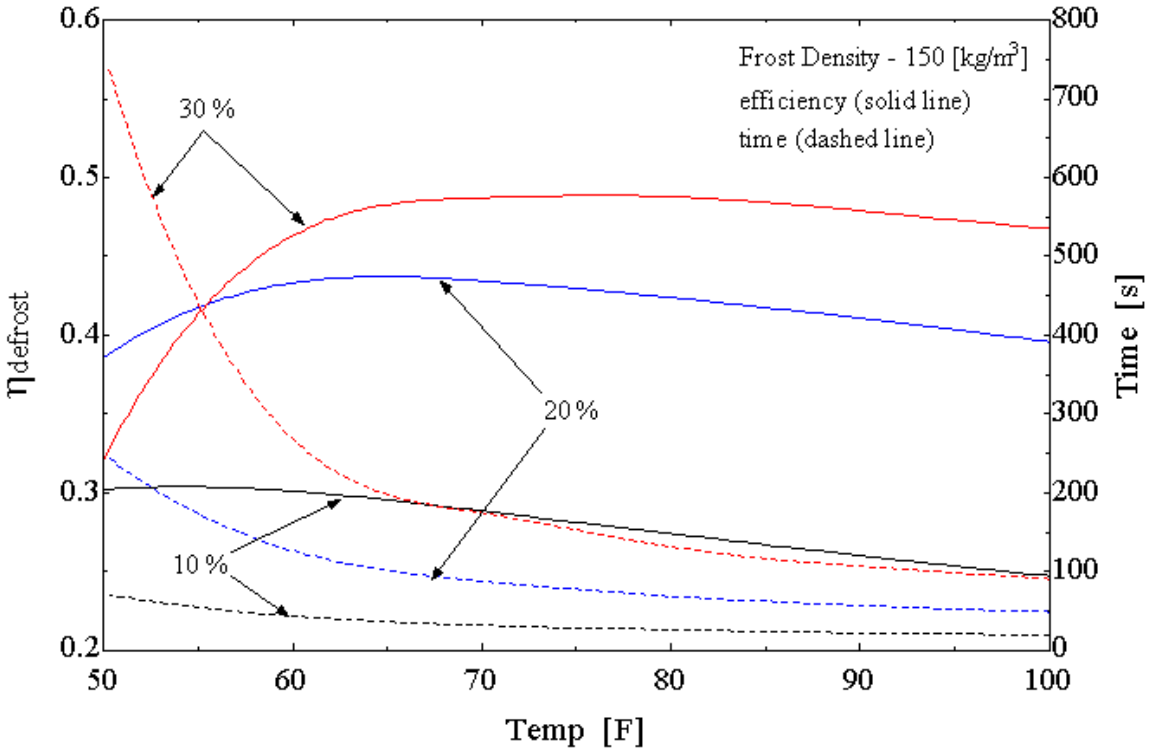

4.2 Distribution of Energy for Defrost

The previous sections defined the different energy terms associated with defrosting. The plots are for a single evaporator of known geometry. This section will cast the various energy terms into non-dimensional values. All of the energy terms discussed in this section will be expressed as percentages based on the total amount of energy that is supplied for a defrost cycle. Though the supplied energy quantities are given are for a half tube-fin assembly, the distributions still apply to whole evaporators as well. The Imeco evaporator described above can be represented by multiplying the supplied energy given in the tables below by multiplying the quantity by 2 due to symmetry, 180 for the number of tubes, and 800 for the number of fins in this evaporator. For instance, to compare the supplied energy (Q_{in}) between the model and the Imeco evaporator using a refrigerant temperature of 50°F

with a frost density of 150 [kg/m^3] and 20% blockage, the value of Q_{in} = 0.4552 kJ from Table 4-3 is multiplied by 2(*half fin/tube*) *x* 180(# *of tubes*) *x* 800(# *of fins*) = 131097.6 kJ ≈ 131.1 MJ, which is the value that can be found in Figure 4-2 for the same refrigerant temperature and frost conditions.

The efficiency of the defrost process can never reach 100%. At the very least, energy has to provide heating to the fins and tubes of the evaporator in order to melt the frost from its surfaces. There will also be evaporative and convective losses due to the temperature differences between the freezer and the warming of both frost and metal while defrosting. Given below are charts that break up the energies associated with various defrosting temperatures, frost densities, and frost blockages.

Table 4-2: Energy distribution for a defrost cycle having a frost density of 150 [kg/m^3] and frost blockage of 10%

Variable	units	Frost Density = 150 [kg/m^3], Frost Blockage = 10%					
		100˚F	90˚F	80˚F	70˚F	60˚F	50˚F
Qin	kJ	**0.2925**	**0.2779**	**0.2638**	**0.2506**	**0.2401**	**0.2393**
Qconv	%	2.8%	3.3%	3.9%	5.0%	6.9%	11.5%
Qconv\tot	%	6.8%	7.0%	7.3%	7.8%	9.1%	12.9%
Qevap	%	1.8%	2.0%	2.3%	2.8%	3.7%	5.9%
Qfin	%	20.9%	20.9%	20.8%	20.6%	20.0%	18.5%
Qtube	%	45.7%	44.1%	42.2%	40.0%	37.1%	32.6%
Qexcess	%	4.0%	3.7%	3.3%	2.8%	2.2%	1.4%
Qmelt	%	24.7%	26.0%	27.4%	28.8%	30.1%	30.2%
Total	%	100.0%	100.0%	100.0%	100.0%	100.0%	100.0%
Time	sec	18.9	21.6	25.5	31.5	42.7	71.2

The row with the variable name '*Total*' is the sum of all of the energy terms listed in the table with respect to the energy supplied for defrost (Q_{in}), excluding the Q_{conv}, and Q_{excess} since the $Q_{conv/tot}$, the total convected energy, is a combination of the two. The *defrost efficiency* is the same value as Q_{melt} in the tables, since Q_{melt} is a percentage of the energy that went into melting the frost with respect to the total amount of supplied energy, Q_{in}.

Table 4-3: Energy distribution for a defrost cycle having a frost density of 150 [kg/m^3] and frost blockage of 20%

Variable	units	Frost Density = 150 [kg/m^3], Frost Blockage = 20%					
		100˚F	90˚F	80˚F	70˚F	60˚F	50˚F
Q_{in}	kJ	**0.4433**	**0.4272**	**0.414**	**0.4039**	**0.4051**	**0.4552**
Q_{conv}	%	4.6%	5.5%	6.7%	8.7%	12.3%	21.5%
$Q_{conv\backslash tot}$	%	12.0%	12.1%	12.5%	13.4%	15.8%	23.4%
Q_{evap}	%	2.7%	3.0%	3.6%	4.5%	6.3%	10.8%
Q_{fin}	%	15.6%	15.1%	14.6%	13.8%	12.6%	10.1%
Q_{tube}	%	30.2%	28.7%	26.9%	24.8%	22.0%	17.1%
Q_{excess}	%	7.4%	6.6%	5.8%	4.7%	3.5%	1.9%
Q_{melt}	%	39.6%	41.1%	42.4%	43.4%	43.3%	38.5%
Total	%	100.0%	100.0%	100.0%	100.0%	100.0%	100.0%
Time	sec	48.5	56.2	68.2	87.3	125.9	248.6

Table 4-4: Energy distribution for a defrost cycle having a frost density of 150 [kg/m^3] and frost blockage of 30%

Variable	units	Frost Density = 150 [kg/m^3], Frost Blockage = 30%					
		100˚F	90˚F	80˚F	70˚F	60˚F	50˚F
Q_{in}	kJ	**0.5959**	**0.5818**	**0.5713**	**0.572**	**0.6018**	**0.8685**
Q_{conv}	%	6.2%	7.5%	9.2%	12.1%	17.7%	34.9%
$Q_{conv\backslash tot}$	%	15.2%	15.5%	16.0%	17.6%	21.4%	36.4%
Q_{evap}	%	3.3%	3.9%	4.7%	6.1%	8.8%	17.2%
Q_{fin}	%	12.3%	11.7%	11.0%	10.1%	8.7%	5.4%
Q_{tube}	%	22.4%	21.1%	19.5%	17.5%	14.8%	9.0%
Q_{excess}	%	9.0%	8.0%	6.8%	5.4%	3.7%	1.5%
Q_{melt}	%	46.8%	47.9%	48.8%	48.7%	46.3%	32.1%
Total	%	100.0%	100.0%	100.0%	100.0%	100.0%	100.0%
Time	sec	89.9	106.3	130.7	173.6	267.9	761.2

Table 4-5: Energy distribution for a defrost cycle having a frost density of 300 [kg/m^3] and frost blockage of 10%

Variable	units	Frost Density = 300 [kg/m^3], Frost Blockage = 10%					
		100˚F	90˚F	80˚F	70˚F	60˚F	50˚F
Q_{in}	kJ	**0.3881**	**0.3727**	**0.3584**	**0.3464**	**0.3393**	**0.3511**
Q_{conv}	%	3.7%	4.3%	5.2%	6.5%	9.0%	14.6%
$Q_{conv\backslash tot}$	%	9.9%	9.9%	10.1%	10.7%	12.2%	16.5%
Q_{evap}	%	2.4%	2.7%	3.0%	3.6%	4.8%	7.5%
Q_{fin}	%	16.0%	15.8%	15.5%	15.0%	14.2%	12.6%
Q_{tube}	%	34.4%	32.9%	31.1%	29.0%	26.3%	22.2%
Q_{excess}	%	6.2%	5.6%	5.0%	4.2%	3.2%	2.0%
Q_{melt}	%	37.2%	38.7%	40.3%	41.7%	42.6%	41.1%
Total	%	100.0%	100.0%	100.0%	100.0%	100.0%	100.0%
Time	sec	31.7	36.5	43.5	54.7	75.4	128.9

Table 4-6: Energy distribution for a defrost cycle having a frost density of 300 [kg/m^3] and frost blockage of 20%

Variable	units	Frost Density = 300 [kg/m^3], Frost Blockage = 20%					
		100˚F	90˚F	80˚F	70˚F	60˚F	50˚F
Q_{in}	kJ	**0.6781**	**0.6622**	**0.6506**	**0.6465**	**0.6635**	**0.7743**
Q_{conv}	%	5.6%	6.6%	8.0%	10.3%	14.4%	24.2%
$Q_{conv\backslash tot}$	%	15.1%	15.1%	15.3%	16.2%	18.6%	26.5%
Q_{evap}	%	3.2%	3.7%	4.3%	5.4%	7.4%	12.2%
Q_{fin}	%	10.2%	9.8%	9.3%	8.6%	7.7%	5.9%
Q_{tube}	%	19.7%	18.5%	17.1%	15.5%	13.4%	10.1%
Q_{excess}	%	9.5%	8.5%	7.3%	5.9%	4.2%	2.2%
Q_{melt}	%	51.7%	53.0%	53.9%	54.3%	52.9%	45.3%
Total	%	100.0%	100.0%	100.0%	100.0%	100.0%	100.0%
Time	sec	88.0	102.9	125.3	162.1	235.8	469.5

Table 4-7: Energy distribution for a defrost cycle having a frost density of 300 [kg/m^3] and frost blockage of 30%

Variable	units	Frost Density = 300 [kg/m^3], Frost Blockage = 30%					
		100˚F	90˚F	80˚F	70˚F	60˚F	50˚F
Q_{in}	kJ	**0.9782**	**0.9651**	**0.9617**	**0.9779**	**1.052**	**1.56**
Q_{conv}	%	7.2%	8.6%	10.5%	13.7%	19.5%	36.5%
$Q_{conv\backslash tot}$	%	18.1%	18.1%	18.5%	19.9%	23.8%	38.2%
Q_{evap}	%	3.8%	4.5%	5.4%	6.9%	9.8%	18.1%
Q_{fin}	%	7.5%	7.1%	6.5%	5.9%	5.0%	3.0%
Q_{tube}	%	13.7%	12.7%	11.6%	10.3%	8.5%	5.0%
Q_{excess}	%	10.8%	9.5%	8.0%	6.3%	4.3%	1.7%
Q_{melt}	%	57.0%	57.7%	57.9%	57.0%	53.0%	35.7%
Total	%	100.0%	100.0%	100.0%	100.0%	100.0%	100.0%
Time	sec	168.0	198.6	246.0	328.0	509.3	1418.0

Table 4-8: Energy distribution for a defrost cycle having a frost density of 450 [kg/m^3] and frost blockage of 10%

Variable	units	Frost Density = 450 [kg/m^3], Frost Blockage = 10%					
		100˚F	90˚F	80˚F	70˚F	60˚F	50˚F
Q_{in}	kJ	**0.4827**	**0.4669**	**0.4527**	**0.4415**	**0.438**	**0.4623**
Q_{conv}	%	4.2%	4.9%	5.9%	7.4%	10.1%	16.1%
$Q_{conv\backslash tot}$	%	11.7%	11.7%	11.8%	12.3%	13.8%	18.3%
Q_{evap}	%	2.8%	3.0%	3.4%	4.1%	5.4%	8.3%
Q_{fin}	%	12.9%	12.6%	12.3%	11.8%	11.0%	9.6%
Q_{tube}	%	27.7%	26.3%	24.6%	22.7%	20.4%	16.9%
Q_{excess}	%	7.5%	6.8%	5.9%	4.9%	3.7%	2.2%
Q_{melt}	%	44.9%	46.4%	47.9%	49.1%	49.5%	46.9%
Total	%	100.0%	100.0%	100.0%	100.0%	100.0%	100.0%
Time	sec	44.4	51.4	61.5	77.6	107.7	186.0

Table 4-9: Energy distribution for a defrost cycle having a frost density of 450 [kg/m^3] and frost blockage of 20%

Variable	units	Frost Density = 450 [kg/m^3], Frost Blockage = 20%					
		100˚F	90˚F	80˚F	70˚F	60˚F	50˚F
Q_{in}	kJ	**0.9132**	**0.8969**	**0.8863**	**0.8884**	**0.9208**	**1.092**
Q_{conv}	%	6.1%	7.1%	8.6%	11.0%	15.2%	25.3%
$Q_{conv\backslash tot}$	%	16.7%	16.5%	16.6%	17.4%	19.8%	27.6%
Q_{evap}	%	3.5%	3.9%	4.6%	5.8%	7.8%	12.8%
Q_{fin}	%	7.6%	7.2%	6.8%	6.3%	5.5%	4.2%
Q_{tube}	%	14.6%	13.7%	12.6%	11.3%	9.7%	7.1%
Q_{excess}	%	10.6%	9.4%	8.0%	6.4%	4.6%	2.4%
Q_{melt}	%	57.6%	58.7%	59.4%	59.2%	57.1%	48.2%
Total	%	100.0%	100.0%	100.0%	100.0%	100.0%	100.0%
Time	sec	127.3	149.1	181.7	236.0	344.3	687.1

Table 4-10: Energy distribution for a defrost cycle having a frost density of 450 [kg/m^3] and frost blockage of 30%

Variable	units	Frost Density = 450 [kg/m^3], Frost Blockage = 30%					
		100˚F	90˚F	80˚F	70˚F	60˚F	50˚F
Q_{in}	kJ	**1.359**	**1.348**	**1.351**	**1.382**	**1.499**	**2.236**
Q_{conv}	%	7.7%	9.0%	11.1%	14.3%	20.2%	37.0%
$Q_{conv\backslash tot}$	%	19.3%	19.1%	19.5%	20.9%	24.7%	38.7%
Q_{evap}	%	4.0%	4.7%	5.7%	7.2%	10.1%	18.3%
Q_{fin}	%	5.4%	5.0%	4.7%	4.2%	3.5%	2.1%
Q_{tube}	%	9.8%	9.1%	8.2%	7.3%	5.9%	3.5%
Q_{excess}	%	11.6%	10.1%	8.5%	6.6%	4.5%	1.8%
Q_{melt}	%	61.5%	62.0%	61.9%	60.5%	55.8%	37.4%
Total	%	100.0%	100.0%	100.0%	100.0%	100.0%	100.0%
Time	sec	244.8	289.9	359.6	479.9	745.7	2050.0

4.2.1 Time Required to Defrost

The way the energy is distributed during defrost affects the time needed to completely remove the frost from the coils. Using lower refrigerant temperatures for defrosting process may result in higher defrost efficiencies, but if defrosting takes longer and only has a slightly higher efficiency it may be suitable to use higher refrigerant temperatures that are less efficient to the process so the evaporator can return to service sooner. Below are plots of defrosting time with respect to frost density and frost blockage using refrigerant temperatures ranging from 50˚F to 100˚F.

Figure 4-9: Time to defrost for a frost density of 150 [kg/m^3] using different refrigerant temperatures

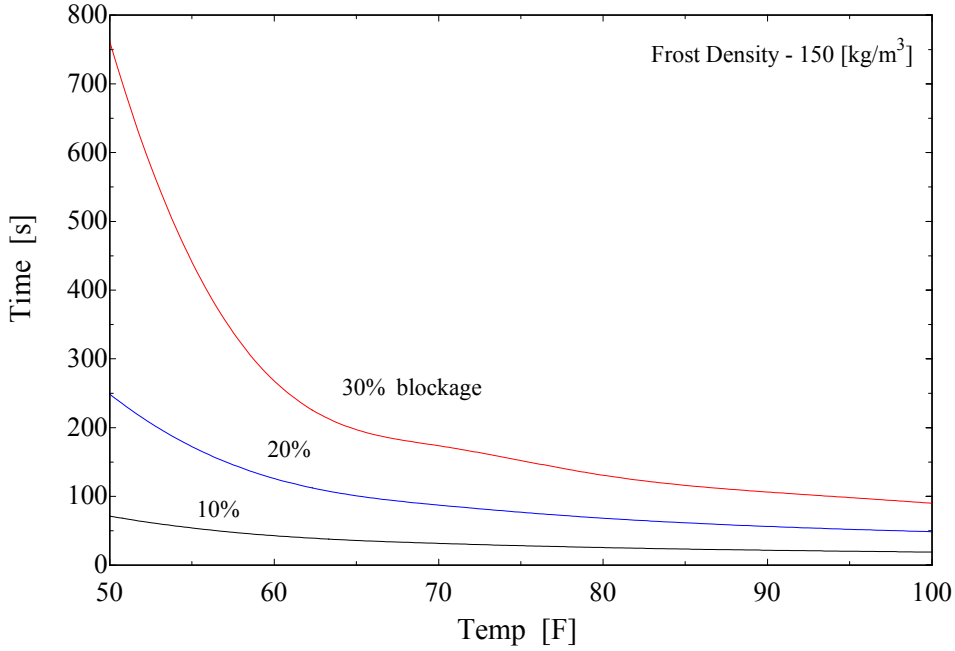

Figure 4-9, Figure 4-10, and Figure 4-11 show the same trends for the time required to melt the frost with respect to accumulated frost. At low frost accumulations, the time required is nearly linear. As the frost builds up, the defrost time increases significantly with decreasing hot gas temperature. The outside layer of frost, now further away from the heat source (evaporator fin) receives less energy because the interior frost nodes which have melted remain almost constant in temperature. The losses due to convection and evaporation of water into the freezer are almost as great as the amount of energy that the interior frost nodes supply to the outer frost nodes.

Figure 4-10: Time to defrost for a frost density of 300 [kg/m^3] using different refrigerant temperatures

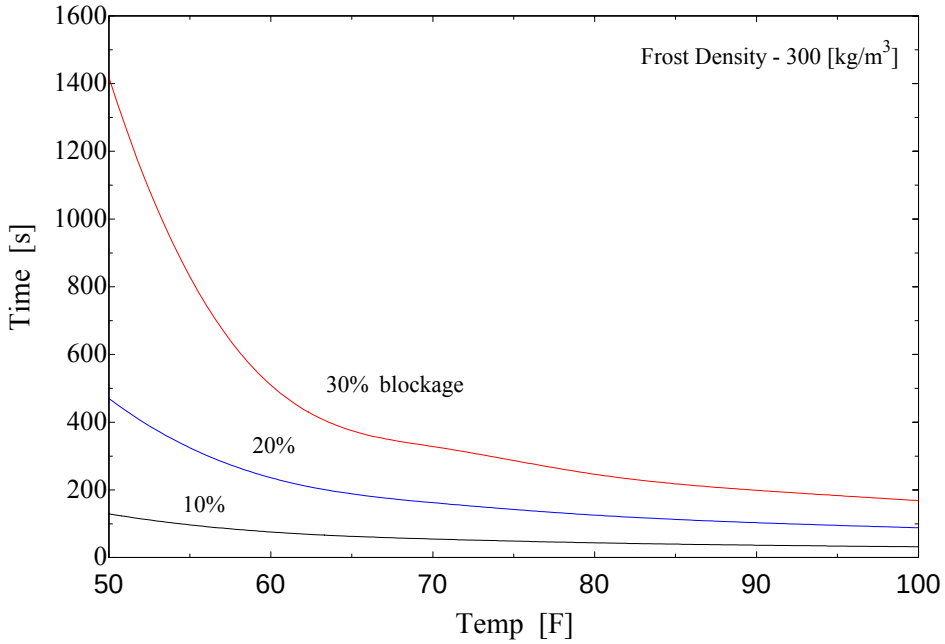

Figure 4-11: Time to defrost for a frost density of 450 [kg/m^3] using different refrigerant temperatures

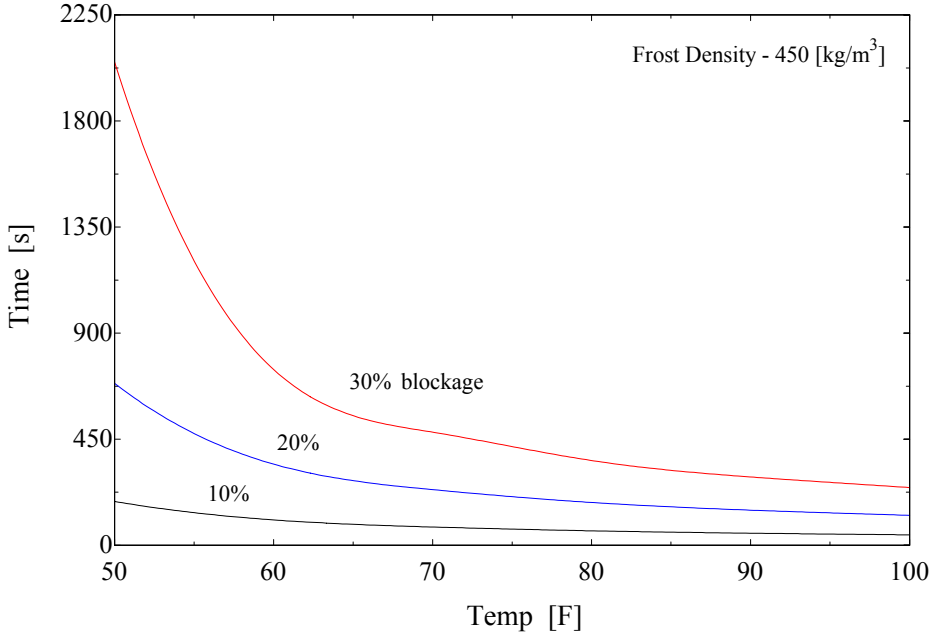

Figure 4-12: Time to defrost for a frost blockage of 10% using different refrigerant temperatures

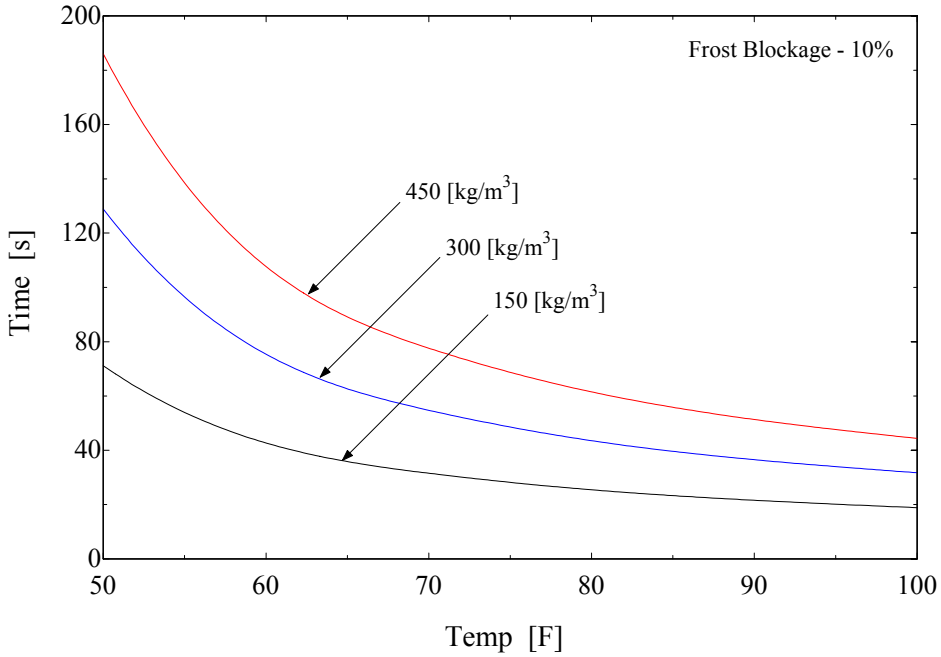

Figure 4-13: Time to defrost for a frost blockage of 20% using different refrigerant temperatures

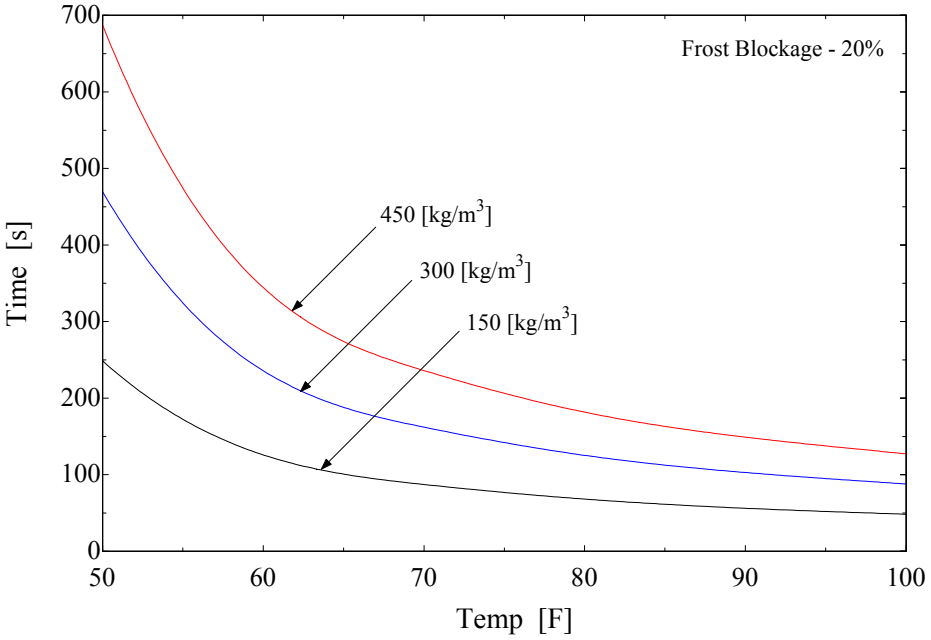

Figure 4-14: Time to defrost for a frost blockage of 30% using different refrigerant temperatures

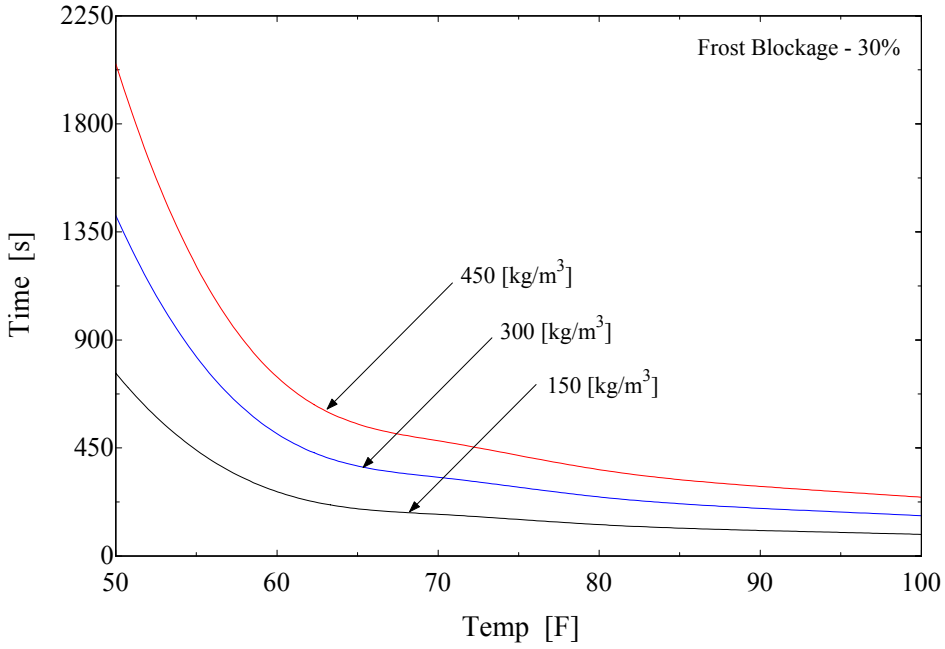

Figure 4-12, Figure 4-13, and Figure 4-14 are defrost times dependent on frost densities. The times for defrost are proportionate to the density of the frost. The time increments for defrost times at the same refrigerant temperatures are almost identical from 150 [kg/m^3] to 300 [kg/m^3] and 300 [kg/m^3] to 450 [kg/m^3]. The transfer of energy from frost node to frost node depends on the thermal conductivity of the frost. Since the thermal conductivity is based on frost density (Eq. 3-6), the variance between the defrost times should be equal because the equation used in correlating the frost conductivity to the density was fairly linear for the range of frost densities used.

4.2.2 Excess Energy after Melting is Complete

The section above shows the distribution of the supplied defrost energy only for the time it takes to melt the mass of frost on the fin. In practice, there are no reliable indicators to measure for determining when to terminate the supply of hot gas at the end of a defrost cycle (i.e. when the frost is gone).

Most defrost cycles in refrigeration systems are controlled with a timer. After a set load time, whether it is liquid feed hours or a set schedule, the evaporator goes into defrost mode. Once a defrost sequence begins, the evaporator initiates a “pump-down” during which the

residual cold refrigerant in the coil is boiled out of the evaporator by continued fan operation. Next, hot gas is supplied to the coil to begin the process of melting the accumulated frost. After the hot gas, the evaporator goes through a pre-chill process to cool down the coil with the cold refrigerant prior to re-starting fans.

With set timers for each sequence, the time needed to defrost the coils may be much less than the time set by the operators. If a coil defrosts within 15 minutes and the time allotted for hot gas is 45 minutes, there are significant energy penalties for operating the hot gas for the extra 30 minutes due to energy convecting from the coils to the freezer surroundings as well as the extra time the evaporator provides no cooling for the space.

The penalties for running a defrost cycle on set timers are of great concern. The model of the dry fin estimates the energy penalties for excess hot gas defrost by keeping track of the energy that enters the fin surface after a defrost cycle is complete. The excess time for a clock-driven defrost is found by subtracting the time recorded in the frosted fin model from the total amount of time allotted for the defrost. Tables of defrost efficiencies are provided for which hot refrigerant is supplied for 45 minutes. Accompanying the defrost efficiency tables are tables of excessive energy supplied to the coils for a set defrost cycle. The percentage of excessive energy is based on the ratio of supplied energy for a given time interval over the supplied energy needed to melt the frost, Q_{in}.

Table 4-11: Defrost efficiency for a set hot gas supply of 45 minutes for a frost density of 150 [kg/m^3] and frost blockage of 10%

Time [min]	**Frost Density = 150 [kg/m^3], Frost Blockage = 10%**					
	100˚F	90˚F	80˚F	70˚F	60˚F	50˚F
Melt time	**18.9 sec**	**21.6 sec**	**25.5 sec**	**31.5 sec**	**42.7 sec**	**1 min 11.2 sec**
5 minutes	8.6%	9.5%	10.6%	11.9%	13.6%	15.7%
10 minutes	5.8%	6.4%	7.3%	8.3%	9.6%	11.3%
15 minutes	4.3%	4.9%	5.5%	6.3%	7.4%	8.8%
20 minutes	3.5%	3.9%	4.5%	5.1%	6.0%	7.2%
25 minutes	2.9%	3.3%	3.7%	4.3%	5.1%	6.1%
30 minutes	2.5%	2.8%	3.2%	3.7%	4.4%	5.3%
35 minutes	2.2%	2.5%	2.8%	3.3%	3.9%	4.7%
40 minutes	1.9%	2.2%	2.5%	2.9%	3.5%	4.2%
45 minutes	1.7%	2.0%	2.3%	2.6%	3.1%	3.8%

Table 4-12: Percent of excess energy into defrost at various timed intervals for a frost density of 150 [kg/m^3] and frost blockage of 10%

Time	Frost Density = 150 [kg/m^3], Frost Blockage = 10%					
	100˚F	90˚F	80˚F	70˚F	60˚F	50˚F
Melt time	**18.9 sec**	**21.6 sec**	**25.5 sec**	**31.5 sec**	**42.7 sec**	**1 min 11.2 sec**
5 minutes	187%	173%	158%	141%	120%	91%
10 minutes	328%	303%	277%	247%	213%	166%
15 minutes	468%	433%	395%	354%	305%	241%
20 minutes	609%	563%	514%	460%	398%	316%
25 minutes	749%	693%	633%	567%	490%	391%
30 minutes	889%	823%	752%	673%	583%	466%
35 minutes	1030%	953%	870%	780%	675%	541%
40 minutes	1170%	1083%	989%	886%	768%	616%
45 minutes	1311%	1213%	1108%	993%	860%	691%

Viewing the tables above, it is noticed that the defrost efficiency continues to decrease as the time for hot gas increases, which is expected. As the losses continue through convecting from the fin surface to the freezer, the defrost efficiency decreases. Table 4-12 shows the percent of excess energy that is supplied during the hot gas time of the defrost cycle. Supplying hot gas for 45 minutes at the various temperatures shown above it is noticed that 13 separate defrosts could have been accomplished using the 100 ˚F refrigerant. At 50˚F, nearly 7 evaporators could have gone through defrost, assuming the frost density and percent of frost blockage were the same.

The rest of this section includes tables expressing the defrost efficiencies as well as the percentages of excessive supplied energy for simulations using different frost densities and frost blockages. The entries in the tables below that have no data mean that the frost has not yet melted for that time period.

Table 4-13: Defrost efficiency for a set hot gas supply of 45 minutes for a frost density of 150 [kg/m^3] and frost blockage of 20%

Time	Frost Density = 150 [kg/m^3], Frost Blockage = 20%					
	100˚F	90˚F	80˚F	70˚F	60˚F	50˚F
Melt time	**48.5 sec**	**56.2 sec**	**1 min 8.2 sec**	**1 min 27.3 sec**	**2 min 5.9 sec**	**4 min 8.6 sec**
5 minutes	18.4%	20.2%	22.3%	24.8%	27.7%	30.8%
10 minutes	12.9%	14.3%	15.9%	18.0%	20.5%	23.4%
15 minutes	9.9%	11.0%	12.4%	14.1%	16.3%	18.9%
20 minutes	8.0%	9.0%	10.2%	43.4%	13.5%	15.8%
25 minutes	6.8%	7.6%	8.6%	9.9%	11.5%	13.6%
30 minutes	5.8%	6.6%	7.5%	8.6%	10.1%	12.0%
35 minutes	5.1%	5.8%	6.6%	7.6%	8.9%	10.7%
40 minutes	4.6%	5.2%	5.9%	6.8%	8.0%	9.6%
45 minutes	4.1%	4.7%	5.3%	6.2%	7.3%	8.8%

Table 4-14: Percent of excess energy into defrost at various timed intervals for a frost density of 150 [kg/m^3] and frost blockage of 20%

Time	Frost Density = 150 [kg/m^3], Frost Blockage = 20%					
	100˚F	90˚F	80˚F	70˚F	60˚F	50˚F
Melt time	**48.5 sec**	**56.2 sec**	**1 min 8.2 sec**	**1 min 27.3 sec**	**2 min 5.9 sec**	**4 min 8.6 sec**
5 minutes	114%	103%	90%	75%	56%	25%
10 minutes	207%	187%	165%	141%	111%	64%
15 minutes	300%	272%	241%	207%	165%	103%
20 minutes	392%	357%	317%	273%	220%	143%
25 minutes	485%	441%	392%	339%	275%	182%
30 minutes	578%	526%	468%	405%	330%	221%
35 minutes	670%	610%	544%	471%	385%	261%
40 minutes	763%	695%	619%	537%	440%	300%
45 minutes	856%	779%	695%	603%	494%	340%

Table 4-15: Defrost efficiency for a set hot gas supply of 45 minutes for a frost density of 150 [kg/m^3] and frost blockage of 30%

Time	Frost Density = 150 [kg/m^3], Frost Blockage = 30%					
	100˚F	90˚F	80˚F	70˚F	60˚F	50˚F
Melt time	**1 min 29.9 sec**	**1 min 46.3 sec**	**2 min 10.7 sec**	**2 min 53.6 sec**	**4 min 27.9 sec**	**12 min 41.2 sec**
5 minutes	26.6%	28.9%	31.7%	34.8%	38.4%	-
10 minutes	19.1%	21.0%	23.4%	26.1%	29.4%	-
15 minutes	14.9%	16.5%	18.5%	20.9%	23.8%	26.9%
20 minutes	12.2%	13.6%	15.3%	17.4%	20.0%	23.0%
25 minutes	10.4%	11.6%	13.1%	14.9%	17.3%	20.0%
30 minutes	9.0%	10.1%	11.4%	13.1%	15.2%	17.7%
35 minutes	7.9%	8.9%	10.1%	11.6%	13.5%	15.9%
40 minutes	7.1%	8.0%	9.1%	10.4%	12.2%	14.4%
45 minutes	6.4%	7.2%	8.2%	9.5%	11.1%	13.2%

Table 4-16: Percent of excess energy into defrost at various timed intervals for a frost density of 150 [kg/m^3] and frost blockage of 30%

Time	Frost Density = 150 [kg/m^3], Frost Blockage = 30%					
	100˚F	90˚F	80˚F	70˚F	60˚F	50˚F
Melt time	**1 min 29.9 sec**	**1 min 46.3 sec**	**2 min 10.7 sec**	**2 min 53.6 sec**	**4 min 27.9 sec**	**12 min 41.2 sec**
5 minutes	75%	65%	54%	39%	20%	-
10 minutes	144%	127%	108%	86%	57%	-
15 minutes	213%	189%	163%	133%	94%	19%
20 minutes	282%	251%	218%	179%	131%	39%
25 minutes	351%	313%	273%	226%	168%	60%
30 minutes	420%	376%	328%	273%	205%	81%
35 minutes	489%	438%	382%	319%	241%	101%
40 minutes	558%	500%	437%	366%	278%	122%
45 minutes	627%	562%	492%	413%	315%	143%

Table 4-17: Defrost efficiency for a set hot gas supply of 45 minutes for a frost density of 300 [kg/m^3] and frost blockage of 10%

Time	Frost Density = 300 [kg/m^3], Frost Blockage = 10%					
	100˚F	90˚F	80˚F	70˚F	60˚F	50˚F
Melt time	**31.7 sec**	**36.5 sec**	**43.5 sec**	**54.7 sec**	**1 min 15.4 sec**	**2 min 8.9 sec**
5 minutes	15.7%	17.2%	19.1%	21.2%	23.9%	26.9%
10 minutes	10.9%	12.0%	13.5%	15.2%	17.5%	20.2%
15 minutes	8.3%	9.3%	10.4%	11.9%	13.8%	16.1%
20 minutes	6.7%	7.5%	8.5%	9.8%	11.4%	13.4%
25 minutes	5.6%	6.3%	7.2%	8.3%	9.7%	11.5%
30 minutes	4.9%	5.5%	6.2%	7.2%	8.4%	10.1%
35 minutes	4.3%	4.8%	5.5%	6.3%	7.5%	9.0%
40 minutes	3.8%	4.3%	4.9%	5.7%	6.7%	8.1%
45 minutes	3.4%	3.9%	4.4%	5.1%	6.1%	7.3%

Table 4-18: Percent of excess energy into defrost at various timed intervals for a frost density of 300 [kg/m^3] and frost blockage of 10%

Time	Frost Density = 300 [kg/m^3], Frost Blockage = 10%					
	100˚F	90˚F	80˚F	70˚F	60˚F	50˚F
Melt time	**31.7 sec**	**36.5 sec**	**43.5 sec**	**54.7 sec**	**1 min 15.4 sec**	**2 min 8.9 sec**
5 minutes	137%	124%	111%	96%	78%	52%
10 minutes	242%	221%	198%	173%	143%	103%
15 minutes	348%	318%	286%	250%	209%	154%
20 minutes	454%	415%	373%	327%	274%	205%
25 minutes	560%	512%	461%	404%	340%	257%
30 minutes	666%	609%	548%	481%	405%	308%
35 minutes	772%	706%	635%	558%	471%	359%
40 minutes	878%	803%	723%	635%	536%	410%
45 minutes	983%	900%	810%	712%	601%	461%

Table 4-19: Defrost efficiency for a set hot gas supply of 45 minutes for a frost density of 300 [kg/m^3] and frost blockage of 20%

Time	Frost Density = 300 [kg/m^3], Frost Blockage = 20%					
	100˚F	90˚F	80˚F	70˚F	60˚F	50˚F
Melt time	**1 min 28.0 sec**	**1 min 42.9 sec**	**2 min 5.3 sec**	**2 min 42.1 sec**	**3 min 55.8 sec**	**7 min 49.5 sec**
5 minutes	31.0%	33.5%	36.4%	39.7%	43.3%	-
10 minutes	22.7%	24.9%	27.4%	30.5%	34.0%	37.5%
15 minutes	18.0%	19.8%	22.0%	24.7%	28.0%	31.5%
20 minutes	14.8%	16.5%	18.4%	20.8%	23.8%	27.1%
25 minutes	12.6%	14.1%	15.8%	18.0%	20.7%	23.8%
30 minutes	11.0%	12.3%	13.9%	15.8%	18.3%	21.2%
35 minutes	9.8%	10.9%	12.3%	14.1%	16.4%	19.2%
40 minutes	8.8%	9.8%	11.1%	12.7%	14.8%	17.4%
45 minutes	7.9%	8.9%	10.1%	11.6%	13.6%	16.0%

Table 4-20: Percent of excess energy into defrost at various timed intervals for a frost density of 300 [kg/m^3] and frost blockage of 20%

Time	Frost Density = 300 [kg/m^3], Frost Blockage = 20%					
	100˚F	90˚F	80˚F	70˚F	60˚F	50˚F
Melt time	**1 min 28.0 sec**	**1 min 42.9 sec**	**2 min 5.3 sec**	**2 min 42.1 sec**	**3 min 55.8 sec**	**7 min 49.5 sec**
5 minutes	67%	58%	48%	36%	22%	-
10 minutes	127%	112%	96%	78%	55%	20%
15 minutes	188%	167%	144%	119%	89%	43%
20 minutes	248%	221%	192%	160%	122%	67%
25 minutes	309%	276%	240%	201%	156%	90%
30 minutes	369%	330%	289%	243%	189%	113%
35 minutes	430%	385%	337%	284%	223%	136%
40 minutes	491%	440%	385%	325%	256%	159%
45 minutes	551%	494%	433%	367%	289%	182%

Table 4-21: Defrost efficiency for a set hot gas supply of 45 minutes for a frost density of 300 [kg/m^3] and frost blockage of 30%

Time	Frost Density = 300 [kg/m^3], Frost Blockage = 30%					
	100˚F	90˚F	80˚F	70˚F	60˚F	50˚F
Melt time	**2 min 48.0 sec**	**3 min 18.6 sec**	**4 min 6.0 sec**	**5 min 28.0 sec**	**8 min 29.3 sec**	**23 min 38.0 sec**
5 minutes	42.1%	45.1%	48.5%	-	-	-
10 minutes	32.1%	34.9%	38.1%	41.7%	45.7%	-
15 minutes	26.0%	28.5%	31.4%	34.8%	38.7%	-
20 minutes	21.8%	24.0%	26.7%	29.8%	33.5%	-
25 minutes	18.8%	20.8%	23.2%	26.1%	29.6%	32.9%
30 minutes	16.5%	18.3%	20.5%	23.2%	26.4%	29.8%
35 minutes	14.7%	16.4%	18.4%	20.9%	23.9%	27.2%
40 minutes	13.3%	14.8%	16.7%	19.0%	21.8%	25.0%
45 minutes	12.1%	13.5%	15.2%	17.4%	20.1%	23.1%

Table 4-22: Percent of excess energy into defrost at various timed intervals for a frost density of 300 [kg/m^3] and frost blockage of 30%

Time	Frost Density = 300 [kg/m^3], Frost Blockage = 30%					
	100˚F	90˚F	80˚F	70˚F	60˚F	50˚F
Melt time	**2 min 48.0 sec**	**3 min 18.6 sec**	**4 min 6.0 sec**	**5 min 28.0 sec**	**8 min 29.3 sec**	**23 min 38.0 sec**
5 minutes	35%	28%	19%	-	-	-
10 minutes	77%	65%	52%	36%	15%	-
15 minutes	119%	102%	84%	63%	36%	-
20 minutes	161%	140%	117%	91%	58%	-
25 minutes	203%	177%	149%	118%	79%	8%
30 minutes	245%	215%	182%	145%	100%	19%
35 minutes	287%	252%	214%	172%	121%	31%
40 minutes	329%	290%	247%	200%	142%	42%
45 minutes	371%	327%	280%	227%	163%	54%

Table 4-23: Defrost efficiency for a set hot gas supply of 45 minutes for a frost density of 450 [kg/m^3] and frost blockage of 10%

Time	Frost Density = 450 [kg/m^3], Frost Blockage = 10%					
	100˚F	90˚F	80˚F	70˚F	60˚F	50˚F
Melt time	**44.4 sec**	**51.4 sec**	**1 min 1.5 sec**	**1 min 17.6 sec**	**1 min 47.7 sec**	**3 min 6.0 sec**
5 minutes	21.7%	23.7%	26.0%	28.7%	31.9%	35.3%
10 minutes	15.4%	17.0%	18.9%	21.2%	10.8%	27.3%
15 minutes	11.9%	13.2%	14.8%	16.8%	19.3%	22.3%
20 minutes	9.7%	10.8%	12.2%	13.9%	16.1%	18.8%
25 minutes	8.2%	9.2%	10.4%	11.9%	13.8%	16.3%
30 minutes	7.1%	8.0%	9.0%	10.4%	12.1%	14.4%
35 minutes	6.3%	7.0%	8.0%	9.2%	10.8%	12.8%
40 minutes	5.6%	6.3%	7.2%	8.3%	9.7%	11.6%
45 minutes	5.1%	5.7%	6.5%	7.5%	8.8%	10.6%

Table 4-24: Percent of excess energy into defrost at various timed intervals for a frost density of 450 [kg/m^3] and frost blockage of 10%

Time	Frost Density = 450 [kg/m^3], Frost Blockage = 10%					
	100˚F	90˚F	80˚F	70˚F	60˚F	50˚F
Melt time	**44.4 sec**	**51.4 sec**	**1 min 1.5 sec**	**1 min 17.6 sec**	**1 min 47.7 sec**	**3 min 6.0 sec**
5 minutes	106%	95%	84%	71%	55%	32%
10 minutes	191%	173%	153%	131%	359%	71%
15 minutes	276%	250%	222%	191%	156%	110%
20 minutes	361%	327%	291%	252%	207%	149%
25 minutes	446%	405%	360%	312%	258%	187%
30 minutes	532%	482%	430%	373%	308%	226%
35 minutes	617%	559%	499%	433%	359%	265%
40 minutes	702%	637%	568%	494%	410%	304%
45 minutes	787%	714%	637%	554%	460%	343%

Table 4-25: Defrost efficiency for a set hot gas supply of 45 minutes for a frost density of 450 [kg/m^3] and frost blockage of 20%

Time	Frost Density = 450 [kg/m^3], Frost Blockage = 20%					
	100˚F	90˚F	80˚F	70˚F	60˚F	50˚F
Melt time	**2 min 7.3 sec**	**2 min 29.1 sec**	**3 min 1.7 sec**	**3 min 56.0 sec**	**5 min 44.3 sec**	**11 min 27.1 sec**
5 minutes	40.1%	42.9%	46.1%	49.6%	-	-
10 minutes	30.5%	33.1%	36.2%	39.6%	43.5%	-
15 minutes	24.6%	27.0%	29.8%	33.0%	36.8%	35.5%
20 minutes	20.7%	22.8%	25.3%	28.3%	31.8%	31.7%
25 minutes	17.8%	19.7%	22.0%	24.7%	28.1%	28.6%
30 minutes	15.6%	17.4%	19.4%	22.0%	25.1%	26.1%
35 minutes	13.9%	15.5%	17.4%	19.8%	22.7%	23.9%
40 minutes	12.6%	14.0%	15.8%	18.0%	20.7%	22.1%
45 minutes	11.4%	12.8%	14.4%	16.5%	19.0%	20.6%

Table 4-26: Percent of excess energy into defrost at various timed intervals for a frost density of 450 [kg/m^3] and frost blockage of 20%

Time	Frost Density = 450 [kg/m^3], Frost Blockage = 20%					
	100˚F	90˚F	80˚F	70˚F	60˚F	50˚F
Melt time	**2 min 7.3 sec**	**2 min 29.1 sec**	**3 min 1.7 sec**	**3 min 56.0 sec**	**5 min 44.3 sec**	**11 min 27.1 sec**
5 minutes	43%	36%	28%	19%	-	-
10 minutes	88%	77%	64%	49%	31%	-
15 minutes	133%	117%	99%	79%	55%	35%
20 minutes	178%	157%	134%	109%	79%	52%
25 minutes	223%	197%	170%	139%	103%	68%
30 minutes	268%	238%	205%	169%	127%	84%
35 minutes	313%	278%	240%	199%	151%	101%
40 minutes	358%	318%	276%	229%	176%	117%
45 minutes	403%	358%	311%	259%	200%	134%

Table 4-27: Defrost efficiency for a set hot gas supply of 45 minutes for a frost density of 450 [kg/m^3] and frost blockage of 30%

Time	Frost Density = 450 [kg/m^3], Frost Blockage = 30%					
	100˚F	90˚F	80˚F	70˚F	60˚F	50˚F
Melt time	**4 min 4.8 sec**	**4 min 49.9 sec**	**5 min 59.6 sec**	**7 min 59.9 sec**	**12 min 25.7 sec**	**34 min 10.0 sec**
5 minutes	52.3%	55.6%	-	-	-	-
10 minutes	41.6%	44.7%	48.2%	52.1%	-	-
15 minutes	34.5%	37.5%	40.8%	44.7%	48.8%	-
20 minutes	29.5%	32.2%	35.4%	39.1%	43.2%	-
25 minutes	25.8%	28.3%	31.3%	34.8%	38.7%	-
30 minutes	22.9%	25.2%	28.0%	31.3%	35.1%	-
35 minutes	20.6%	22.7%	25.3%	28.4%	32.1%	35.6%
40 minutes	18.7%	20.7%	23.1%	26.1%	29.6%	33.1%
45 minutes	17.1%	19.0%	21.3%	24.1%	27.4%	30.9%

Table 4-28: Percent of excess energy into defrost at various timed intervals for a frost density of 450 [kg/m^3] and frost blockage of 30%

Time	Frost Density = 450 [kg/m^3], Frost Blockage = 30%					
	100˚F	90˚F	80˚F	70˚F	60˚F	50˚F
Melt time	**4 min 4.8 sec**	**4 min 49.9 sec**	**5 min 59.6 sec**	**7 min 59.9 sec**	**12 min 25.7 sec**	**34 min 10.0 sec**
5 minutes	17%	11%	-	-	-	-
10 minutes	47%	38%	28%	16%	-	-
15 minutes	78%	65%	51%	35%	14%	-
20 minutes	108%	92%	74%	54%	29%	-
25 minutes	138%	119%	97%	74%	43%	-
30 minutes	168%	145%	121%	93%	58%	-
35 minutes	199%	172%	144%	112%	73%	5%
40 minutes	229%	199%	167%	131%	88%	13%
45 minutes	259%	226%	190%	151%	103%	21%

Using lower refrigerant temperatures is more beneficial when operating with defrost cycles that utilize long hot gas periods. Though the efficiencies of the defrost cycle are

always higher at lower refrigerant temperatures, an attempt should be made observe the hot gas portion of the defrost cycle to determine a suitable time allotted for defrosting the coils of the evaporator.

Looking at Table 4-27 and at temperatures of 100˚F and 50˚F for 45 minutes, the efficiency of the defrost cycle is 31% for 50˚F, compared to just 17% for 100˚F. If an attempt is made to lower the hot gas supply time, an efficiency of up to 52% can be obtained for a refrigerant temperature of 100˚F, whereas using 50˚F does not even melt the entire mass of frost in this time period. For operators that like to run the hot gas supply longer to ensure that no frost is left can still get an efficiency of 41% using 100˚F refrigerant for 10 minutes which is a higher defrost efficiency for 50˚F refrigerant at any time.

4.3 References

Cole, R.A. *Refrigeration Loads in a Freezer Due to Hot Gas Defrost and Their Associated Costs*. ASHRAE Trans. 1989, vol. 95, part 2, 1149-1154.

Chapter 5 Atlas Cold Storage Experimentation and Results

5.1 Atlas Freezer Layout

Atlas Cold Storage, located in Jefferson Wisconsin is a storage facility that refrigerates and stores food items from around the state of Wisconsin. Atlas Cold Storage consists of two separate buildings and has multiple freezers in each. Depending on the freezer, the food items stored vary from frozen processed meat products, to ice cream, to fresh cranberries harvested from bogs across the state. Each freezer is made up of 'zones'. Zones are described as a number of evaporators that share the cooling load in a specified area.

The zones that were studied in the facility were 9, 10, and 11 located in freezer 11. Each zone consisted of only one Imeco evaporator, which was detailed in section 4.1. All three zones were used primarily for freezing and storing fresh cranberries. The figure below is the layout for building #2.

Figure 5-1: Atlas Cold Storage Plant #2 ammonia piping map

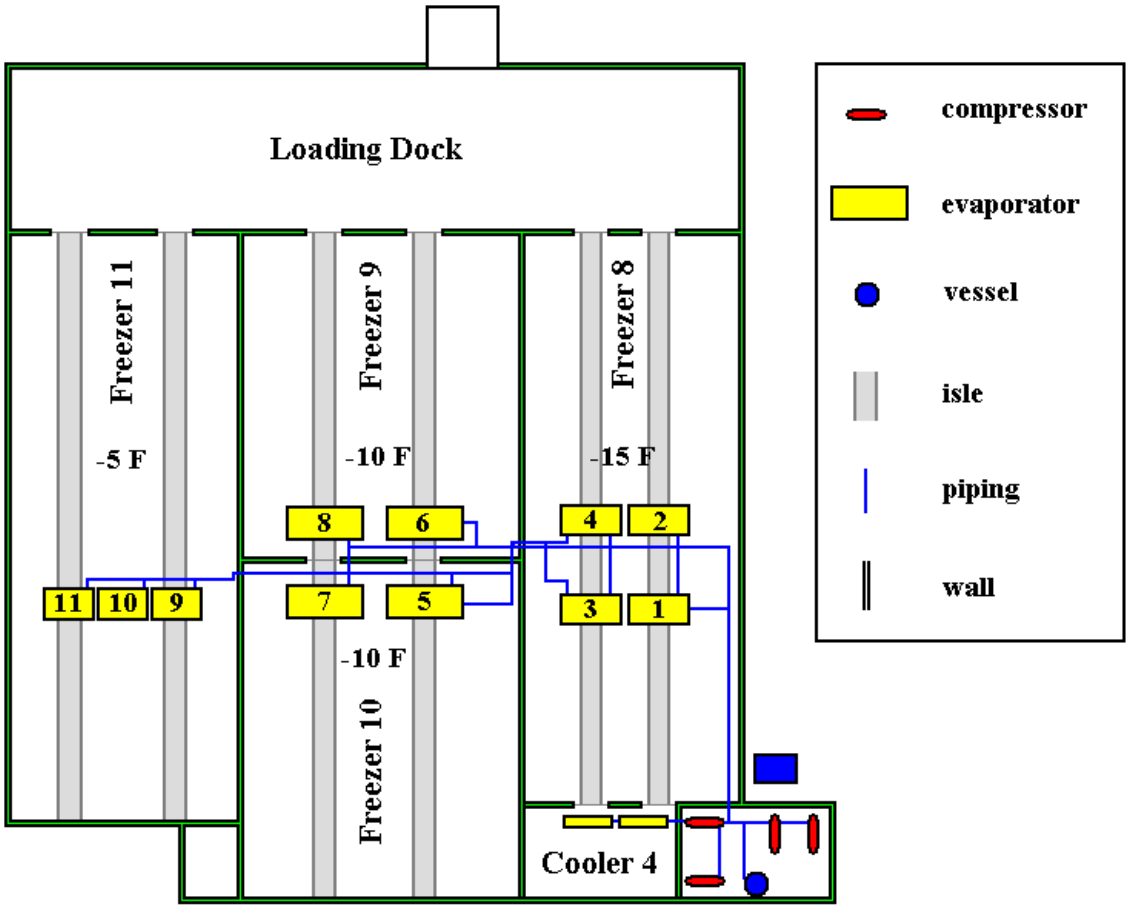

Freezer #11 is used primarily for freezing and storing cranberries straight from the bogs. The cranberries are unloaded from semi-trucks and stored in wooden crates with no covers. Depending on the time of year and the type of cranberry (white or red) the shipments are received having a temperature from anywhere between 45˚F to 70˚F. The cranberries are also very wet when they arrive since the harvesting process involves picking the berries from flooded bogs. Figure 5-2 through Figure 5-6 show the cranberries as they arrive and where they are stored.

Figure 5-2: Cranberries are unloaded into a hopper

Figure 5-3: From the hopper, the cranberries are stored in wooden crates

The cranberries come straight from the bogs by way of semi-trucks. The trailers are then hoisted in the air and the cranberries are dumped into a hopper. The hopper fills individual crates that are then stored in freezers.

Figure 5-4: Forklifts transport the crates to a freezer as is

Figure 5-5: The crates of cranberries are stacked up to the ceiling and left to freeze

Figure 5-6: The cranberries after a period of freezing release moisture and shrink

5.2 Atlas Data Collection

Field data for the evaporators in freezer #11 were taken during defrost operations in late September 2003. Late September is, typically, the period coinciding with shipments of white cranberries arriving for freezing. The freezer was only partially full of new cranberries. Some cranberries from the previous year were still stored in the freezer as well.

The evaporators in Freezer #11 were on a defrost cycle schedule that initiated after an eight-hour liquid feed time was accumulated. The defrosting sequence starts by allowing the fans to continue running for 10 minutes after the liquid refrigerant solenoid valve is closed in order to boil off any remaining refrigerant in the evaporator. After the boil off period, hot gaseous refrigerant passes through the evaporator coils at a 50˚F saturation temperature for 45 minutes in which the metal of the evaporator is raised and the frost is melted. At that point, a 15 minute cool-down period is initiated where cold refrigerant is again passed through the evaporator to lower the coil temperature. The fans start at the end of the cool down period and the evaporator once again assists in meeting the freezer load.

To collect data from a single evaporator defrosting, the liquid feed time of the evaporator was controlled manually in order to initiate a defrost sequence when desired. First, a bucket

was placed outside of the freezer where the defrost drain pipe exited the building to collect the defrost water from the evaporator. The evaporator was then manually initiated into a defrost sequence. Equipped with a stopwatch, spotlight, and a digital camera a forklift hoisted a cage in front of the evaporator for observation of the evaporator during the defrost process. Once the fans ceased, the hot gas supply was initiated and the stopwatch was started. Pictures of the defrost process (Figure 5-7 through Figure 5-16) were then taken during each two minute interval.

Figure 5-7: Initial amount of frost on evaporator coils

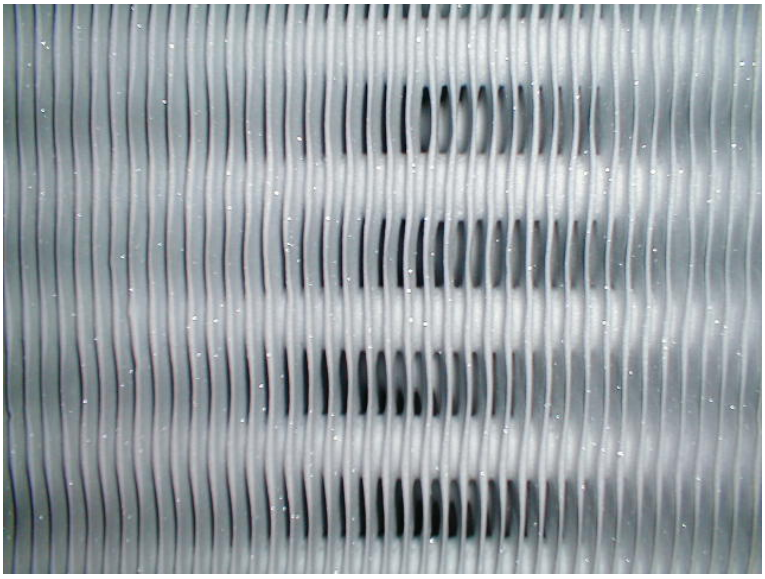

Figure 5-8: Face of evaporator with hot refrigerant circulating for 2 minutes

Figure 5-9: Coil face at 4 minutes of hot gas; melting frost is visible

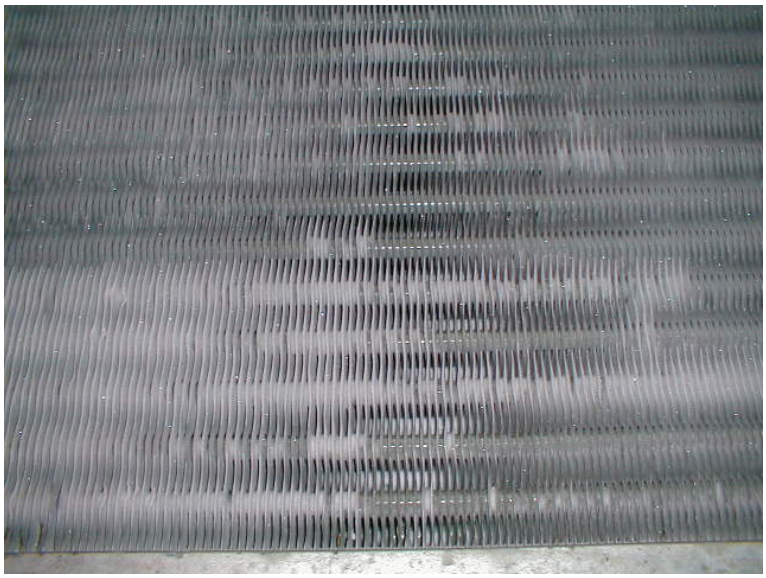

Figure 5-10: Evaporator face at 4-6 minutes of hot gas; the coil is mostly wetted

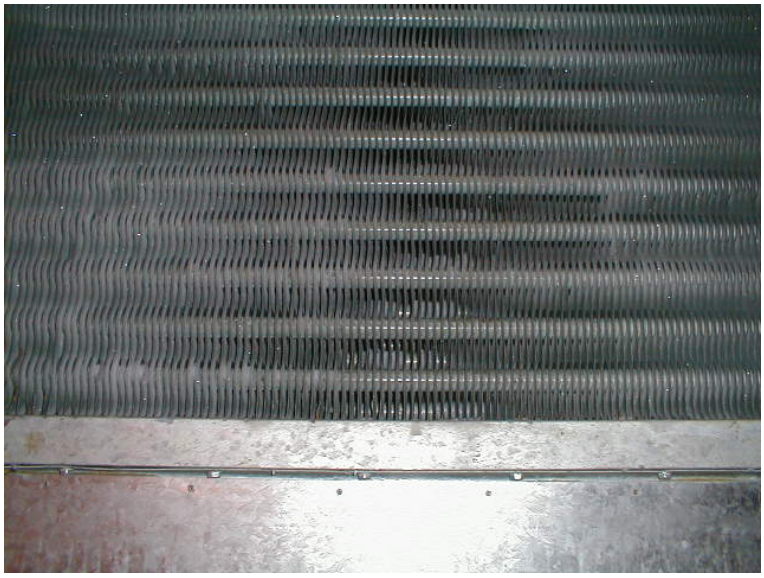

Figure 5-11: Drain pan at 6-8 minutes of hot gas; the water is draining at a fast rate

Figure 5-12: Evaporator face at 8-10 minutes of hot gas; the surface is frost free

Figure 5-13: Drain pan at 10-12 minutes of hot gas; the draining water is mostly halted minus a few drops

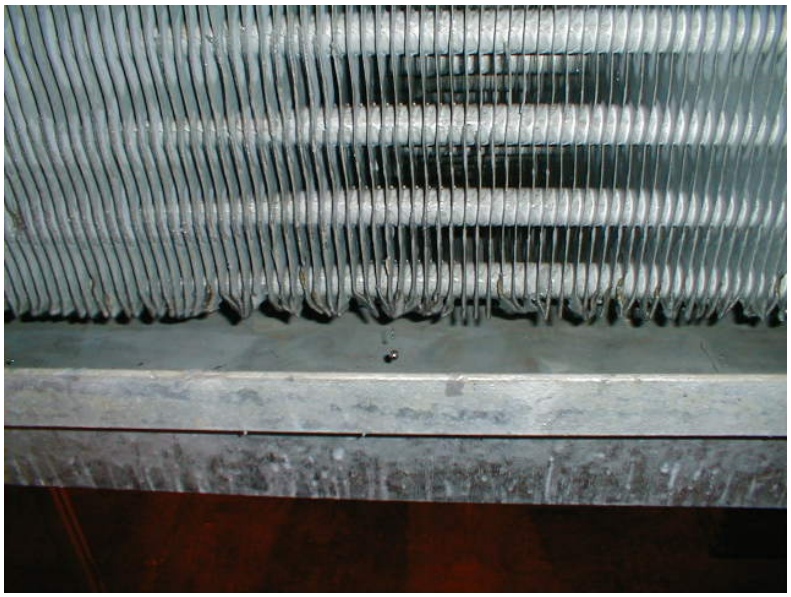

Figure 5-14: Face of evaporator at 12-14 minutes of hot gas supply; the surface is mostly dry

Figure 5-15: Drain pan at 12-14 minutes into hot gas defrost; the drain pan is drying out

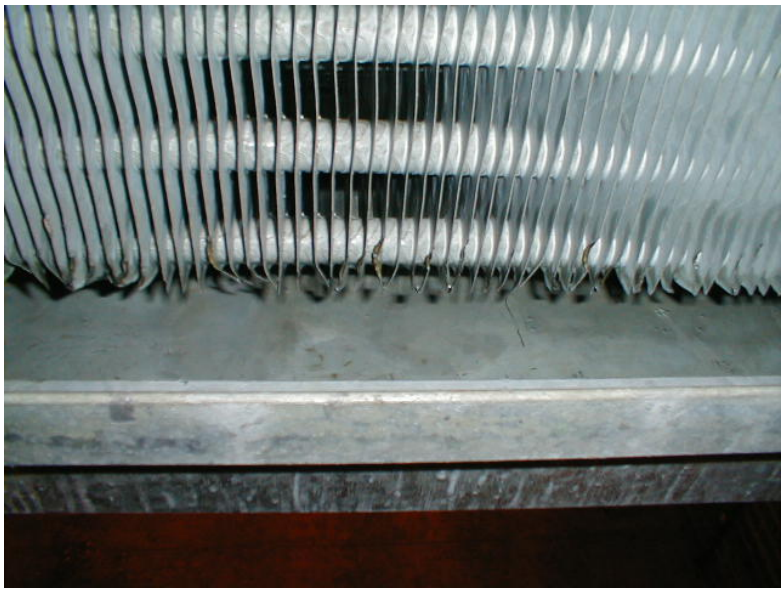

Figure 5-16: Drain pan at 14-16 minutes of hot gas; the pan is nearly dry

Examining the pictures above, the time it takes to melt the frost from the evaporator is in the range of 10 ~ 14 minutes. The excess hot refrigerant passing through the coils assists only in drying the drain pan for the remaining time. However, the excess hot gas supply significantly increases the cooling load in the freezer.

The water collected at the exit of the drain pipe was found to be 70 gallons. Knowing the volume of water and its density, the density of frost was calculated by using the evaporator's geometry and the pictures to estimate the amount of frost between the fins. A frost density of 300 [kg/m^3] was estimated, corresponding to a frost blockage of 23%.

5.3 Atlas Defrost Simulation

Simulations were conducted using the same frost properties as observed in zone 11. Table 5-1 shows the frost properties and freezer conditions that were used in the defrost simulation.

Table 5-1: Frost properties and freezer conditions used for Atlas defrost simulation in Freezer #11, Plant #2

Frost Properties and Freezer Conditions		
Frost density	300	kg/m^3
Frost blockage	23	%
Freezer temperature	5	˚F
Coil temperature	-20	˚F
Refrigerant temperature	50	˚F

The simulation indicated that the defrost period required a total of 10 minutes and 45 seconds – in good agreement with field observation. Table 5-2 shows the distribution of energy during a defrost cycle with respect to the total supplied energy for a single fin/tube assembly. The distribution of energy is the same for the scaled up evaporator. The energy supplied to defrost the evaporator in units of [MJ] is found by multiplying the Q_{in} for the model by a factor of 288,000 which scales up the model to represent the Imeco evaporator in section 4.1 having 2(*half fin/tube*) *x* 180(*# of tubes*) *x* 800(*# of fins*); the same factor that was calculated in section 4.2. Thus, the energy supplied (Q_{in}) for defrosting the whole evaporator is 272.1 [MJ].

Table 5-2: Distribution of supplied defrost energy in model

Model		
Frost Density = 300 [kg/m^3] Frost Blockage = 23%		
Variable	units	50˚F
Q_{in}	kJ	**0.9448**
Q_{conv}	%	29.4%
Q_{evap}	%	13.7%
Q_{fin}	%	4.9%
Q_{tube}	%	8.3%
Q_{melt}	%	43.7%
Total	%	100.0%
Time	sec	645.4

The actual "as-found" hot gas defrost dwell period for the evaporator at Atlas Cold Storage was set for 45 minutes. In order to simulate the amount of energy that was supplied

to the coils for the time remaining after ice was removed from the evaporator; the dry fin model described in Chapter 2 was used. The dry fin model was run for a time period of 45 minutes minus the time the frosted fin model took to complete (10 min 45 sec), which was 34 minutes and 15 seconds. Table 5-3 shows the amount of energy that is supplied for a 45 minute set hot gas supply time. Since the frost melted in 10 minutes and 45 seconds, data provided with the dry fin program starts at 15 minutes. As the time increases the amount of excess energy increases. This excess energy must then be removed by the refrigeration equipment, increasing the cost of providing the cooling.

Table 5-3: Excess amount of supplied energy for a defrost period of 45 minutes

Excess Supplied Energy [%]		
Frost Density = 300 [kg/m^3] Frost Blockage = 23%		
Melt time	**10 minutes 45.4 seconds**	
Time	**[%]**	**[MJ]**
Melt	**0.0%**	**0.0**
15 minutes	**16.1%**	**43.8**
20 minutes	**35.1%**	**95.5**
25 minutes	**54.1%**	**147.1**
30 minutes	**73.1%**	**198.8**
35 minutes	**92.0%**	**250.4**
40 minutes	**111.0%**	**302.1**
45 minutes	**130.0%**	**353.7**

Table 5-4 shows the defrost efficiency for a cycle that utilizes 45 minutes of hot refrigerant. At the moment the frost melts, the maximum defrost efficiency (defined in Eq. 4-9) that is reached is 43.7%. As the time increases the efficiency decreases, finally to a value of 19.0% for 45 minutes of hot gas.

Table 5-4: Defrost efficiency given at 5 minute intervals for a 45 minute defrost set time

Defrost Efficiency	
Time	**Frost Density = 300 [kg/m^3] Frost Blockage = 23%**
Melt time	**10 minutes, 45.4 seconds**
Melt	**43.7%**
15 minutes	**37.6%**
20 minutes	**32.3%**
25 minutes	**28.4%**
30 minutes	**25.3%**
35 minutes	**22.8%**
40 minutes	**20.7%**
45 minutes	**19.0%**

5.4 Calculation of Savings

The preceding section suggests that significant energy savings can be achieved resulting in lower operating costs at the Atlas Cold Storage facility by operating defrost cycles for shorter periods of time. Excess time allotted for defrosting hurts the performance of the compressors by introducing false loads on the system after the frost is melted from the coils of the evaporator.

Atlas Cold Storage's compressor setup is different for each plant. In Plant #1 compressors are run in a single stage, taking the refrigerant at suction pressure and compressing it to the condensing pressure. Plant #2 has a two stage setup. A booster (low stage) compressor receives refrigerant at the operating suction pressure and discharges the refrigerant at the intermediate pressure to an intercooler where the hot refrigerant discharging from the booster compressor(s) is de-superheated to the intercooler's saturation temperature. The saturated vapor at the intermediate temperature as well as the flash gas produced from the throttled refrigerant from the high-pressure receiver to the intercooler then travels to the (high stage) compressor. The high stage compressor then discharges to the operating condensing pressure.

The following calculations are presented as costs to perform a single defrost per 1000 ft^2 of evaporator surface area. The initial step in calculating savings for defrosts is to use general operating condensing pressures and temperatures typical for this plant. The operating condensing pressure varies throughout the year so breaking up the pressures into groups of months is necessary to get a better estimate of operating costs. Table 5-5 shows the operating condensing temperatures and pressures that are run throughout a typical year. The data used for the single stage and the two stage setup is different because the provided manufacturer's data used to compute the compressor ratings are in relation to the sets of condensing pressures and temperatures that are shown in Table 5-5.

Table 5-5: Condensing pressures and temperatures corresponding to the months of operation

Month	Jan	Feb	Mar	Apr	May	June	July	Aug	Sep	Oct	Nov	Dec
Condensing Pressure/Temperature Data for Single Stage Compressor Rating												
[psig]	130	130	150	150	150	170	170	170	150	150	150	130
[˚F]	77	77	84	84	84	91	91	91	84	84	84	77
Condensing Pressure/Temperature Data for Two Stage Compressor Rating												
[psig]	125.8	125.8	151.7	151.7	151.7	181.1	181.1	181.1	151.7	151.7	151.7	125.8
[˚F]	75	75	85	85	85	95	95	95	85	85	85	75

Knowing the condensing pressures and their corresponding temperatures makes it possible to estimate the compressor power requirements. The data sheet that notes the brake horsepower and refrigerant capacity for given suction and condensing pressures and temperatures are provided by compressors manufacturers. The data sheet for the 180S compressor used for the high stage compressor ratings in the two stage system appears in Figure 5-17 below. The efficiency of the compressors can be found by dividing the brake horse power by the refrigerant capacity (given as tons of refrigerant) for a given suction/condensing pressure operating range.

Figure 5-17: FES compressor rating data sheet for 180S compressor (high stage and economized ratings)

FES

Model 180S R717/3550 RPM

MODEL 180S (High Stage/Economized Ratings)

SUCTION TEMP [F] AND CORRESPONDING PRESSURE [psig]		CONDENSING TEMP [F] AND CORRESPONDING PRESSURE [psig]							
		75 125.8		85 151.7		95 181.1		105 214.2	
		H.S.	ECON.	H.S.	ECON.	H.S.	ECON.	H.S.	ECON.
-40	TR	46.3	54.6	44.4	53.5	42.5	52.3	40.3	50.8
*8.7	BHP	135.7	138.3	154.6	157.9	176	180.1	200.1	205.1
-35	TR	53.8	62.8	51.8	61.8	49.6	60.6	47.3	59.1
*5.4	BHP	138.4	141	157.4	160.7	178.9	183	203.1	208.1
-30	TR	62.2	72	60	70.9	57.7	69.7	55.2	68.2
*1.6	BHP	141.4	144	160.4	163.7	182	186.1	206.2	211.5
-25	TR	71.6	82	69.2	81	66.6	79.8	63.9	78.3
1.3	BHP	144.7	147.2	163.7	167	185.3	189.5	209.7	214.9
-20	TR	82.1	93	79.4	92	76.6	90.8	73.6	89.3
3.6	BHP	148.3	150.8	167.3	170.6	188.9	193.1	213.4	218.6
-15	TR	93.7	105.1	90.7	104.1	87.7	102.9	84.4	101.4
6.2	BHP	152.4	154.7	171.3	174.5	192.9	197.1	217.4	222.7
-10	TR	106.8	118.6	103.2	117.2	99.9	116	96.3	114.5
9	BHP	157	159.1	175.7	178.7	197.3	201.4	221.8	227.1
-5	TR	121.1	133.1	117	131.5	113.3	130.3	109.5	128.8
12.2	BHP	160.9	162.9	180.5	183.4	202.1	206.1	226.6	231.8
0	TR	136.7	148.6	132.7	147.5	128.2	145.8	123.9	144.3
15.7	BHP	165.3	167.1	185.5	188.2	207.4	211.2	231.9	236.9
5	TR	154.5	166.2	149.5	164.4	144.9	163.1	139.8	161.1
19.6	BHP	170	171.5	190.2	192.6	213.3	216.8	237.6	242.5
10	TR	173.8	184.9	167.7	182.4	162.9	181.4	157.6	179.6
23.8	BHP	171.2	172.4	195.4	197.5	218.4	221.7	244.5	249.1
15	TR	194.7	204.8	189	203.3	182.3	200.7	176.8	199.4
28.4	BHP	172.5	173.5	198.5	200.4	224	226.9	250.1	254.4
20	TR	217.3	226	211.4	224.9	204.7	222.9	197.5	220.3
33.5	BHP	174	174.6	200	201.5	229.6	232.2	256.1	260.1
25	TR	241.9	-	235.4	-	228.6	-	219.8	-
39	BHP	175.6	-	201.5	-	231.1	-	262.7	-
30	TR	268.4	-	261.4	-	254.2	-	246.3	-
45	BHP	177.3	-	203.2	-	232.8	-	266.2	-
35	TR	297	-	289.5	-	281.7	-	273.7	-
51.6	BHP	179.2	-	205.1	-	234.6	-	268	-
40	TR	327.8	-	319.7	-	311.3	-	302.7	-
58.6	BHP	181.3	-	207.1	-	236.6	-	269.9	-

Refrigeration capacity based on saturated suction conditions, the use of a shell and tube type economizer with high pressure liquid cooled to within 10 °F of saturated side port temperature, and 10 °F liquid subcooling from the condenser

* Inches of mercury below one standard atmosphere (29.92")

Ratings include use of external cooling systems

The first sets of calculations are representative of a single stage compressor. For a single stage 450 hp compressor operating at a suction temperature of 0˚F (-17.8˚C) and a condensing pressure of 130 psig the compressor efficiency rating is 1.2 [hp/ton]. When the head pressure increases to 150 psig the compressor efficiency decreases to 1.33 [hp/ton]. In

the summer months the compressor operates at 1.48 [hp/ton] when the condensing pressure is 170 psig.

Next, the excess load that the fin model predicts is scaled to 1000 ft^2 (92.9 [m^2]). The fin model has an outside tube diameter of 1.05 inches (2.667 [cm]) and an outside fin diameter of 3.05 inches (7.747 [cm]). The fin spacing in the model is set to three fins per inch, making the tube length 0.16164 inches (0.41 [cm]) (subtracting half the fin thickness due to geometrical conditions). The total surface area of the fin tube assembly is therefore 6.974 in^2 (45 [cm^2]). To approximate 1000 ft^2 of evaporator surface area the model would have to be duplicated 20,648 times for a total of 10,324 single tube/fin assemblies. For example, if an evaporator had 120 total tubes, the number of fins that would be needed to approximate 1000 ft^2 of evaporator area would be 86 if the tubes were spaced 2 inches apart.

The cost per kilowatt hour to operate the compressor is taken to be 3 cents. (Note that the cost of electricity for residential applications in the Madison area is currently about 10 cents per kilowatt hour). The compressor load, given in kilowatt hours, is multiplied by the cost to obtain the price for a defrost for a given time period.

Figure 5-18 is the cost to melt frost that has a density of 300 [kg/m^3] and a frost blockage of 20% for 1000 ft^2 (92.9 [m^2]) of evaporator surface area using a refrigerant temperature of 50˚F (10˚C). The estimate includes the changing condensing pressures throughout the year.

Figure 5-18: Cost to defrost 1000 ft^2 of evaporator surface area at different operating head pressures (single stage compression)

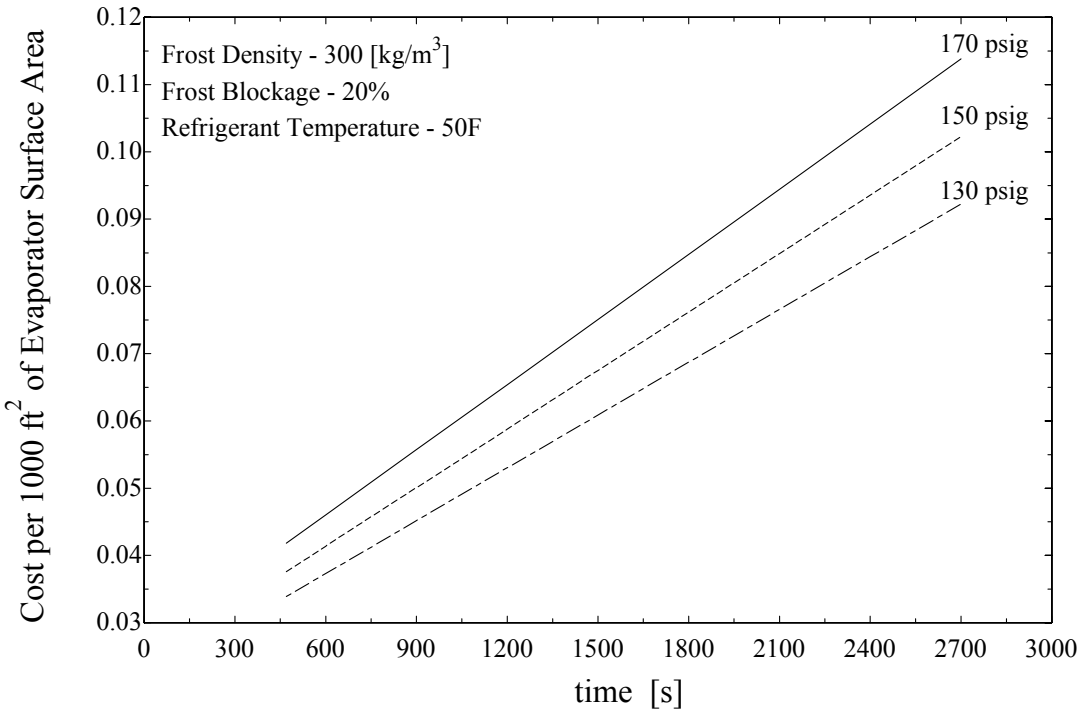

Figure 5-18 shows that as time increases the cost to defrost also increases, which is intuitive. What is noticed is that as the condensing pressure increases, the cost to defrost increases at a greater rate than the lower operating pressures. Excessive defrosting (i.e., operating the defrost cycle after ice has been removed from the evaporator) has a greater impact on the cost while operating in the summer months than any other time of the year even though frost conditions at initiation of defrost are the same.

Figure 5-18 shows the impact that the condensing pressure has on the cost of defrosting for a single refrigerant temperature. Figure 5-19, Figure 5-20, and Figure 5-21 show different refrigerant temperatures at a set condensing pressure. The trends are similar in all three figures, however, when the condensing pressures are lower, which is typical in the winter months, the maximum achievable defrost temperatures decrease. The cost of defrosting is also reduced and the energy benefits of lowering the refrigerant temperature for defrosting also diminish.

Figure 5-19: Cost to defrost 1000 ft^2 of evaporator surface area at 170 psig condensing pressure for a frost density of 300 [kg/m^3] and frost blockage of 20%

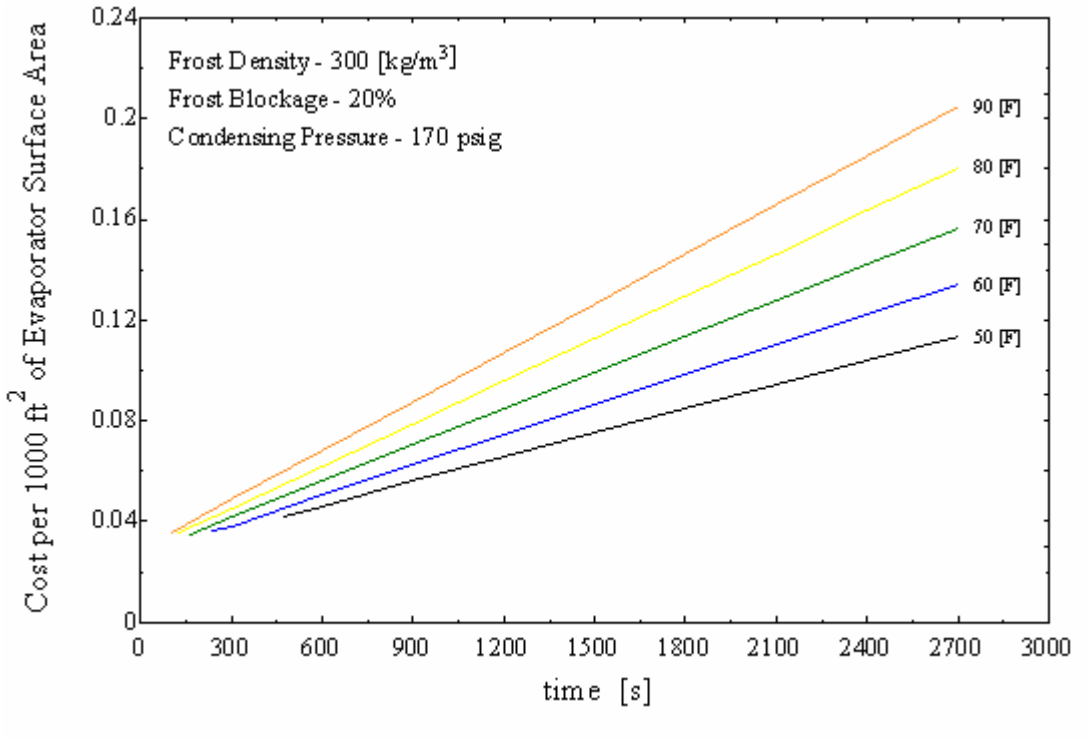

Figure 5-20: Cost to defrost 1000 ft^2 of evaporator surface area at 150 psig condensing pressure for a frost density of 300 [kg/m^3] and frost blockage of 20%

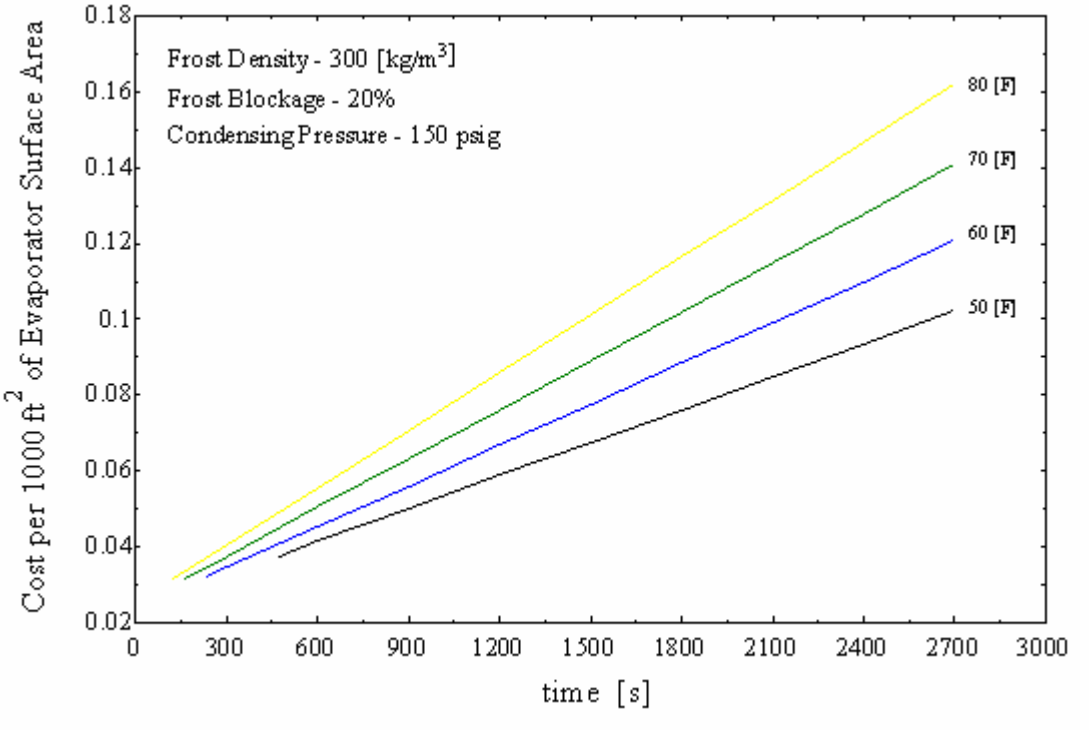

Figure 5-21: Cost to defrost 1000 ft^2 of evaporator surface area at 130 psig condensing pressure for a frost density of 300 [kg/m^3] and frost blockage of 20%

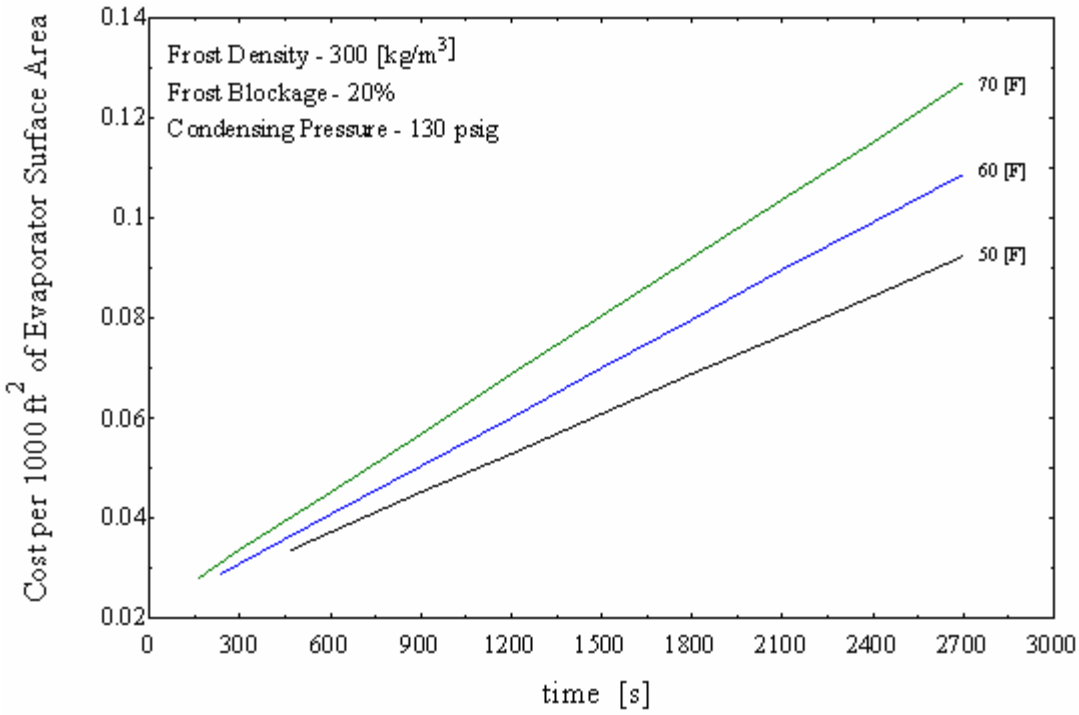

Figure 5-22 is a plot showing the defrost cost as frost blockage varies from 10% to 30% while all other variables remain constant. The lines for the different blockages start at different times because the time to achieve a full defrost increases as the amount of frost increases; however, once the fin is dry the rate at which the price of defrost increases at the same rate for all three frost amounts. The rate of defrost cost is dependant on the refrigerant temperature, but the amount of frost dictates the lowest cost one can achieve per defrost.

Figure 5-22: Cost to defrost 1000 ft^2 of evaporator surface area for a frost density of 300 [kg/m^3] at 170 psig condensing pressure

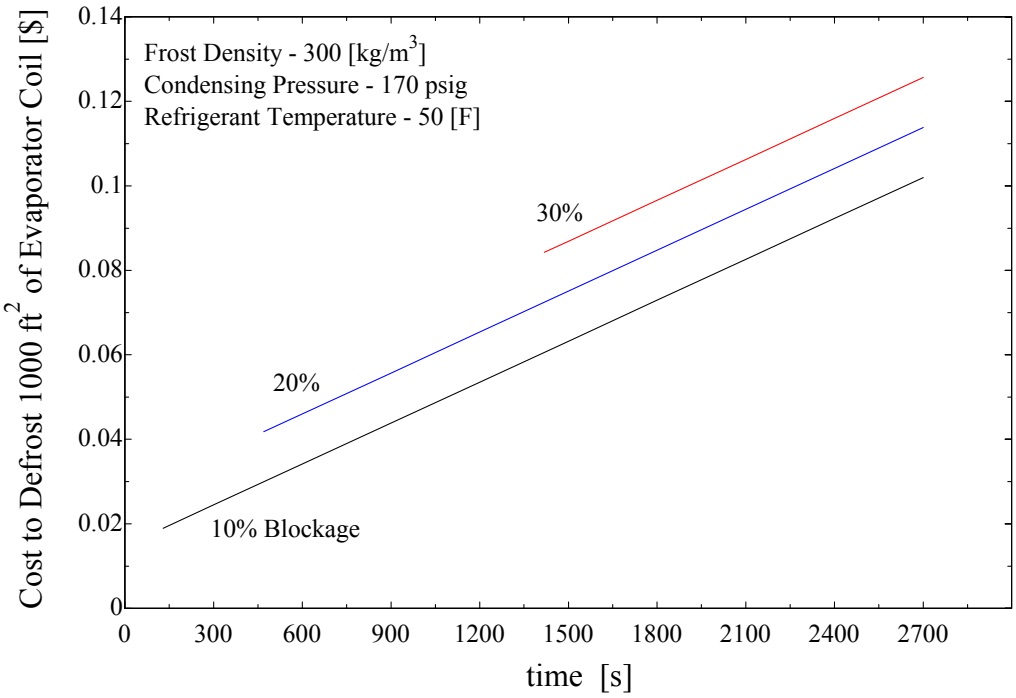

To estimate a savings for Plant #1 at Atlas Cold Storage, a single stage compressor setup operating at a suction temperature of 0 ˚F (-17.7 ˚C) and a condensing pressure of 150 psig (the intermediate condensing pressure experienced throughout a typical year) running a 45 minute defrost for a typical frost density of 300 [kg/m^3] and frost blockage of 20% is taken. Plant #1 is much older than Plant #2 and was built in small sections; adding on to the building when needed. The evaporators in Plant #1 are of all different sorts. To find estimate an evaporator area representative of the mean size found in Plant #1, the Imeco evaporators found in Freezer #11 at Plant #2 are scaled down by ¼ to represent a three fan, 8,000 ft^2 coil area evaporator. A cost to defrost per 1000 ft^2 of evaporator area in Plant #1 with an operating freezer temperature of 0 ˚F for 45 minutes is $0.102. The cost to defrost per 1000 ft^2 to melt the frost is $0.038. A savings potential is then approximated to be $0.064 for every 1000ft^2 of evaporator area. For an evaporator having ¾ the capacity of the large evaporators that are located in Freezer #11, the savings per evaporator is around $0.53. Adding up the total number of defrosts Plant #1 completes in 2003 (given in Table 5-6) a total savings can be estimated. Table 5-6 shows a total of 2,795 defrosts in 2003.

Multiplying the number of defrosts by the savings for each defrost per evaporator yields a total savings for Plant #1 of $1,481.

Table 5-6: Number of defrosts in 2003 for evaporators located Plant #1 at Atlas Cold Storage

		Jan	Feb	Mar	Apr	May	June	July	Aug	Sep	Oct	Nov	Dec	Total
PLANT 1	13	16	11	15	14	18	20	19	24	21	18	10	5	191
	14	2	0	3	2	6	16	19	25	16	15	7	1	112
	15	0	0	2	1	0	1	3	1	37	44	45	13	147
	16	4	7	5	4	10	7	11	4	64	65	55	18	254
	17	C	O	O	L	E	R							0
	18	C	O	O	L	E	R							0
	19	2	1	1	6	9	9	9	12	8	4	6	6	73
	20	25	23	5	5	9	9	9	11	8	5	3	1	113
	21	3	3	5	6	6	10	15	17	9	17	15	4	110
	22	1	1	1	3	4	2	2	3	2	2	4	3	28
	23	0	0	0	0	0	0	0	0	0	0	0	0	0
	24	7	24	29	23	26	14	16	16	8	39	40	5	247
	25	28	24	29	25	29	29	26	29	25	30	15	9	298
	26	16	20	21	17	24	35	39	43	37	34	39	44	369
	27	C	O	O	L	E	R							0
	28	C	O	O	L	E	R							0
	29	7	5	1	4	5	9	10	10	5	16	19	2	93
	30	7	10	13	7	13	17	18	19	8	19	19	4	154
	31	7	7	16	15	18	19	22	10	5	5	3	5	132
	32	7	7	11	9	13	18	20	8	5	5	2	3	108
	33	29	18	21	17	17	14	14	22	19	18	19	22	230
	34	3	5	10	7	12	19	17	18	16	13	11	5	136

Calculating the costs of a two stage system is similar to the one stage system. The booster (low stage) compressor ratings are found by finding the operating suction pressure and the intermediate pressure in which the booster supplies the high stage compressor with. The high stage compressor rating is found from the incoming intermediate pressure and the operating head pressure for the system. There are two energy penalties for a two stage compression system because the high stage compressor not only has the load from the freezer but also the added work from the booster compressor.

Figure 5-23 shows the cost to defrost 1000 ft^2 of evaporator area for the data collected at Atlas Cold Storage. At the time of defrost, the amount of money that it takes to complete the defrost is $0.0717, assuming the operating condensing pressure in September was 151.7 psig,

corresponding to a temperature of 85 ˚F (29.44 ˚C). At 45 minutes the cost of defrost goes up to $0.1649 for every 1000 ft^2 of evaporator area. There are three evaporators in freezer #11 with a total surface area of 33,357 ft^2. A savings for each defrost for the three evaporators could have been $3.11 if the defrost time was cut to the time it took to melt the frost.

Figure 5-23: Cost to defrost 1000 ft^2 of evaporator surface area at different operating head pressures for data observed at Atlas Cold Storage

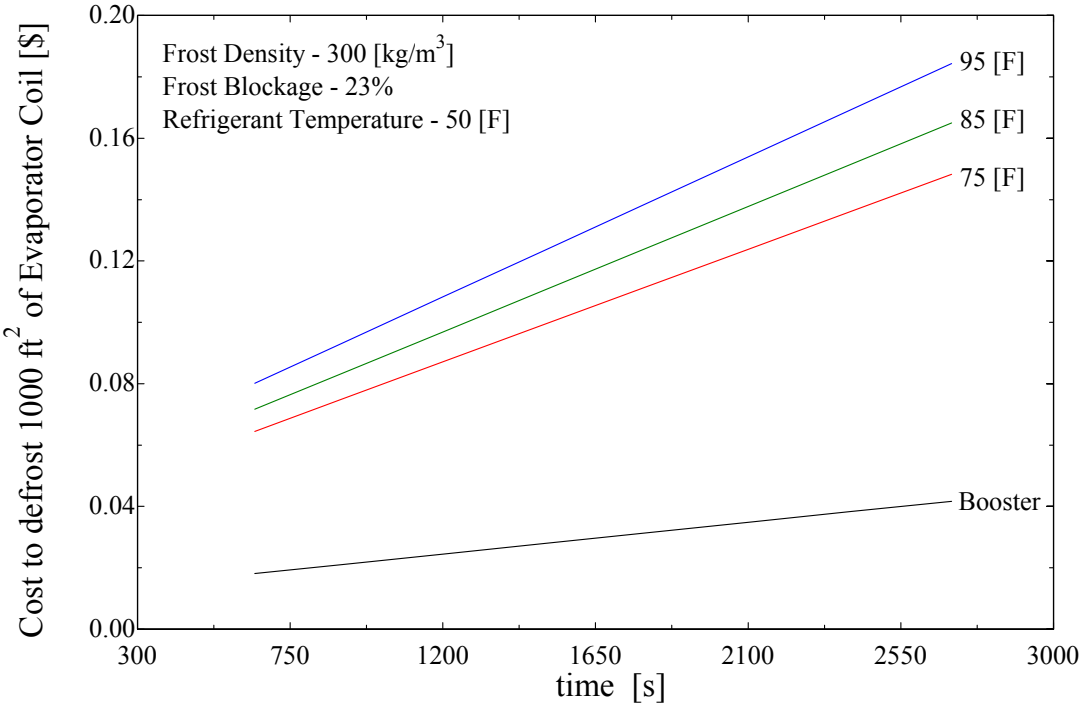

Energy savings for an entire year for Freezer #11 can be estimated by viewing the number of defrosts that the freezer goes through in an entire year. Table 5-7 shows the evaporators located in Freezer #11 and their number of defrosts on a month to month basis. If each evaporator had a saving potential of $1.04 per defrost, and the average operating condensing pressure was 151.7 psig, as is typical in the spring and fall months, a total savings for the freezer could reach $636.51.

Table 5-7: Number of defrosts in 2003 for evaporators located in freezer #11 at Atlas Cold Storage

	Jan	Feb	Mar	Apr	May	June	July	Aug	Sep	Oct	Nov	Dec	Total
9	2	0	7	8	13	8	4	1	66	45	41	11	**206**
10	0	0	3	2	0	0	0	0	64	53	43	3	**168**
11	16	6	16	5	16	14	7	5	51	55	39	10	**240**

In Plant #2 there are a total of eleven evaporators, 5 are the Imeco evaporators that are representative of the ones located in Freezer #11 and the remaining six are Imeco evaporators that have ¾ the capacity of the ones located in Freezer #11. A total of 1,594 defrosts were completed in 2003 at Plant #2. 814 defrosts were for the Imeco evaporators that are representative of the evaporators located in Freezer #11, and 780 defrosts were completed for the six remaining evaporators. By scaling the savings by 0.75 for the smaller evaporators and summing the total with the larger evaporators, a total savings for plant #2 in 2003 could have reached as high as $1,455. Combining the total with the one estimated for Plant #1 gives a total cost savings for Atlas Cold Storage of approximately $2,936.

Figure 5-24 shows the cost to defrost 1000 ft^2 of evaporator coil area operating at a condensing pressure of 181.1 psig (corresponding to a condensing temperature of 95˚F).

Figure 5-24: Cost to defrost 1000 ft^2 of evaporator coil area for a frost density of 300 [kg/m^3] and frost blockage of 20% operating at a condensing pressure of 181.1 psig

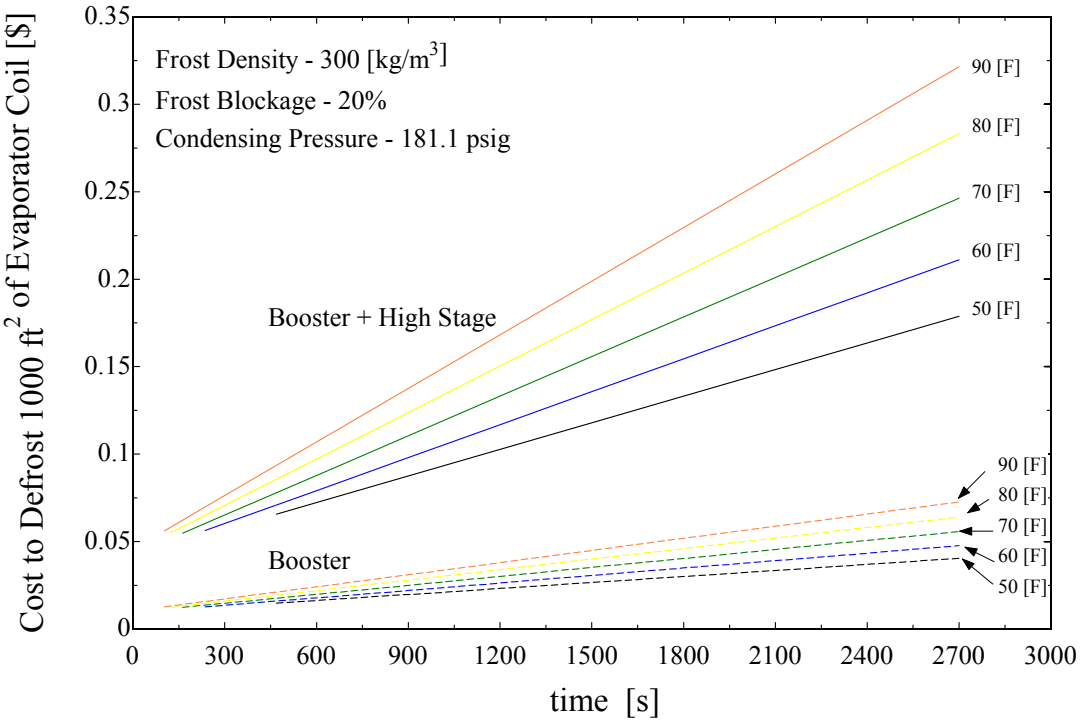

Looking at Figure 5-24, it is seen that for these frost properties and compressor setup while operating during the summer months (increased head pressure) the savings for a defrost can be as high as 9 cents per 1000 ft^2 of evaporator area when using a refrigerant temperature of 50˚F (10˚C) to defrost if the time is decreased from 45 minutes to about 7 minutes. If a high refrigerant temperature is used (90˚F) then the savings reach 26 cents per 1000 ft^2 of evaporator coil area. The different frost properties and operating condensing pressures have similar trends, but the savings potential is greater with higher operating condensing pressures. Though the cost to defrost is based on 1000 ft^2 of coil surface area, it can also be applied to the floor area in a freezer space as well. To get the cost of operating a defrost for 1000 ft^2 of freezer floor area, a relationship of the evaporator surface area of the floor space has to be made. At Atlas Cold Storage three evaporators are utilized, each having a coil surface area of 11,119 ft^2. The freezer in which the evaporators are operated has a floor area of 30,225 ft^2. The cost to operate a defrost for 1000 ft^2 of freezer floor area is therefore a ratio of 1.104 of the cost to defrost 1000 ft^2 of evaporator area. The cost to defrost per cubic foot of freezer area is done in the same manner. Atlas Cold Storage's freezer in which the three evaporators operate has a space of 876,525 ft^3. The cost to defrost per 1000 ft^3 of freezer area is a ratio of 0.038 of the cost to defrost 1000 ft^2 of evaporator area.

5.5 Comparisons with Data in the Literature

In a paper presented by R.A. Cole, *Refrigeration Loads in a Freezer Due to Hot Gas Defrost and Their Associated Costs*, a review is done on a the heating requirements for a copper tube/aluminum fin coil that was studied by Stoecker (1983).

Tests of a coil having 6 rows of tubes in the direction of the air flow and 14 tubes in each row with fins spaced ¼ inch apart across a 28 inch wide span, a crude estimate of the energy required to melt 20.1 lbs of frost from the coils was done. Table 5-8 is the energy required to melt the frost from the coil assuming that the condensate is heated to 45˚F and the coil is heated to 55˚F.

Table 5-8: Table of distributed energy for a copper tube/aluminum fin coil (R.A. Cole)

Item	Mass		Energy		Ratio [%]
	[lb_m]	[kg]	[Btu]	[kJ]	
Aluminum Fins	54.5	24.7	629	664	13.9%
Copper Tubes	93.0	42.2	471	497	10.4%
Warming the Frost	20.1	9.1	294	310	6.5%
Thawing the Frost	20.1	9.1	2880	3038	63.5%
Warming the Water	20.1	9.1	260	274	5.7%
Total	-	-	4534	4783	-

Cole estimates the defrost efficiency of 76% because the heating of the metal in the evaporator requires 1161 [kJ] or roughly 24% of the total energy required, assuming no other losses associated with the defrost. From the frosted fin model, a defrost efficiency of 79.7% is found if the convective and evaporative losses are neglected. If the convective and evaporative losses were not included in the total energy supplied, an efficiency of 73% would be obtained. Given the frost conditions and coil material the two tables are in good agreement with the amount of energy that is distributed to the evaporator coils.

Table 5-9: Distribution of defrost energy from the frosted fin model using same evaporator materials and frost conditions as Table 5-8

Item	Variable	Mass		Energy [kJ]	Ratio [%]
		[lb_m]	[kg]		
Frost/Metal	Q_{in}	167.6	76	6499.0	-
Frost	Q_{melt}	20.1	9.1	3561.9	54.8%
Frost	Q_{evap}	20.1	9.1	495.4	7.6%
Frost	Q_{conv}	20.1	9.1	1121.3	17.3%
Aluminum	Q_{fin}	54.5	24.7	749.1	11.5%
Copper Tubes	Q_{tube}	93.0	42.2	570.3	8.8%

In W.F. Stoecker's, *Energy Considerations in Hot-Gas Defrosting of Industrial Refrigeration Coils,* the energy required to melt 9.1 [kg] (20.1 [lb_m]) of frost on a coil weighing 66.9 [kg] (147.5 [lb_m]) was found to be 4783 [kJ] (4534 [Btu]). The energy supplied to the evaporator was from hot gaseous refrigerant (R-22 with a latent heat of 202 [kJ/kg] (87 [Btu/lb_m])) passing though the coils at 0.136 [kg/s] (18 [lb_m/min]). The analysis

uses only the heating of the coils and the warming and melting of the frost as the factors. Convective and evaporative energy losses are not accounted for.

To compare the frosted fin model with the Stoecker data, the model was run using frost properties that would yield the same amount of frost that was noted in the literature.

The frosted fin model was used applying two different methods to supply the defrost energy (Q_{in}). The first model used the convective coefficient method that was used for all of the previous data. The second method was to implement a mass flow rate of R-22 with the enthalpy of vaporization at the specified refrigerant temperature as what was done by Stoecker (1983). Table 5-10 and Table 5-11 show the amount of energy and their distribution with respect to the total energy supplied.

Table 5-10: Frosted fin model using 'lumped' convection coefficient for supplied energy

Item	Variable	Mass		Energy		Ratio [%]
		[lb_m]	[kg]	[Btu]	[kJ]	
Frost/Metal	Q_{in}	167.6	76	6160.2	6499.0	-
Frost	Q_{melt}	20.1	9.1	3376.2	3561.9	54.8%
Frost	Q_{evap}	20.1	9.1	469.6	495.4	7.6%
Frost	Q_{conv}	20.1	9.1	1062.8	1121.3	17.3%
Aluminum	Q_{fin}	54.5	24.7	710.0	749.1	11.5%
Copper	Q_{tube}	93.0	42.2	540.6	570.3	8.8%

Table 5-11: Frosted fin model using a mass flow rate of refrigerant

Item	Variable	Mass		Energy		Ratio [%]
		[lb_m]	[kg]	[Btu]	[kJ]	
Frost/Metal	Q_{in}	167.6	76	6203.0	6544.2	-
Frost	Q_{melt}	20.1	9.1	3376.2	3561.9	54.8%
Frost	Q_{evap}	20.1	9.1	398.3	420.2	6.5%
Frost	Q_{conv}	20.1	9.1	1061.3	1119.7	17.2%
Aluminum	Q_{fin}	54.5	24.7	825.7	871.7	13.4%
Copper	Q_{tube}	93.0	42.2	540.6	570.3	8.8%

Both methods of the frosted fin program are in good agreement with the energy required to melt the frost and heat the coils reported by Stoecker, as presented in Table 5-8.

In the paper, *Frosting and Defrosting Effects on Coil Heat Transfer*, Niederer (1976) indicates that only 15% to 25% of the heat required to defrost is actually carried out by the refrigerant condensate. He refers to a figure in his paper where 25.5 lb_m of condensate is removed by defrosting at a rate of 13.351 kW. The figure shows that 4,105 Btu are required to remove the condensate whereas 26,580 Btu where actually needed to accomplish the defrost; taking 35 minutes.

The frosted fin program was used to compare its results to Niederer's findings. The frosted fin program used a refrigerant temperature of 40˚F (4.44˚C) at a mass flow rate of 1.417 [lb_m/sec] to equal the total kW input specified by D.H. Niederer. After 35 minutes, the total energy input was found to be 0.3656 kJ (0.3465 Btu) per one half tube/fin assembly. Multiplying that figure by the total number of fins (408 for fins spaced at 4 per inch), the total number of tubes (12 rows, 8 columns), and by a factor of 2 for symmetrical conditions, the value obtained was 28,640 kJ (27,145 Btu). The amount of energy to melt the frost from the coils was 0.051 kJ (0.0483 Btu). Using the same multipliers, the total amount of energy required to melt the frost was 3,995 kJ (3,786 Btu) which compares well with the 4,105 Btu reported by Niederer.

5.6 References

Cole, R.A. *Refrigeration Loads in a Freezer Due to Hot Gas Defrost and Their Associated Costs*. ASHRAE Trans. 1989, vol. 95, part 2, 1149-1154.

Stoecker, W.F., J.J. Lux, Jr., R.J. Kooy. *Energy Considerations in Hot-Gas Defrosting of Industrial Refrigeration Coils.* ASHRAE Trans 1983, vol. 89, part 2, 549-573.

Niederer, D.H. *Frosting and Defrosting Effects on Coil Heat Transfer.* ASHRAE Trans 1976, vol. 82, part 1, 467-473.

Chapter 6 Conclusions and Recommendations

6.1 Study Summary

Frost accumulation on the coil surface increases the resistance for cooling and decreases the efficiency of the evaporator. To clear the coil of accumulated frost, evaporators must initiate a defrost, whether it be from electrical resistance heating, water defrost, or hot gaseous refrigerant. The latter is the most common way to defrost and was therefore the focus of the present investigation.

The primary contribution of the present study was the development of a dry air-cooling evaporator coil model as well as a frosted coil model that can be used to predict, energy and temperature flows during the process of hot gas defrosting the coil. This information forms the basis for developing estimates of energy costs associated with the parasitic effects of the defrost process of an evaporator. Evaporators that operate below the freezing point will have frost accumulate on its surface.

The energy impacts associated with defrosting evaporator coils heavily depend on the temperature of the refrigerant that is used for the hot gas defrost process. The lower the refrigerant gas temperature supplied to the coil for defrosting, the longer time period required to achieve a complete melt of the accumulated frost. The higher the refrigerant temperature, the shorter the defrost period; however, the higher rate at which both sensible and latent energy will be convected from the warm coil to the surrounding conditioned warehouse. Higher refrigerant temperatures also raise the mass of the coil to higher temperatures leading to a greater parasitic cooling load on the refrigeration system at the conclusion of the hot gas defrost process. The parasitic energy is due to the required removal of heat stored in the tubes and fins of the evaporator that must be removed prior to bringing the evaporator back on-line for useful conditioning of the warehouse space.

As many facilities have their defrost dwell time controlled by the use of a simple set-timer, the frost often completely melts off the coil long before the hot gas supply portion of the defrost sequence is terminated. The added heat load to the freezer, by over-hot gassing the coil results in diminished refrigeration system efficiency. The costs associated with the parasitic effects incurred to perform a defrost per 1000 ft^2 of evaporator area in a freezer that

was maintained at -5˚F was calculated by computing the total energy that went into defrosting that area for varying periods of time. The cost of operating the compressors to meet the excess load was then computed for a single stage compression and two-stage compression systems.

6.2 Conclusions

The frosted fin model, used in combination with the dry fin model, provides a good estimate of the energy needed for a defrost process, including the heating of the coil mass, the melting accumulated frost, sensible space load and latent space loads.

The frosted fin model compared quite well with the time to melt the accumulated frost that was observed at a local cold storage warehouse facility (Atlas Cold Storage). Using the same frost properties, freezer conditions, and refrigerant temperature observed in the field at Atlas, the model estimated a complete defrost at 10 minutes and 45 seconds. The time observed to complete a defrost of the actual coil ranged between 10 and 14 minutes. Variation in defrost time observed could be due to a number of factors including: evaporator piping variations, variations in frost thickness accumulated on the coil, presence of contaminants within the coil (e.g. oil) and other factors not readily apparent in the coil's installation.

As found, the defrost set time for hot gas supply to the evaporators at Atlas was 45 minutes. The dry fin model was used to calculate the energy into the evaporator coil during the period after a complete frost melt; thereby, representing the parasitic sensible load to the space for excessive hot gas supply. With an estimate of the additional load associated with excessive hot gas supply, the energy costs for operating a compressor to meet the load was calculated for the entire 45 minutes of hot gas, taken at 5 minute intervals. At the instant when the frost completely melts from the coil, the cost to perform the defrost per 1000 ft^2 of evaporator coil area is estimated to be $0.08 (based on the system operating with a saturated condensing temperature of 95 ˚F (35 ˚C)). The cost for defrosting the area of coil during system operation under other condensing temperatures is $0.0717 and $0.0645 for 85 ˚F (29.44 ˚C) and 75 ˚F (23.89 ˚C), respectively. At the 45 minute set time, the cost for defrosting 1000 ft^2 increases to $0.1843 for a condensing temperature of 95 ˚F (35 ˚C). At

condensing temperatures of 85 ˚F (29.44 ˚C) and 75 ˚F (23.89 ˚C), the cost of defrost is $0.1649 and $0.1483 for the 45 minutes of scheduled operation. Figure 5-23 shows the cost to defrost 1000 ft^2 of evaporator area for a range of hot gas saturation temperatures, with respect to varying system condensing temperatures.

In cases where operators may not easily know how much surface area their evaporators are, a more readily available measure such as the square footage of their freezers might be a better measure to scale defrost cost. The -5 ˚F freezer in the present study had a ratio of coil surface area to freezer floor area of 1.104. This ratio can be used to scale the defrost cost based on evaporator area to freezer floor area. So, the cost to melt the frost for evaporators serving a 1000 ft^2 of freezer floor area is $0.0884 when operating at a condensing temperature of 95 ˚F (35 ˚C). The cost at other condensing temperatures is $0.0792 and $0.0712 for 85 ˚F (29.44 ˚C) and 75 ˚F (23.89 ˚C), respectively. At the 45 minute set time, the cost for defrosting evaporators serving a 1000 ft^2 of freezer area increases to $0.2035 for a condensing temperature of 95 ˚F (35 ˚C). At condensing temperatures of 85 ˚F (29.44 ˚C) and 75 ˚F (23.89 ˚C), the cost of defrost is $0.1820 and $0.1637 per 1000 ft^2 of freezer floor area.

Since freezers have varying ceiling heights, the cost to defrost per 1000 ft^3 of storage volume is also beneficial to know. A ratio of 0.038 was calculated back in section 5.4 that relates the cost to defrost 1000 ft^3 of freezer space to 1000 ft^2 of evaporator coil for a freezer maintained at -5 ˚F. The cost to melt the frost in relation to 1000 ft^3 of freezer area is $0.00304 when operating at a condensing temperature of 95 ˚F (35 ˚C). The cost at other condensing temperatures is $0.00272 and $0.00245 for 85 ˚F (29.44 ˚C) and 75 ˚F (23.89 ˚C), respectively. At the 45 minute set time the cost for defrosting 1000 ft^3 of freezer space increases to $0.00700 for a condensing temperature of 95 ˚F (35 ˚C). At condensing temperatures of 85 ˚F (29.44 ˚C) and 75 ˚F (23.89 ˚C), the cost of defrost is $0.00627 and $0.00564.

The model developed in this project also compares well with papers written by W.F. Stoecker and D.H. Niederer. In Stoecker's paper [2], *Considerations in Hot-Gas Defrosting of Industrial Refrigeration Coils,* he states that using R-22 refrigerant at a flow rate of 18 [lb_m/min], heating the coils to 55 ˚F and melting 20.1 [lb_m] (9.1 kg) of frost, it would take

4,534 Btu (4783 kJ) of energy to achieve a complete defrost. Using the frosted coil program where the energy input is taken to be the mass flow rate of refrigerant times the enthalpy of vaporization of R-22 the frosted coil model required an estimated 6,544 kJ of energy to complete defrost. The total energy flow predicted by the present model also included the energy losses from convection and evaporation. Taking into account the thermal capacitance of the evaporator coil mass and frost-only, the total amount of energy supplied to the defrost is 4,881 kJ, which agrees closely with Stoecker's reported value.

The frosted fin model was run again; only the energy into defrosting the coil was taken to be a high convective term in order to keep the base temperature of the fin constant. The total amount of energy that went into the defrost was 6,499 kJ. Assuming no convective or evaporative losses the total amount of energy supplied for the defrost would have been 5,003 kJ. The total amount is also very close to Stoecker's reported values.

D.H. Niederer's paper [1], *Frosting and Defrosting Effects on Coil Heat Transfer,* states that only 15% to 25% of all energy that is supplied in a defrost cycle actually goes into melting the frost. He refers to a figure in his paper where 25.5 lb_m of condensate is removed by defrosting at a rate of 13.4 kW. The figure shows that 4,105 Btu are required to remove the condensate whereas 26,580 Btu where actually needed to accomplish the defrost; taking 35 minutes.

The frosted coil program used a refrigerant temperature of 40˚F (4.44˚C) at a mass flow rate of 1.417 [lb_m/sec] to equal the total kW input specified by D.H. Niederer. After 35 minutes, the total energy obtained was 28,640 kJ (27,145 Btu). The amount of energy to melt the frost from the coils was 3,995 kJ (3,786 Btu) which compares well with the 4,105 Btu reported by Niederer (1976). The calculated percent of the energy provided to the defrost cycle that is used to melt the ice is 14%, compared to Niederer's efficiency of 15%.

6.3 Recommendations for Future Model Work

Though the model developed during the course of this project is a first step in predicting the energy that is involved with defrosting air-cooling evaporators, the program itself has limitations. The convective heat transfer that the outside layer of frost encounters is based on natural convection on a vertical plate. The true nature of the convective forces present is

different due to the presence of evaporator tubes that disrupt air flow through the evaporator fins. Thus there is uncertainty in the value of the convection coefficient that should be used in this analysis.

The model is made up of many nodes that represent both frost and metal. Though the nodes that represent the evaporator fin are good in comparison with the fin efficiencies and temperature distributions found in Incropera and DeWitt (2002), the nodes that make up the frost present some particular difficulties under a change in phase. The frost, once it is melted, is assumed to be drained from the grid area and replaced by air. The justification for keeping the density of the node constant and changing the thermal conductivity is as follows: When the frost in a node melts, the water will drain, resulting in the infiltration of air into the vacant space created by the drained water. In a realistic situation, the temperature of that nodal space will stay relatively constant because it has a nearly infinite heat sink from the huge amount of air in the freezer space continuously removing the air in the nodal space by new air. This effect is captured by not changing the density of the node to air, to retain a larger effective nodal mass. Having a larger mass for the node makes it possible for the sum of its superficially large amount of mass times the specific heat of the air to result in a relatively constant temperature, which would be expected due to the continuous infiltration of new freezer air. Though this is a plausible estimate, future work with modeling defrost processes should include greater detail in where the melted frost nodes are permitted to leave the computational domain and are replaced by nodes that represent the conditions of the freezer air inside the evaporator casing.

The supplied energy to defrost should also be modeled in greater detail. Although attempts in using the mass flows of refrigerant times their enthalpy of vaporization were made when comparing the model to the paper presented by Stoecker and Niederer, a greater understanding of the refrigerant passing through the tubes of the evaporator would be beneficial. In reality, not all of the refrigerant will condense over the entire period of a defrost cycle. After the frost has melted and the refrigerant continues to flow through the evaporator coils, some refrigerant will pass through the coil without condensing and be returned to the compressors presenting a “hot gas bypass” of sorts.

6.4 Recommendations for Field Practice

In most facilities defrost sequences are established by a time clock set. The defrost sequence has a timer which controls the time to initiate a defrost and the defrost sequence itself including refrigerant pump-out, hot gas supply, hot gas supply termination, cool down period, and defrost sequence termination. Though there are alternatives to the whole clock driven sequences, clock driven sequences are certainly the easiest to implement. Attempts should be made to observe a defrost cycle and determine if the sequence timing (particularly the hot gaseous refrigerant supply dwell time) is reasonably consistent with the actual time required to completely melt accumulated frost. Further attempts should also be taken in determining whether a coil even needs to go defrost. Many evaporators are set on schedules and the evaporator initiates a defrost whether there is frost on the coils or not. By scaling the defrost timers at larger intervals between defrosts, the extra load introduced in the system is less and the operating costs go down.

To insure all moisture is gone from the coil surface and drain pan, many operators tend to run excessive defrosts. The result of excessive defrost is that compressors work harder because of the false load introduced by hot gas bypassing the evaporator once the frost is melted. A way to conserve compressor power would be to introduce a ball float into the piping arrangement. A ball float would make sure that as the defrosting times grow, the hot gas, that would otherwise bypass the evaporator, would condense before leaving the evaporator to a low pressure receiver and not create any false loads on the system.

From observing defrost sequences, it was noticed that from the start of the hot gas supply water did not start to drain for at least 4 ~ 5 minutes. By piping the evaporator in a way so that the refrigerant first passes through the coils before it heats the drain pan would decrease in the amount of energy needed to defrost. Otherwise the pan simply acts as a space heater for the initial five minutes.

If set defrost times are used in the field, using lower temperature refrigerant for the defrost process is more beneficial. Although lower temperatures are always better if it removes frost from the coils in the same set time as higher refrigerants would, instead of leaving a defrost last for an hour with a low temperature refrigerant, higher temperature refrigerants could be used with lower set times to decrease the overall defrost load.

6.5 References

[1] Niederer, D.H. *Frosting and Defrosting Effects on Coil Heat Transfer.* ASHRAE Trans 1976, vol. 82, part 1, 467-473.

[2] Stoecker, W.F., J.J. Lux, Jr., R.J. Kooy. *Energy Considerations in Hot-Gas Defrosting of Industrial Refrigeration Coils.* ASHRAE Trans 1983, vol. 89, part 2, 549-573.

Incropera, F. P., and D. P. DeWitt. *Introduction to Heat Transfer 4th Ed*. John Wiley & Sons, 2002.

Appendix A: Dry Fin Model

```
"!_____""N O D E   M A T R I X""!_____"

jj=10                                                    "# of fin nodes"

DELTAi = 0.010[inch]*convert(inch, m)                    "fin thickness"

"_____R A D I U S   E Q U A T I O N
S_____"

r[jj] = 1.525[inch]*convert(inch,m)                      "outside fin radius"
r[1] = 0.525[inch]*convert(inch,m)                       "inside fin radius"
DELTAr = (r[jj] - r[1])/(jj - 1)                         "change in nodal radius"
r_out[jj] = r[jj]                                        "outside radius of outer node "
r_in[jj] = r_out[jj]-DELTAr/2                            "inside radius of outer node"
r_in[1] = r[1]                                           " inside radius of inner node "
r_out[1] = r[1]+DELTAr/2                                 " outside radius of inner node "


Duplicate j = 2,jj-1                                     “incremental radius for interior
nodes”
r[j] = r[j-1] + DELTAr
r_out[j] = r[j] + 0.5*DELTAr
r_in[j] = r[j] - 0.5*DELTAr
End

"_____""!E N E R G Y   B A L A N C E""_____"

"Energy In      (q_in)      (from the bottom of the fin)"
Q_dot_in = (h_base*(dI\2)*(2*pi*r_in[1])*(T_base-T[1]))*convert(W,kW)
Q_in = integral(Q_dot_in, time, 0, time_final, step) + Q_stored_tube      "Energy In [kJ]"


"Total Energy Out  (Q|stored\out)"
Q|stored\out = Q_conv_fin  + Q_stored_fin + Q_stored_tube          "Total Energy (Q_stored +
Q_out + Q_evap) should eQual Q_in in [kJ]"


"Energy Convected Out     (Q_out)"
Q_conv_fin = -(Q_conv_J + Q_conv_K + Q_conv_L)
Q_dot_conv_fin = -(Q_dot_conv_J + Q_dot_conv_K + Q_dot_conv_L)

Q_dot_conv_J = (h_bar_C[jj]*pi*(r_out[jj]^2 - r_in[jj]^2)*(T_infinity-T[jj]))*convert(W,kW)
    Q_conv_J = integral(Q_dot_conv_J, time, 0, time_final, step)
Q_dot_conv_K = (SUM(h_bar_C[j]*pi*(r_out[j]^2 - r_in[j]^2)*(T_infinity-T[j]),  j=2,jj-
1))*convert(W,kW)
    Q_conv_K = integral(Q_dot_conv_K, time, 0, time_final, step)
Q_dot_conv_L = (h_bar_C[1]*pi*(r_out[1]^2 - r_in[1]^2)*(T_infinity-T[1]))*convert(W,kW)
    Q_conv_L = integral(Q_dot_conv_L, time, 0, time_final, step)

"Energy Stored in Fin"
```

```
Q_stored_fin = Q_fin_J_stored+Q_fin_K_stored+Q_fin_L_stored


Q_dot_J_stored = (rho_f*(dI\2)*pi*(r_out[jj]^2 - r_in[jj]^2))*C*(dT\dt[jj])
    Q_fin_J_stored = integral(Q_dot_J_stored, time, 0, time_final, step)
Q_dot_K_stored = SUM((rho_f*(dI\2)*pi*(r_out[j]^2 - r_in[j]^2))*C*(dT\dt[j]),j=2,jj-1)
    Q_fin_K_stored = integral(Q_dot_K_stored, time, 0, time_final, step)
Q_dot_L_stored = (rho_f*(dI\2)*pi*(r_out[1]^2 - r_in[1]^2))*C*(dT\dt[1])
    Q_fin_L_stored = integral(Q_dot_L_stored, time, 0, time_final, step)


"Energy Stored in Steel Tubes"

"!Tube Dimensions"
   D_o = 1[inch]*convert(inch,m)                    "Outside Diameter of Tube"
   D_i = D_o - 2*t_tube                             "Inside Diameter of Tube"
   t_tube = 0.06[inch]*convert(inch,m)              "Thickness of Tube"
   A_x_tube = (pi*(D_o^2 - D_i^2))/4                "Cross-Sectional Area of Tube"

"!Total Mass and Volume of Tube"
   V_tube_total = A_x_tube*L_tube_total                          "Volume of Tube"
   mass_tube = V_tube_total*rho_tube                             "Mass of Tube"
   V_tube = A_x_tube*0.16665[inch]*convert(inch,m)
   m_tube = V_tube*rho_tube
   L_tube = 15[ft]*convert(ft, m)                                "Length of Evaporator"
   rho_tube = 489[lb_m/ft^3]*convert(lb_m/ft^3, kg/m^3)          "Density of Fin/Tube"
   Cp_tube = 0.12[Btu/lb_m-F]*convert(Btu/lb_m-F, kJ/kg-K)"Specific Heat of Tube"

V_fin = pi*(r[jj]^2 - r[1]^2)*(DELTAi/2)
   m_fin = V_fin*rho_f
   mass_fin = m_fin*2*N_tubes*N_fins
   L_tube_total = L_tube*N_tubes                          "Total Length of Tubes"
   N_tubes = N_rows*N_columns                             "Number of Tubes"
   N_rows = 18                                            "rows of tubes in evaporator"
   N_columns = 10                                         "columns of tubes in evaporator"
   N_fins = 800                                           "Number of Fins"

"!Energy into the Tube: Total,  Per (1) Tube and Fin Assembly"
Q_tubes_total = mass_tube*Cp_tube*(T_base - T_initial)   "Energy Input to Heat All Tubes
total length"
Q_stored_tube = m_tube*Cp_tube*(T_base - T_initial)      "Energy Input to Tube of [1/6]
inch long"

"Energy Stored in Total Fin Area"
Q_fin_total = Q_stored_fin*2*N_rows*N_columns*N_fins

"!_____""D I F F U S I O
N""!_____"

Duplicate dup=1,jj

   Nus_bar_L[dup] = 0.13*(Gr_L[dup]*Pr[dup])^(1/3)        "Nusselt Number (4.86) pp.347"
   h_bar_C[dup] = (k_air[dup]/Length_fin*Nus_bar_L[dup])  "Heat transfer coefficient"
```

```
   Gr_L[dup] = ((DELTArho[dup]/rho_m[dup])*g*Length_fin^3)/nu[dup]^2   "Grasholf
number"

   Pr[dup] = nu[dup]/ALPHA[dup]                          "Prandtl Number"


    rho_s[dup] = rho_1_s[dup] + rho_2_s[dup]      "density of moist air at node surface"
    rho_1_s[dup] = (P_1_s[dup]*MW_H2O)/(R*T[dup])"density of water at node surface"
    rho_2_s[dup] = (P_2_s[dup]*MW_Air)/(R*T[dup])   "density of dry air at node surface"

    rho_m[dup] = 0.5*(rho_s[dup] + rho_e)          "mean density"
    DELTArho[dup] = rho_e - rho_s[dup]             "density difference between node surface
and freezer"

    P_sat_s[dup] = PRESSURE(Water,T=T[dup],x=1)   "satuation pressure of water at node
surface"

        P_1_s[dup] = P_sat_s[dup]              "saturated pressure of water at temperature 'T'"
        P_2_s[dup] = P_atm - P_1_s[dup]        "partial pressure of dry air at temperature 'T'"

    nu[dup] = mu[dup]/rho_m[dup]                          "dynamic viscosity"
    mu[dup] = VISCOSITY(Air,T=T_m[dup])                   "viscosity"
    ALPHA[dup] = k_air[dup]/(rho_m[dup]*C_air[dup])       "thermal diffusivity"
    C_air[dup] = CP(Air,T=T_m[dup])*convert(kJ/kg-K, J/kg-K)
    k_air[dup] = CONDUCTIVITY(Air,T=T_m[dup])             "thermal conductivity of pure air"
    T_m[dup] = (T[dup]+T_infinity)/2
End


"Diffusion Parameters"

rho_e = rho_1_e + rho_2_e                                 "density of moist air in freezer"
rho_1_e = (P_1_e*MW_H2O)/(R*T_infinity)                   "density of water in freezer air"
rho_2_e = (P_2_e*MW_Air)/(R*T_infinity)                   "density of dry air in freezer"

P_sat_infinity = PRESSURE(Water,T=T_infinity,x=1)  "saturation pressure in freezer"
P_atm = Po#
P_1_e = RH*P_sat_infinity
P_2_e = P_atm - P_1_e

RH = 0.80                                                 "relative humidity"
g = g#                                                    "gravitational constant"
R = R#                                                    "Universal gas constant"
MW_H2O = MOLARMASS(Water)                                 "molecular weight of water"
MW_Air = MOLARMASS(Air)                                   "molecular weight of air"
Length_fin = 60[inch]*convert(inch, m)

"_____""!N O D A L     E Q U A T I O N S""_____"

"J  Exterior Fin Node"
0 = ((k_f*(2*pi*dI\2)*(T[jj-1]-T[jj]))/(ln(r[jj]/(r[jj]-DELTAr))) + h_bar_C[jj]*pi*(r_out[jj]^2 -
r_in[jj]^2)*(T_infinity-T[jj]))*convert(W, kW) - ((rho_f*dI\2*pi*(r_out[jj]^2 -
r_in[jj]^2))*C*dT\dt[jj])
```

```
"K Fin Interior Nodes"
Duplicate j=2,jj-1
0 = ((k_f*(2*pi*dI\2)*(T[j-1]-T[j]))/(ln(r[j]/(r[j]-DELTAr)))+(k_f*(2*pi*dI\2)*(T[j+1]-
T[j]))/(ln((r[j]+DELTAr)/r[j]))+h_bar_C[j]*pi*(r_out[j]^2 - r_in[j]^2)*(T_infinity-T[j]))*convert(W,
kW) - ((rho_f*dI\2*pi*(r_out[j]^2 - r_in[j]^2))*C*dT\dt[j])
End

"L Base of Fin Node"
0 = (h_base*(2*pi*dI\2)*r_in[1]*(T_base-T[1])+(k_f*(2*pi*dI\2)*(T[2]-
T[1]))/(ln((r[1]+DELTAr)/r[1]))+h_bar_C[1]*(pi*(r_out[1]^2 - r_in[1]^2))*(T_infinity-
T[1]))*convert(W, kW) - ((rho_f*dI\2*pi*(r_out[1]^2 - r_in[1]^2))*C*dT\dt[1])

"!_____""I N T E G R A T I O N""!_____"

"Temperature of Fin"
Duplicate j=1,jj
T[j] = T_initial + integral(dT\dt[j], time, 0, time_final, step)
End

"_____""!K N O W N S""_____"

C = 0.9                                  "Specific Heat of Fin [kJ/kg-K]"
rho_f = 2707                             "Density of Fin"
k_f = 240                                "Thermal Conductivity of Fin"
dI\2 = DELTAi/2                          "variable names to shorten computational time"
time_final = 3600                        "Stop Time of Simulation"

"!_____""V A R I A B L E S""!_____"

T_initial = ConvertTEMP(F,K, 0)          "INITIAL TEMP (2) of (2) places in program"
T_infinity = ConvertTEMP(F,K, -5)        "AMBIENT TEMPERATURE"
T_base = ConvertTEMP(F,K, 100)           "conversion from [F] to [K]"
h_base = 100000.0                        "Convection Coefficient for Q in bottom of fin"
step = 0.5                               "STEP SIZE"

"Integral Table"
$integraltable time: 0.5, Q_in

$tabstops0.1, 0.15, 0.2, 0.4
```

Appendix B: Frosted Fin Model

"Frosted Fin Finite Difference Model"

```
"_____""!S I M U L A T I O N   S T O P""_____"
"Simulation is stopped when T[1,jj] > 273.16[K] (top left corner node)"
function checkstop(T_corner)
   checkstop = 1
IF (T_corner > 273.16[K] ) THEN Call Error('Simulation Complete')
End

"!_____""S U M   F U N C T I O N""!_____"

"Function used to SUM interior nodes stored energy"
function Sum2D(i_1,i_2,j_1,j_2)
jj =10                                          Number of nodes in Y direction""! (1) of (2)"
ii = 10                                         Number of nodes in the X direction""! (1) of (2)"
T_initial = {252.6} {-5} {249.8} {-10} 244.26 {-20}     "INITIAL TEMPERATURE""! (1) of (2)"
P_atm = Po#                                     "Atmospheric pressure"
rho = 150 {300} {450}                           "Density of Frost (assumed constant)""!(2) of (3)"
h_initial = ENTHALPY(Ice,T=T_initial,P=P_atm)       "initial enthalpy"
DELTAi = 0.010[inch]*convert(inch, m)               "fin thickness"
Percent_Blockage = 0.20                         "!(1) of (3)"
Fins_Per_Inch = 3                               "Number of fins per inch"
Adiabatic = 0.5                                 "Used to get 1/2 of the spacing of fin to fin"
Fin_Space = (1/Fins_Per_Inch)*convert(inch, m)*Adiabatic     "Spacing between fins"
Length_FROST = Percent_Blockage*Fin_Space - DELTAi/2        "Length used in FIN/Frost"
r[jj] = 1.525[inch]*convert(inch,m)                         "Outside fin radius"
r[1] = 0.525[inch]*convert(inch,m)                          "Inside fin radius"
DELTAr = (r[jj] - r[1])/(jj - 1)                "Height of Nodes"
DELTAx = Length_FROST/(ii - (3/2))              "Length of Node in the X Direction"

r_out[jj] = r[jj]                               "Outside radius of Outer nodes j=jj"
r_in[jj] = r_out[jj]-DELTAr/2                   "Inside radius of Outer nodes j=jj"
r_in[1] = r[1]                                  "Inside radius of Inner nodes j=1"
r_out[1] = r[1]+DELTAr/2                        "Outside radius of Inner nodes j=1"

Duplicate j = 2,jj-1
r[j] = r[j-1] + DELTAr                          "Mean radius of nodes"
r_out[j] = r[j] + 0.5*DELTAr                    "Outside radius of nodes j=2,jj-1"
r_in[j] = r[j] - 0.5*DELTAr                     "Inside radius of nodes j=2,jj-1"
End

 $common h[1..20,1..20]                         "Common enthalpy matrix encountered"
 i: = i_1-1
 sum=0
 repeat
   i: = i+1
   j = j_1-1
   repeat
     j = j+1
     sum = sum+(rho*DELTAx*pi*(r_out[j]^2 - r_in[j]^2)*(h[i,j]-h_initial))
   until (j>= j_2)
```

```
  until (i>= i_2)
  sum2d = sum
end

"!_____""S U M   F U N C T I O N""!_____"
"Function used to SUM interior nodes excess stored energy"
function Sum2D_excess(i_1,i_2,j_1,j_2)
jj = 10                                   "Number of nodes in Y direction""! (1) of (2)"
ii = 10                                   "Number of nodes in the X direction""! (1) of (2)"
T_initial = {252.6} {-5} {249.8} {-10} 244.26 {-20}     "INITIAL TEMPERATURE""! (1) of (2)"
P_atm = Po#                               "Atmospheric pressure"
rho = 150 {300} {450}                     Density of Frost (assumed constant)""!(2) of (3)"
h_initial = ENTHALPY(Ice,T=T_initial,P=P_atm)     "initial enthalpy"
DELTAi = 0.010[inch]*convert(inch, m)             "fin thickness"
Percent_Blockage = 0.20                   "!(2) of (3)"
Fins_Per_Inch = 3                         "Number of fins per inch"
Adiabatic = 0.5                           "Used to get 1/2 of the spacing of fin to fin"
Fin_Space = (1/Fins_Per_Inch)*convert(inch, m)*Adiabatic
Length_FROST = Percent_Blockage*Fin_Space - DELTAi/2      "Length used in FIN/Frost"
r[jj] = 1.525[inch]*convert(inch,m)                       "Outside fin radius"
r[1] = 0.525[inch]*convert(inch,m)                "Inside fin radius"
DELTAr = (r[jj] - r[1])/(jj - 1)                  "Height of Nodes"
DELTAx = Length_FROST/(ii - (3/2))                Length of Node in the X Direction"

r_out[jj] = r[jj]                                 "Outside radius of Outer nodes j=jj"
r_in[jj] = r_out[jj]-DELTAr/2                     "Inside radius of Outer nodes j=jj"
r_in[1] = r[1]                                    "Inside radius of Inner nodes j=1"
r_out[1] = r[1]+DELTAr/2                          "Outside radius of Inner nodes j=1"

Duplicate j = 2,jj-1
r[j] = r[j-1] + DELTAr                            "Mean radius of nodes"
r_out[j] = r[j] + 0.5*DELTAr                      "Outside radius of nodes j=2,jj-1"
r_in[j] = r[j] - 0.5*DELTAr                       "Inside radius of nodes j=2,jj-1"
End

  $common h[1..20,1..20]                  "Common enthalpy matrix encountered"
  i: = i_1-1
  sum=0
  repeat
    i: = i+1
    j = j_1-1
    repeat
      j = j+1
      sum = sum+(rho*DELTAx*pi*(r_out[j]^2 - r_in[j]^2)*h[i,j])
    until (j>= j_2)
  until (i>= i_2)
  sum2d_excess = sum
end

"_____""!P  R  O  C  E  D  U  R  E""_____"

"Procedure to determine Temperatures from Enthalpies in a lookup table"
```

```
PROCEDURE T_water(h:T{,x},k{,rho})          "properties, given h"
T = Interpolate1('ice','h','T',h=h)         "Temperature"
{T_C = Interpolate1('ice','h','T_C',h=h)    "Temperature in Celcius"}
{k = Interpolate1('ice','h','k_450',h=h)    "Thermal Conductivity of Frost/Water"}
{k = Interpolate1('ice','h','k_300',h=h)    "Thermal Conductivity of Frost/Water"}
k = Interpolate1('ice','h','k_150',h=h)     "Thermal Conductivity of Frost/Water"

{x = Interpolate1('ice','h','x',h=h)        "Quality"}
{rho = {Interpolate1('ice','h','rho',h=h)}900   "Density of Frost/Water"}
END

"!_____""N O D E   M A T R I X""!_____"

jj=10                          "!Number of nodes in Y direction (2) of (2) places in
program"
ii=10                          "!Number of nodes in the X diredtion (2) of (2) places in
program"

DELTAx = Length_FROST/(ii - (3/2))          "Length of Node in the X Direction"
DELTAi = 0.010[inch]*convert(inch, m)       "fin thickness"
Length_FROST = Percent_Blockage*Fin_Space - DELTAi/2   "Length used in FIN/Frost"
Fins_Per_Inch = 3                           "Number of fins per inch"
Fin_Space = (1/Fins_Per_Inch)*convert(inch, m)*Adiabatic   "Spacing between fins"
Adiabatic = 0.5                "Used to get 1/2 of the spacing of fin to fin"
Percent_Blockage = 0.20                     "!(3) of (3)"

"_____R A D I U S   E Q U A T I O N
S_____"
r[jj] = 1.525[inch]*convert(inch,m)         "Outside fin radius"
r[1] = 0.525[inch]*convert(inch,m)          "Inside fin radius"
DELTAr = (r[jj] - r[1])/(jj - 1)            "Height of Nodes"
r_out[jj] = r[jj]                           "Outside radius of Outer nodes j=jj"
r_in[jj] = r_out[jj]-DELTAr/2               "Inside radius of Outer nodes j=jj"
r_in[1] = r[1]                              "Inside radius of Inner nodes j=1"
r_out[1] = r[1]+DELTAr/2                    "Outside radius of Inner nodes j=1"

Duplicate j = 2,jj-1
r[j] = r[j-1] + DELTAr                      "Mean radius of nodes"
r_out[j] = r[j] + 0.5*DELTAr                "Outside radius of nodes j=2,jj-1"
r_in[j] = r[j] - 0.5*DELTAr                 "Inside radius of nodes j=2,jj-1"
End

"_____""!E N E R G Y   B A L A N C E""_____"


"Energy In                     (q_in)              (from the bottom of the fin)"
Q_dot_in = (h_base*(dI\2)*(2*pi*r_in[1])*(T_base-T[ii,1]))*convert(W,kW)"Energy rate in to
defrost [kW]"
Q_in = integral(Q_dot_in, time, 0, time_final, step) + Q_tube     "Energy In to defrost [kJ]"

"Energy In to Melt Frost w/o Excess Energy to Raise Water Temperature above 0 [C]"
Q_in\melt = Q_in - Q_excess_FROST
```

```
"Total Energy Out        (Q|stored\out)"
Q|stored\out = Q_conv + Q_evap + Q_stored + Q_tube  "Total Energy stored and released =
Q_in"

"Energy Evaporated Out"
Q_evap = Q_evap_A + Q_evap_D + Q_evap_G              "Energy evaporated out [kJ]"
Q_dot_evap = Q_dot_evap_A + Q_dot_evap_D + Q_dot_evap_G     "Energy rate evaporated
out [kW]"

"Energy rate of evap. for node A"
Q_dot_evap_A =  g_bar_m[1,jj]*pi*(r_out[jj]^2 - r_in[jj]^2)*(m_1_s[1,jj] - m_1_e)*h_ig[1,jj]
"Energy evap. out for node A"
   Q_evap_A = integral(Q_dot_evap_A, time, 0, time_final, step)

"Energy rate of evap. for node D"
   Q_dot_evap_D = SUM(g_bar_m[1,j]*pi*(r_out[j]^2 - r_in[j]^2)*(m_1_s[1,j] - m_1_e)*h_ig[1,j],
j=2,jj-1)
"Energy evap. out for node D"
   Q_evap_D = integral(Q_dot_evap_D, time, 0, time_final, step)

"Energy rate of evap. for node G"
Q_dot_evap_G = g_bar_m[1,1]*pi*(r_out[1]^2 - r_in[1]^2)*(m_1_s[1,1] - m_1_e)*h_ig[1,1]
"Energy evap. out for node G"
   Q_evap_G = integral(Q_dot_evap_G, time, 0, time_final, step)


"Energy Convected Out                        (Q_out)"

"Energy convected out [kJ]"
Q_conv = -(Q_conv_A+Q_conv_D+Q_conv_G+Q_conv_H+Q_conv_I)
"Energy rate convected out [kW]"
Q_dot_conv = -(Q_dot_conv_A+Q_dot_conv_D+Q_dot_conv_G+Q_dot_conv_H+Q_dot_conv_I)

"Energy rate of conv. for node A"
Q_dot_conv_A = h_bar_C[1,jj]*pi*(r_out[jj]^2 - r_in[jj]^2)*(T_infinity-T[1,jj])*convert(W,kW)
"Energy  conv. for node A"
Q_conv_A = integral(Q_dot_conv_A, time, 0, time_final, step)

"Energy rate of conv. for node D"
Q_dot_conv_D = (SUM(h_bar_C[1,j]*pi*(r_out[j]^2 - r_in[j]^2)*(T_infinity-T[1,j]),  j=2,jj-
1))*convert(W,kW)
"Energy  conv. for node D"
Q_conv_D = integral(Q_dot_conv_D, time, 0, time_final, step)

"Energy rate of conv. for node G"
Q_dot_conv_G = (h_bar_C[1,1]*pi*(r_out[1]^2 - r_in[1]^2)*(T_infinity-T[1,1]) +
h_bar_C[1,1]*(dX\2)*(2*pi*r_in[1])*(T_infinity-T[1,1]))*convert(W,kW)
"Energy  conv. for node G"
Q_conv_G = integral(Q_dot_conv_G, time, 0, time_final, step)
```

```
"Energy rate of conv. for node H"
Q_dot_conv_H = (SUM(h_bar_C[1,1]*DELTAx*(2*pi*r_in[1])*(T_infinity-T[i,1]),  i=2,ii-
2))*convert(W,kW)
"Energy  conv. for node H
Q_conv_H = integral(Q_dot_conv_H, time, 0, time_final, step)

"Energy rate of conv. for node I"                    "
Q_dot_conv_I = h_bar_C[1,1]*DELTAx*(2*pi*r_in[1])*(T_infinity-T[ii-1,1])*convert(W,kW)
"Energy  conv. for node I"
Q_conv_I = integral(Q_dot_conv_I, time, 0, time_final, step)


"Energy Stored                                          (Q_stored)"

"Energy Stored in frost and fin"
Q_stored = Q_stored_FROST+Q_stored_fin

"Energy Stored in Frost"
Q_stored_FROST=Q_A_stored+Q_B_stored+Q_C_stored+Q_D_stored+Q_E_stored+Q_F_store
d+Q_G_stored+Q_H_stored+Q_I_stored

"Energy Stored in Fin"
Q_stored_fin = Q_fin_J_stored+Q_fin_K_stored+Q_fin_L_stored


"Excess Energy Used to Raise Frost Nodes above 0 [C]"
Q_excess_FROST=Q_A_excess+Q_B_excess+Q_C_excess+Q_D_excess+Q_E_excess+Q_F_exc
ess+Q_G_excess+Q_H_excess+Q_I_excess                    "Excess energy in frost"

"Energy Used to Raise Frost Nodes to 0 [C]"
Q_FROST_melt = Q_stored_FROST - Q_excess_FROST"Energy used to melt mass of frost"

"Stored energy rate in node A"
Q_dot_A_stored = (rho*(dX\2)*pi*(r_out[jj]^2 - r_in[jj]^2))*(dh\dt[1,jj])
"Stored energy in node A"
Q_A_stored = integral(Q_dot_A_stored, time, 0, time_final, step)

"Stored energy rate in node B"
Q_dot_B_stored = SUM((rho*DELTAx*pi*(r_out[jj]^2 - r_in[jj]^2))*(dh\dt[i,jj]),i=2,ii-2)
"Stored energy in node B"
Q_B_stored = integral(Q_dot_B_stored, time, 0, time_final, step)

"Stored energy rate in node C"
Q_dot_C_stored = (rho*DELTAx*pi*(r_out[jj]^2 - r_in[jj]^2))*(dh\dt[ii-1,jj])
"Stored energy in node C"
Q_C_stored = integral(Q_dot_C_stored, time, 0, time_final, step)

"Stored energy rate in node D"
Q_dot_D_stored = SUM((rho*(dX\2)*pi*(r_out[j]^2 - r_in[j]^2))*(dh\dt[1,j]),j=2,jj-1)
"Stored energy in node D"
Q_D_stored = integral(Q_dot_D_stored, time, 0, time_final, step)
```

```
"Stored energy in node E"
Q_E_stored = sum2D(2,ii-2,2,jj-1)

"Stored energy rate in node F"
Q_dot_F_stored = SUM((rho*DELTAx*pi*(r_out[j]^2 - r_in[j]^2))*(dh\dt[ii-1,j]),j=2,jj-1)
"Stored energy in node F"
Q_F_stored = integral(Q_dot_F_stored, time, 0, time_final, step)

"Stored energy rate in node G"
Q_dot_G_stored = (rho*(dX\2)*pi*(r_out[1]^2 - r_in[1]^2))*(dh\dt[1,1])
"Stored energy in node G"
Q_G_stored = integral(Q_dot_G_stored, time, 0, time_final, step)

"Stored energy rate in node H"
Q_dot_H_stored = SUM((rho*DELTAx*pi*(r_out[1]^2 - r_in[1]^2))*(dh\dt[i,1]),i=2,ii-2)
"Stored energy in node H"
Q_H_stored = integral(Q_dot_H_stored, time, 0, time_final, step)

"Stored energy rate in node I"
Q_dot_I_stored = (rho*DELTAx*pi*(r_out[1]^2 - r_in[1]^2))*(dh\dt[ii-1,1])
"Stored energy in node I"
Q_I_stored = integral(Q_dot_I_stored, time, 0, time_final, step)

"Stored energy rate in node J"
Q_dot_J_stored = (rho_f*(dI\2)*pi*(r_out[jj]^2 - r_in[jj]^2))*C*(dT\dt[ii,jj])
"Stored energy in node J"
Q_fin_J_stored = integral(Q_dot_J_stored, time, 0, time_final, step)
"Stored energy rate in node K"
Q_dot_K_stored = SUM((rho_f*(dI\2)*pi*(r_out[j]^2 - r_in[j]^2))*C*(dT\dt[ii,j]),j=2,jj-1)
"Stored energy in node K"
Q_fin_K_stored = integral(Q_dot_K_stored, time, 0, time_final, step)

"Stored energy rate in node L"
Q_dot_L_stored = (rho_f*(dI\2)*pi*(r_out[1]^2 - r_in[1]^2))*C*(dT\dt[ii,1])
"Stored energy in node L"
Q_fin_L_stored = integral(Q_dot_L_stored, time, 0, time_final, step)

"Energy in frost to exceed 0 deg. C in node A"
Q_A_excess = (rho*(dX\2)*pi*(r_out[jj]^2 - r_in[jj]^2))*(h[1,jj])

"Energy in frost to exceed 0 deg. C in node B"
Q_B_excess = SUM((rho*DELTAx*pi*(r_out[jj]^2 - r_in[jj]^2))*(h[i,jj]),i=2,ii-2)

"Energy in frost to exceed 0 deg. C in node C"
Q_C_excess = (rho*DELTAx*pi*(r_out[jj]^2 - r_in[jj]^2))*(h[ii-1,jj])

"Energy in frost to exceed 0 deg. C in node D"
Q_D_excess = SUM((rho*(dX\2)*pi*(r_out[j]^2 - r_in[j]^2))*(h[1,j]),j=2,jj-1)

"Energy in frost to exceed 0 deg. C in node E"
Q_E_excess = sum2D_excess(2,ii-2,2,jj-1)
```

```
"Energy in frost to exceed 0 deg. C in node F"
Q_F_excess = SUM((rho*DELTAx*pi*(r_out[j]^2 - r_in[j]^2))*(h[ii-1,j]),j=2,jj-1)

"Energy in frost to exceed 0 deg. C in node G"
Q_G_excess = (rho*(dX\2)*pi*(r_out[1]^2 - r_in[1]^2))*(h[1,1])

"Energy in frost to exceed 0 deg. C in node H"
Q_H_excess = SUM((rho*DELTAx*pi*(r_out[1]^2 - r_in[1]^2))*(h[i,1]),i=2,ii-2)

"Energy in frost to exceed 0 deg. C in node I"
Q_I_excess = (rho*DELTAx*pi*(r_out[1]^2 - r_in[1]^2))*(h[ii-1,1])


"Energy Stored in Steel Tubes"


"!Tube Dimensions"
   D_o = 2*r[1]                                          "Outside Diameter of Tube"
   D_i = D_o - 2*t_tube                                  "Inside Diameter of Tube"
   t_tube = 0.06[inch]*convert(inch,m)                   "Thickness of Tube"
   A_x_tube = (pi*(D_o^2 - D_i^2))/4                     "Cross-Sectional Area of Tube"

"!Total Mass and Volume of Tube"
   V_tube_total = A_x_tube*L_tube_total                  "Volume of Tube"
   mass_tube = V_tube_total*rho_tube                     "Mass of Tube"
   V_tube = A_x_tube*Fin_Space                           "Volume of one model tube"
   m_tube = V_tube*rho_tube                              "Mass of model tube"
   L_tube = 22.25[ft]*convert(ft, m)                     "Length of Evaporator"
   rho_tube = 489[lb_m/ft^3]*convert(lb_m/ft^3, kg/m^3)        "Density of Fin/Tube"
   Cp_tube = 0.12[Btu/lb_m-F]*convert(Btu/lb_m-F, kJ/kg-K)     "Specific Heat of Tube"

V_fin = pi*(r[jj]^2 - r[1]^2)*(DELTAi/2)                 "Volume of model fin"
   m_fin = V_fin*rho_f                                   "Mass of model fin"
   mass_fin = (m_fin/Adiabatic)*N_tubes*N_fins           "Mass of Evaporator fin"
   L_tube_total = L_tube*N_tubes                         "Total Length of Tubes"
   N_tubes = N_rows*N_columns                            "Number of Tubes"
   N_rows = 18                                           "rows of tubes in evaporator"
   N_columns = 10                                        "columns of tubes in evaporator"
   N_fins = 800                                          "Number of Fins"

"!Energy into the Tube: Total,  Per (1) Tube and Fin Assembly"
Q_tubes_total = mass_tube*Cp_tube*(T_base - T_initial)   "Energy Input to Heat All Tubes
total length"
Q_tube = m_tube*Cp_tube*(T_base - T_initial)     "Energy Input to Tube of [1/6] inch long"

"Energy Stored in Total Fin Area"
Q_fin_total = Q_stored_fin*2*N_rows*N_columns*N_fins  "Energy Into All Evaporator Fins"


"!_____""D I F F U S I O
N""!_____"

"LOWER LIMIT"
```

```
m_FROST = Length_FROST*pi*(r[jj]^2 - r[1]^2)*rho      "Mass of frost on model"

mass_FROST = m_FROST/Adiabatic*N_tubes*N_fins  "Total mass of frost on evaporator"

"Fraction of water evaporated"
fraction_evaporated = (m_evap_total/(m_evap_total + mass_FROST))*100
"Mass flow of water in model"
m_dot_evap_total = m_dot_evap_A + m_dot_evap_D + m_dot_evap_G
"Mass of water evaporated in model"
m_evap_total = integral(m_dot_evap_total, time, 0, time_final, step)

m_dot_evap_A = g_bar_m[1,jj]*pi*(r_out[jj]^2 - r_in[jj]^2)*(m_1_s[1,jj] - m_1_e)
m_dot_evap_D = SUM(g_bar_m[1,j]*pi*(r_out[j]^2 - r_in[j]^2)*(m_1_s[1,j] - m_1_e), j=2,jj-1)
m_dot_evap_G = g_bar_m[1,1]*pi*(r_out[1]^2 - r_in[1]^2)*(m_1_s[1,1] - m_1_e)

Duplicate j=1,jj

   Nus_bar_L[1,j] = 0.13*(Gr_L[1,j]*Pr[1,j])^(1/3)          "Nusselt Number (4.86) pp.347"
   h_bar_C[1,j] = (k_air[1,j]/Length_fin*Nus_bar_L[1,j]) "Heat transfer coefficient"
   Sh_bar_L[1,j] = 0.13*(Gr_L[1,j]*Sc[1,j])^(1/3)           "Sherwood Number"
   Sc[1,j] = nu[1,j]/D_12[1,j]                              "Schmitt Number  pp.818"
   Gr_L[1,j] = ((DELTArho[1,j]/rho_m[1,j])*g*Length_fin^3)/nu[1,j]^2 "Grasholf number"
"Reynolds Number"
   Re[1,j] = (((DELTArho[1,j]/rho_m[1,j])*g*Length_fin)^(1/2)*Length_fin)/nu[1,j]
   Pr[1,j] = nu[1,j]/ALPHA[1,j]                                    "Prandtl Number"
   Le[1,j] = Sc[1,j]/Pr[1,j]                                       "Lewis Number"
   Le[1,j] = 0.95

   "Diffusion of water into air correlation for (280K < T < 450K)  pp.1181 Table A.17a"
   D_h2o_air[1,j] = 1.87*10^(-10)*(T[1,j]^2.072/Press)

"Mass transfer coefficient"
g_bar_m[1,j] = (rho_m[1,j]*nu[1,j])/(Sc[1,j]*Length_fin)*Sh_bar_L[1,j]
"enthalpy of vaporization"
h_ig[1,j] = h_vapor[1,j] - h_liQuid[1,j]
"enthalpy of water (vapor) at temperature 'T'"
h_vapor[1,j] = ENTHALPY(Water,T=T[1,j],x=1)
"enthalpy of water (liQuid) at temperature 'T'"
h_liQuid[1,j] = (ENTHALPY(Water,T=T[1,j],x=0)) - 332.8[kJ/kg]

   rho_s[1,j] = rho_1_s[1,j] + rho_2_s[1,j]                 "density of moist air at node surface"
   rho_1_s[1,j] = (P_1_s[1,j]*MW_H2O)/(R*T[1,j])            "density of water at node surface"
   rho_2_s[1,j] = (P_2_s[1,j]*MW_Air)/(R*T[1,j])            "density of dry air at node surface"

   rho_m[1,j] = 0.5*(rho_s[1,j] + rho_e)                    "mean density"
   DELTArho[1,j] = max(0.0005,abs(rho_e - rho_s[1,j]))  "density difference between node
surface and freezer"

   P_sat_s[1,j] = PRESSURE(Water,T=T[1,j],x=1)"satuation pressure of water at node surface"

   P_1_s[1,j] = P_sat_s[1,j]                  "saturated pressure of water at temperature 'T'"
   P_2_s[1,j] = P_atm - P_1_s[1,j]            "partial pressure of dry air at temperature 'T'"
```

```
   m_1_s[1,j] = rho_1_s[1,j]/rho_s[1,j]                    "water mass fraction at surface"

   nu[1,j] = mu[1,j]/rho_m[1,j]                            "dynamic viscosity"
   mu[1,j] = VISCOSITY(Air,T=T_m[1,j])                     "viscosity"
   ALPHA[1,j] = k_air[1,j]/(rho_m[1,j]*C_air[1,j])         "thermal diffusivity"
   C_air[1,j] = CP(Air,T=T_m[1,j])*convert(kJ/kg-K, 'J/kg-K')
   k_air[1,j] = CONDUCTIVITY(Air,T=T_m[1,j])               "thermal conductivity of pure air"
   T_m[1,j] = (T[1,j]+T_infinity)/2
End


"Diffusion Parameters"

rho_e = rho_1_e + rho_2_e                                  "density of moist air in freezer"
rho_1_e = (P_1_e*MW_H2O)/(R*T_infinity)                    "density of water in freezer air"
rho_2_e = (P_2_e*MW_Air)/(R*T_infinity)                    "density of dry air in freezer"

P_sat_infinity = PRESSURE(Water,T=T_infinity,x=1)          "saturation pressure in freezer"

P_1_e = RH*P_sat_infinity
P_2_e = P_atm - P_1_e

m_1_e = rho_1_e/rho_e                                      "water mass fraction in freezer"

RH = 0.80                                                  "relative humidity"
g = g#                                                     "gravitational constant"
R = R#                                                     "Universal gas constant"
MW_H2O = MOLARMASS(Water)                                  "molecular weight of water"
MW_Air = MOLARMASS(Air)                                    "molecular weight of air"
Press = P_atm*convert(kPa,atm)
Length_fin = 60[inch]*convert(inch, m)


"_________""!N O D A L     E Q U A T I O N S""_________"

"A                    Top Left Exterior Frost Node"
0 = ((((k[1,jj-1]+k[1,jj]))*(pi*dX\2)*(T[1,jj-1]-T[1,jj])/(ln(r[jj]/(r[jj]-
DELTAr)))+((k[2,jj]+k[1,jj])/2)*((pi*(r_out[jj]^2 - r_in[jj]^2))/DELTAx)*(T[1+1,jj]-
T[1,jj])+h_bar_C[1,jj]*pi*(r_out[jj]^2 - r_in[jj]^2)*(T_infinity-T[1,jj]) + -
(g_bar_m[1,jj]*pi*(r_out[jj]^2 - r_in[jj]^2)*(m_1_s[1,jj] -
m_1_e)*h_ig[1,jj]*convert(kJ,J)))*convert(W, kW)) - ((rho*dX\2*pi*(r_out[jj]^2 -
r_in[jj]^2))*dh\dt[1,jj])

"B                    Top Exterior Frost Nodes"
Duplicate i=2,ii-2
0 = ((((k[i,jj-1]+k[i,jj]))*(pi*DELTAx)*(T[i,jj-1]-T[i,jj])/(ln(r[jj]/(r[jj]-
DELTAr)))+((k[i+1,jj]+k[i,jj])/2)*(pi*(r_out[jj]^2 - r_in[jj]^2)/DELTAx)*(T[i+1,jj]-T[i,jj])+((k[i-
1,jj]+k[i,jj])/2)*(pi*(r_out[jj]^2 - r_in[jj]^2)/DELTAx)*(T[i-1,jj]-T[i,jj]))*convert(W, kW)) -
((rho*DELTAx*pi*(r_out[jj]^2 - r_in[jj]^2))*dh\dt[i,jj])
End

"C                    Top Exterior Frost Node w/ Fin on Right Side"
```

```
0 = ((((k[ii-1,jj-1]+k[ii-1,jj]))*(pi*DELTAx)*(T[ii-1,jj-1]-T[ii-1,jj])/(ln(r[jj]/(r[jj]-DELTAr)))+((k[ii-
1,jj]*(pi*(r_out[jj]^2 - r_in[jj]^2)/DELTAx)*(T[ii,jj]-T[ii-1,jj]))+(k_f*(pi*(r_out[jj]^2 -
r_in[jj]^2)/DELTAi)*(T[ii,jj]-T[ii-1,jj])))+((k[ii-2,jj]+k[ii-1,jj])/2)*(pi*(r_out[jj]^2 -
r_in[jj]^2)/DELTAx)*(T[ii-2,jj]-T[ii-1,jj]))*convert(W, kW)              ) -
((rho*DELTAx*pi*(r_out[jj]^2 - r_in[jj]^2))*dh\dt[ii-1,jj])

"D                    Left Exterior Frost Nodes"
Duplicate j=2,jj-1
0 = ((((k[1,j-1]+k[1,j]))*(pi*dX\2)*(T[1,j-1]-T[1,j])/(ln(r[j]/(r[j]-
DELTAr)))+((k[2,j]+k[1,j])/2)*(pi*(r_out[j]^2 - r_in[j]^2)/DELTAx)*(T[2,j]-
T[1,j])+((k[1,j+1]+k[1,j])*(pi*dX\2)*(T[1,j+1]-
T[1,j])/(ln((r[j]+DELTAr)/r[j])))+h_bar_C[1,j]*pi*(r_out[j]^2 - r_in[j]^2)*(T_infinity-T[1,j]) + -
(g_bar_m[1,j]*pi*(r_out[j]^2 - r_in[j]^2)*(m_1_s[1,j] -
m_1_e)*h_ig[1,j]*convert(kJ,'J')))*convert(W, kW)) - ((rho*dX\2*pi*(r_out[j]^2 -
r_in[j]^2))*dh\dt[1,j])
End

"E                    Interior Frost Nodes"
Duplicate i=2,ii-2
Duplicate j=2,jj-1
0 = ((((k[i,j-1]+k[i,j]))*(pi*DELTAx)*(T[i,j-1]-T[i,j])/(ln(r[j]/(r[j]-
DELTAr)))+((k[i+1,j]+k[i,j])/2)*(pi*(r_out[j]^2 - r_in[j]^2)/DELTAx)*(T[i+1,j]-
T[i,j])+((k[i,j+1]+k[i,j])*(pi*DELTAx)*(T[i,j+1]-T[i,j])/(ln((r[j]+DELTAr)/r[j])))+((k[i-
1,j]+k[i,j])/2)*(pi*(r_out[j]^2 - r_in[j]^2)/DELTAx)*(T[i-1,j]-T[i,j]))*convert(W, kW)) -
((rho*DELTAx*pi*(r_out[j]^2 - r_in[j]^2))*dh\dt[i,j])
End
End

"F                    Interior Frost Nodes w/ Fin on Right Boundary"
Duplicate j=2,jj-1
0 = ((((k[ii-1,j-1]+k[ii-1,j]))*(pi*DELTAx)*(T[ii-1,j-1]-T[ii-1,j])/(ln(r[j]/(r[j]-DELTAr)))+((2*k[ii-
1,j]*(pi*(r_out[j]^2 - r_in[j]^2)/DELTAx)*(T[ii,j]-T[ii-1,j]))+(2*k_f*(pi*(r_out[j]^2 -
r_in[j]^2)/DELTAi)*(T[ii,j]-T[ii-1,j])))+((k[ii-1,j+1]+k[ii-1,j])*(pi*DELTAx)*(T[ii-1,j+1]-T[ii-
1,j])/(ln((r[j]+DELTAr)/r[j])))+((k[ii-2,j]+k[ii-1,j])/2)*(pi*(r_out[j]^2 - r_in[j]^2)/DELTAx)*(T[ii-
2,j]-T[ii-1,j]))*convert(W, kW)) - ((rho*DELTAx*pi*(r_out[j]^2 - r_in[j]^2))*dh\dt[ii-1,j])
 End

"G                    Bottom Corner Frost Node"
0 = ((h_bar_C[1,1]*DELTAx*(pi*r_in[1])*(T_infinity-T[1,1])+((k[2,1]+k[1,1])/2)*(pi*(r_out[1]^2 -
r_in[1]^2)/DELTAx)*(T[2,1]-T[1,1])+(((k[1,2]+k[1,1]))*(pi*dX\2)*(T[1,2]-
T[1,1])/(ln((r[1]+DELTAr)/r[1])))+h_bar_C[1,1]*(pi*(r_out[1]^2 - r_in[1]^2))*(T_infinity-T[1,1])
+ -(g_bar_m[1,1]*pi*(r_out[1]^2 - r_in[1]^2)*(m_1_s[1,1] -
m_1_e)*h_ig[1,1]*convert(kJ,J)))*convert(W, kW)) - ((rho*dX\2*pi*(r_out[1]^2 -
r_in[1]^2))*dh\dt[1,1])

"H                    Bottom Exterior Middle Nodes"
Duplicate i=2,ii-2
0 = ((h_bar_C[1,1]*DELTAx*(2*pi*r_in[1])*(T_infinity-T[i,1])+(k[i+1,1]+k[i,1])/2*pi*(r_out[1]^2
- r_in[1]^2)/DELTAx*(T[i+1,1]-T[i,1])+(((k[i,2]+k[i,1]))*(pi*DELTAx)*(T[i,2]-
T[i,1])/(ln((r[1]+DELTAr)/r[1])))+((k[i-1,1]+k[i,1])/2)*(pi*(r_out[1]^2 - r_in[1]^2)/DELTAx)*(T[i-
1,1]-T[i,1]))*convert(W, kW)) - ((rho*DELTAx*pi*(r_out[1]^2 - r_in[1]^2))*dh\dt[i,1])
End
```

```
"I                    Bottom Exterior Frost Node w/ Fin on Right Side"
0 = ((h_bar_C[1,1]*DELTAx*(2*pi*r_in[1])*(T_infinity-T[ii-1,1])+((k[ii-1,1]*(pi*(r_out[1]^2 -
r_in[1]^2)/DELTAx)*(T[ii,1]-T[ii-1,1]))+(k_f*(pi*(r_out[1]^2 - r_in[1]^2)/DELTAi)*(T[ii,1]-T[ii-
1,1])))+(((k[ii-1,2]+k[ii-1,1]))*(pi*DELTAx)*(T[ii-1,2]-T[ii-1,1])/(ln((r[1]+DELTAr)/r[1])))+((k[ii-
2,1]+k[ii-1,1])/2)*(pi*(r_out[1]^2 - r_in[1]^2)/DELTAx)*(T[ii-2,1]-T[ii-1,1]))*convert(W, kW)) -
((rho*DELTAx*pi*(r_out[1]^2 - r_in[1]^2))*dh\dt[ii-1,1])

"J                    Exterior Fin Node"
0 = (((k_f*(pi*DELTAi)*(T[ii,jj-1]-T[ii,jj])/(ln(r[jj]/(r[jj]-DELTAr))))+((k[ii-1,jj]*(pi*(r_out[jj]^2 -
r_in[jj]^2)/DELTAx)*(T[ii-1,jj]-T[ii,jj]))+(k_f*(pi*(r_out[jj]^2 - r_in[jj]^2)/DELTAi)*(T[ii-1,jj]-
T[ii,jj])))))*convert(W, kW)) - ((rho_f*dI\2*pi*(r_out[jj]^2 - r_in[jj]^2))*C*dT\dt[ii,jj] )


"K                    Fin Interior Nodes"
Duplicate j=2,jj-1
0 = (((k_f*(pi*DELTAi)*(T[ii,j-1]-T[ii,j])/(ln(r[j]/(r[j]-DELTAr))))+(k_f*(pi*DELTAi)*((T[ii,j+1]-
T[ii,j]))/(ln((r[j]+DELTAr)/r[j])))+((2*k[ii-1,j]*(pi*(r_out[j]^2 - r_in[j]^2)/DELTAx)*(T[ii-1,j]-
T[ii,j]))+(2*k_f*(pi*(r_out[j]^2 - r_in[j]^2)/DELTAi)*(T[ii-1,j]-T[ii,j])))))*convert(W, kW)) -
((rho_f*dI\2*pi*(r_out[j]^2 - r_in[j]^2))*C*dT\dt[ii,j] )
End

"L                    Base of Fin Node"
0 = ((h_base*(DELTAi)*(pi*r_in[1])*(T_base-T[ii,1])+(k_f*(pi*DELTAi)*(T[ii,2]-
T[ii,1])/(ln((r[1]+DELTAr)/r[1])))+((k[ii-1,1]*(pi*(r_out[1]^2 - r_in[1]^2)/DELTAx)*(T[ii-1,1]-
T[ii,1]))+(k_f*(pi*(r_out[1]^2 - r_in[1]^2)/DELTAi)*(T[ii-1,1]-T[ii,1])))))*convert(W, kW)) -
((rho_f*dI\2*pi*(r_out[1]^2 - r_in[1]^2))*C*dT\dt[ii,1] )



"!_____""I N T E G R A T I O N""!_____"

"Enthalpy of Frost/Water"
Duplicate i = 1,ii-1
Duplicate j = 1,jj
h[i,j] = h_initial+integral(dh\dt[i,j], time, 0, time_final, step)
          call T_water(h[i,j]:T[i,j]{,x[i,j]},k[i,j]{,rho})
End
End

"Temperature of Fin"
Duplicate j=1,jj
T[ii,j] = T_initial + integral(dT\dt[ii,j], time, 0, time_final, step)
End

"Time of Simulation, used with checkstop function"    "Used with Checkstop Function"
Stop_Time = integral(checkstop(T[1,jj]), time, 0, time_final, step)



"_____""!K N O W N S""_____"
```

```
C = {c_('Aluminum', T_initial)}0.9                "Specific Heat of Fin [kJ/kg-K]"
P_atm = Po#                                       "Atmospheric Pressure"
rho_f = 2707                                      "Density of Fin"
rho = 150 {300} {450}                             "Density of Frost (assumed constant)""!(2) of (3)"
k_f = 240                                         "Thermal Conductivity of Fin"
h_initial = ENTHALPY(Ice,T=T_initial,P=P_atm)          "Initial Convective Coefficient"
time_final = 5000                                 "Stop Time of Simulation"


"!_____""V A R I A B L E S""!_____"

T_initial = {252.6} {-5} {249.8} {-10} 244.26 {-20} "INITIAL TEMP (2) of (2) places in program"
T_infinity = {261.48} 252.6 {-5} {249.8} {-10} {244.26} {-20}          "AMBIENT TEMP"
T_base = ConvertTEMP(F,K, 60)                                  "conversion from [F] to [K]"

h_base = 100000.0                                 "Convection Coefficient for Q in bottom of fin"

step = 0.01

Duplicate i = 1,ii
node[i] = i
End


"Integral Table"
$integraltable time:0.5, Q_in, Q_dot_in, Q_conv, Q_dot_conv, Q_evap, Q_dot_evap,
Q_stored, Q|stored\out, Q_stored_fin, Q_stored_FROST, Q_excess_FROST, h_bar_C[1,1..jj],
g_bar_m[1,1..jj], m_dot_evap_total_low, T[1..ii,1..jj], k[1..ii-1,1..jj]



$tabstops 0.1, 0.11, 0.12
```